Development of highly improved fabrication techniques for colloidal silicon nanocrystals by pulsed laser irradiation in liquid

Development of highly improved fabrication techniques for colloidal silicon nanocrystals by pulsed laser irradiation in liquid

Ze Yuan

February 2018

Development of highly improved fabrication techniques for colloidal silicon nanocrystals by pulsed laser irradiation in liquid

Ze Yuan

Doctoral program in Materials Science

Submitted to the Graduate School of

Pure and Applied Sciences

in Partial Fulfillment of the Requirements

for the Degree of Doctor of Philosophy in

Engineering

at the

University of Tsukuba

Contents

Contents I

List of abbreviations III

Chapter 1 General introduction ..... - 1 -

1.1 luminescent colloidal Silicon nanocrystals ..... - 1 -
1.2 Application of the Si nanocrystals for light-emitting silicon device ..... - 2 -
1.3 Approach to improve photoluminescence properties of silicon nanocrystals ..... - 3 -
1.3.1 Effects of Surface passivation ..... - 3 -
1.3.2 Oxide-terminated Si-nc (O: Si-nc) ..... - 3 -
1.3.3 Hydrogen-terminated Si-nc (H: Si-nc) ..... - 3 -
1.3.4 Carbon-terminated Si-nc (C: Si-nc) ..... - 5 -
1.4 Application for C: Si-ncs in LEDs ..... - 5 -
1.5 Fabrication approach of Si-ncs. ..... - 6 -
1.5.1 Bottom up synthesis method (Solution-phase synthesis) ..... - 6 -
1.5.2 Top down synthesis method (Chemical etching) ..... - 7 -
1.5.3 Laser ablation in solution ..... - 7 -
1.5.4 Starting material for improving laser ablation ..... - 10 -
1.6 Motivation, objectives and outline ..... - 12 -
1.7 Reference ..... - 14 -

Chapter 2 Bright and multicolor luminescent colloidal Si nanocrystals prepared by pulsed laser irradiation in liquid ..... - 20 -

2.1 Introduction ..... - 20 -
2.2 Experimental section ..... - 21 -
2.2.1 Preparation of PSi powder ..... - 21 -
2.2.2 Preparation of colloidal Si-nc ..... - 21 -
2.2.3 Analytical technique ..... - 22 -
2.3 Results and discussion ..... - 23 -
2.4 Conclusion ..... - 29 -
2.5 Reference ..... - 31 -
2.6 Supporting Information ..... - 33 -

Chapter 3 Luminescence color control and quantum-efficiency enhancement of colloidal Si nanocrystals by pulsed laser irradiation in liquid ..... - 35 -

3.1 Introduction ..... - 35 -

3.2 Experimental section ..... - 36 -

3.2.1 Preparation of PSi powder ..... - 36 -

3.2.2 Preparation of colloidal Si-nc ..... - 37 -

3.2.3 Analytical technique ..... - 38 -

3.3 Results and discussion ..... - 39 -

3.4 Conclusions ..... - 49 -

3.5 References ..... - 50 -

3.6 Supporting Information ..... - 54 -

Chapter 4 Improvement of laser processing for colloidal silicon nanocrystal formation in a reactive solvent ..... - 58 -

4.1 Introduction ..... - 58 -

4.2 Experimental section ..... - 59 -

4.2.1 Preparation of PSi powder ..... - 59 -

4.2.2 Preparation of colloidal Si-nc ..... - 60 -

4.2.3 Analytical technique ..... - 61 -

4.3 Results and discussion ..... - 61 -

4.4 Conclusions ..... - 70 -

4.5 References ..... - 71 -

4.6 Supporting Information ..... - 74 -

Chapter 5 Concluding remarks ..... - 76 -

Publications and Presentations ..... - 79 -

Acknowledgments ..... - 82 -

List of abbreviations

Silicon (Si)

Si nanocrystal (Si-nc)

Porous Si (PSi)

Chlorine-terminated silicon nanocrystals (Cl:Si-ncs)

Carbon-terminated silicon nanocrystals (C:Si-ncs)

Hydrogen Fluoride (HF)

Silicon-Carbon (Si-C)

Silicon-Hydrogen (Si-H)

Silicon-Oxygen (Si-O)

Silicon-Chlorine (Si-Cl)

Methyl group (CH_3)

Concentrations (conc)

Ultraviolet (UV)

Transmission electron microscope (TEM)

High-resolution TEM (HRTEM)

Fast Fourier transform (FFT)

Fourier-transform infrared (FTIR)

Photoluminescence (PL)

PL intensity (I_{PL})

Photoluminescence excitation (PLE)

Photoluminescence decay (PL decay)

The intensity for the slow (fast) component ($I_{s(f)}$)

The decay time for the slow (fast) component ($\tau_{s(f)}$)

The β factor for the slow (fast) component ($\beta_{s(f)}$)

The common decay time for the slow decay component (τ_s)

The common decay time for the fast decay component (τ_f)

The β factor for the slow decay component (β_s)

The β factor for the fast decay component (β_f)

Decay rate (w)

Radiative decay rates (w_r)

Non-radiative decay rates (w_{nr})

Emission energies (E_{em})

PLE peak energies (E_{PLE})

The PL intensities for the slow (I_{slow})

The PL intensities for the fast (I_{fast})

Instrument response function (IRF)

Quantum efficiency (QE)

Φ is the PL quantum efficiency.

Quantum dot (QD)

Light emitting diodes (LEDs)

Etching times (t_e)

Chapter 1

General introduction

1.1 luminescent colloidal Silicon nanocrystals

Silicon (Si) is one of the most important and abundant materials on earth. It is abundant and relatively benign, which is widely used in microelectronic industry. Nanometer-size (1–10 nm) silicon is in many ways very interesting materials whose potential is still not fully understood. In particular, we call free-standing silicon nanocrystals as a 'colloidal' silicon nanocrystals (Si-ncs), or freestanding Si-ncs. The optical properties of Si-ncs are dramatically modified by and dependent on the nanocrystal size.[1-5]

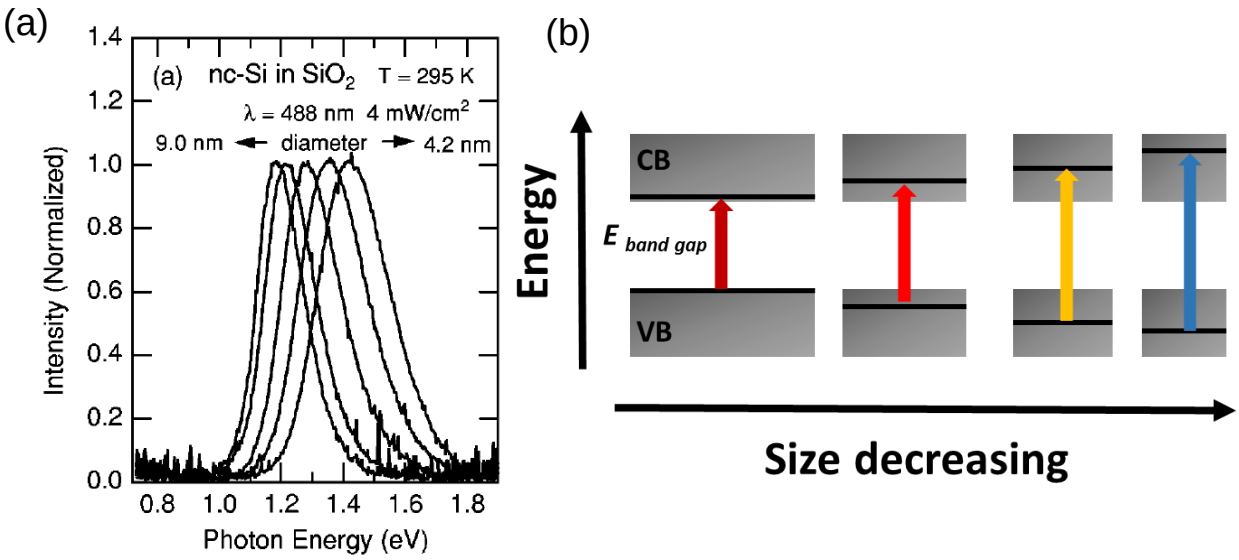

Figure 1.1. (a) Dependence of the PL spectra on the average diameter of Si-nc at 295 K.[1] (b) Schematic illustration of quantum confinement effects.

Canham *et al*[6] was the first to report in 1990 room-temperature photoluminescence from nano-sized silicon (i.e., porous silicon) that were fabricated by electrochemical erosion of crystalline silicon in acidic electrolytes. Many other technologies were subsequently

developed for the fabrication of luminescent nanostructured of silicon. For example, the luminescent Si-ncs fabricated in SiO_2 matrices were synthesized by using rf cosputtering method. As shown in Figure 1.1, the dependence of the PL spectra on particle size are demonstrated at room temperature, i.e., PL peak energy of the Si-nc increases with decreasing its size, due to the confinement of excited carriers (e.g., exciton) in nanometer-sized region, i.e., quantum confinement. As shown in Figure 1.1(b), with decreasing the size of confinement region (a particle) below exciton Bohr radius, the energy band becomes discrete levels and the band gap energy increase.

However, compared to the direct bandgap semiconductor materials, the optical and electronic properties of the nano-sized silicon particle is still not very clear and is under debate. As a result, the research on luminescent colloidal Si-ncs are still very important for future practical applications.

1.2 Application of the Si nanocrystals for light-emitting silicon device

Semiconductor nanocrystals or quantum dots (QDs) are a new class of materials in recent years, combining tailored electronic properties and the advantageous ability in solution-based techniques. Colloidally stable nanocrystals are therefore expected to find widespread application in electronics and optoelectronics.[7-18] Even though QD-LEDs have been intensively investigated, [16-18] the toxicity of the elements used for efficient II–VI QD-LEDs, such as CdS, CdSe, and their Pb containing counterparts, is a severe drawback for many applications. In contrast, Si-ncs with diameters less than 5 nm can exhibit high luminescence efficiencies[1-5] with their high natural abundance and low toxicity.

A significant research effort has been paid for the demonstration of electroluminescence of Si-nc as well as to the development of both all-silicon and hybrid light-emitting-diodes (LEDs) exploiting Si-nc.[13-15] However, despite the relatively high photoluminescence efficiency of Si-ncs,[15,16] electroluminescence efficiencies of Si-LEDs have been reported to be significantly lower than those obtained using II-VI semiconductors. The quantum efficiency (QE) of Si-ncs based LED is less than 1% as shown in Figure 1.2. When the Si nanoparticles were used as a phosphor for blue LED, the conversion efficiency is reported to be less than 10%.[19] Thus, it is important to improve the photoluminescence efficiency of Si-nc.

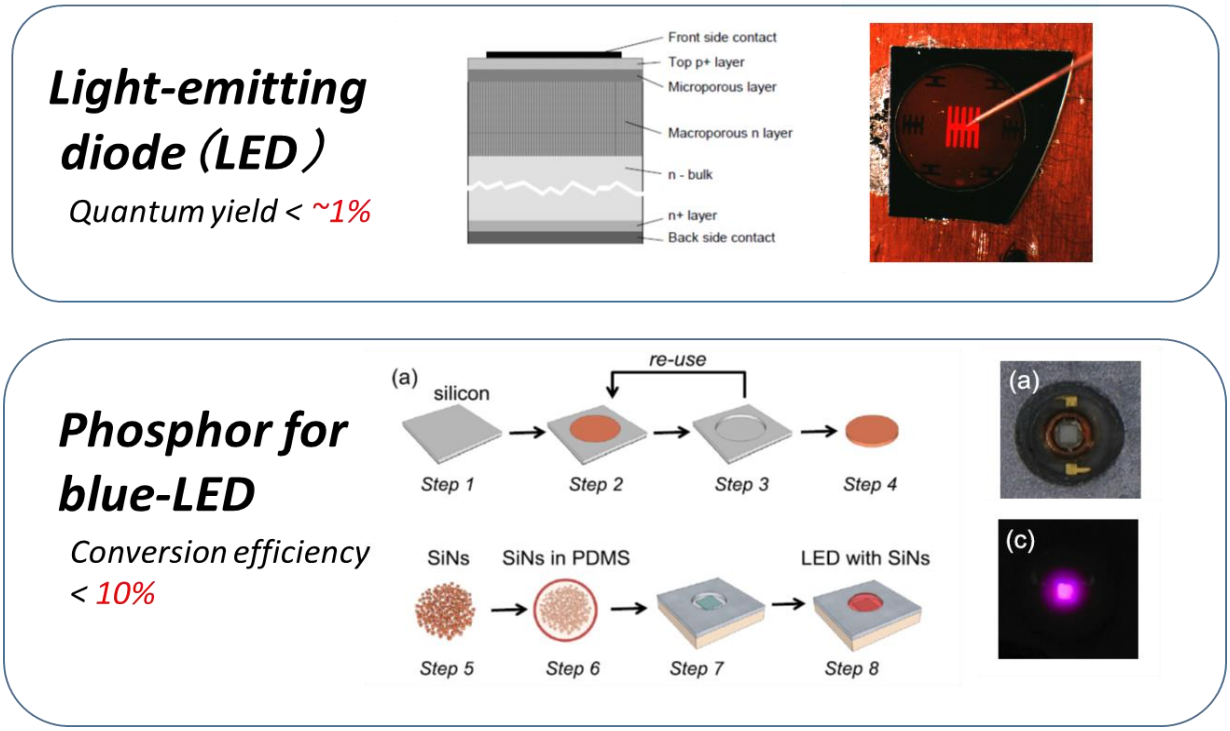

Figure 1.2. Si-nc based LED[14] and Si-nc phosphor for blue LED.[19]

1.3 Approach to improve photoluminescence properties of silicon nanocrystals

1.3.1 Effects of Surface passivation

The semiconductor nanocrystals are sensitive to the surrounding environment and surface reconstructions.[20] When some atoms at the surface remain un-passivated, the changes in the rate of non-radiative rate are induced, thereby possibly impacting emission efficiency.

1.3.2 Oxide-terminated Si-nc (O: Si-nc)

Oxide-terminated Si-ncs (O: Si-ncs) are known for its good photochemical stability. Oxygen can be form a variety of chemcal bonds with the Si-ncs surface, such as bridging oxygen (Si–O–Si),double bonded oxygen in the silanone bond (Si=O), or alkoxy bonds (Si–

O–C-) and single bonded oxygen in the silanol (Si–OH). Furthermore, theoretical modeling has shown that those chemical bonds of oxygen don't migrate to the Si-nc core [21]. Even though the Si=O is not stable[22] as shown in Table 1, formation of a Si=O has been predicted for Si-ncs in amorphous matrices[23]. Theoretical simulations also demonstrates that the Si=O is extremely impressionable in the water and air [24], while the Si–OH and Si–O–Si are expected to be more stable compared with Si=O. Si=O and Si–O–Si are most commonly found in Si-ncs grown in thermal oxides, porous Si and Si-ncs oxidized upon exposure to air[25]. Si–OH, interestingly, forms laser fragmentation[26] and micro-plasma treatment[27] in solvent.

	Bond dissociation energy		
Bond	kJ mol^{-1}	eV	nm
Si–Si (surface)	210	2.18	568
Si–Si (silane)	270–335	2.80–3.47	357–442
Si=O	255	2.64	469
Si–H (surface)	320, *293	3.32, *3.04	373, *408
Si–H (silane)	335–376	3.47–3.90	357–318
Si–C (surface/silane)	370, *356	3.83, *3.69	323, *336
Si–N	418	4.34	285
Si–Cl (surface/silane)	470, *381	4.87, *3.95	255, *314
Si–O (surface/silane, Si–OH, Si–O–Si)	540	5.60	221
Si–F (surface/silane)	670, *552	6.94, *5.72	180, *217

Table 1. Selected dissociation bond energies for Si-ncs and some bonds[29,30]

1.3.3 Hydrogen-terminated Si-nc (H: Si-nc)

Hydrogen terminated Si-nc (H: Si-nc) is obtained in various fabrication techniques such as the HF etching of the silicon or silica shell, electrochemical etching of Si wafers[25], and post-etching of oxide-terminated Si-nc.[20]. Unfortunately, hydrogen[31,25,32] exhibits lower stability against photo-oxidation. The photochemical stability of particle surface essentially is determined by the bond dissociation energy. H-termination is photochemically unstable and H: Si-nc is very easier to be oxidized in air ambient. As shown in Table 1, this instability is promoted by the defect of nanocrystal surface.

1.3.4 Carbon-terminated Si-nc (C: Si-nc)

Carbon-terminated Si-ncs (C: Si-nc) are photochemically stable; it is usually less reactive than the Si-F or Si-O bonds[29] and have a good resistance to oxidation. However, a short organic bonds may react with oxygen [33] and allow oxygen to penetrate the organic bonds termination layer and oxidize the surface of the Si-ncs [34]. Surface termination of particles with longer organic bonds was demonstrated to prevent aggregation of Si-ncs and improve their photochemically stability.[35] The carbon termination can lead to an enhancement of optical properties.[28] The electron and hole can recombine at Γ point as shown in figure 1.4. [28] Carbon-bonds termination samples can be obtained by UV illumination [36] (as shown in Table 1) or heating temperature more than 120℃ in alkenes or alkynes (alkylation) or other unsaturated compounds under oxygen and water free conditions [29]. Thus, the carbon-linked organic ligands termination is very good approach for improving the silicon photoluminescence properties.

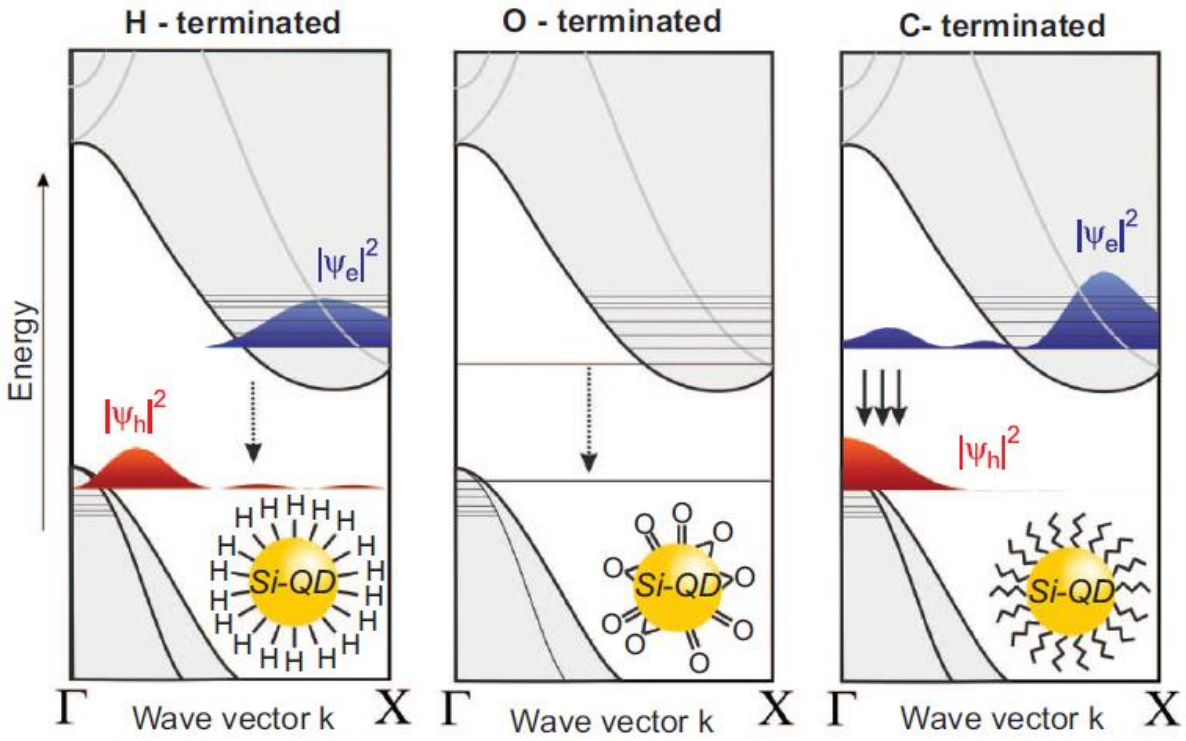

Figure 1.4. Schematic illustration of electronic states in k-space for H, O and C: Si-ncs.[28]

1.4 Application for C: Si-ncs in LEDs

Many nano-sized materials can be applied to optoelectronic devices, such as LEDs or displays, have already been realized based on some typical direct bandgap materials, and prototypes advertised by several companies, such as SHARP and Japan Display Inc. but these materials usually have higher toxic element (e.g. Cd), may face environmental risks with long term use. On the other hand, C: Si-ncs with direct bandgap transitions[28] and tunable luminescence [28] offer an ideal environmentally friendly and readily available substitution for these materials.

Rescently, Maier-Flaig *et al* reported an efficient electroluminescent devices using luminescent C: Si-nc samples. The luminescent color can be changed from the infrared to the orange emission region by monodisperse size-separated nanocrystals. High external QE up to 1.1% as well as lower voltages are fabricated for red emitters compared with H:Si-ncs as light emitting material (QE: 0.1%).[37]

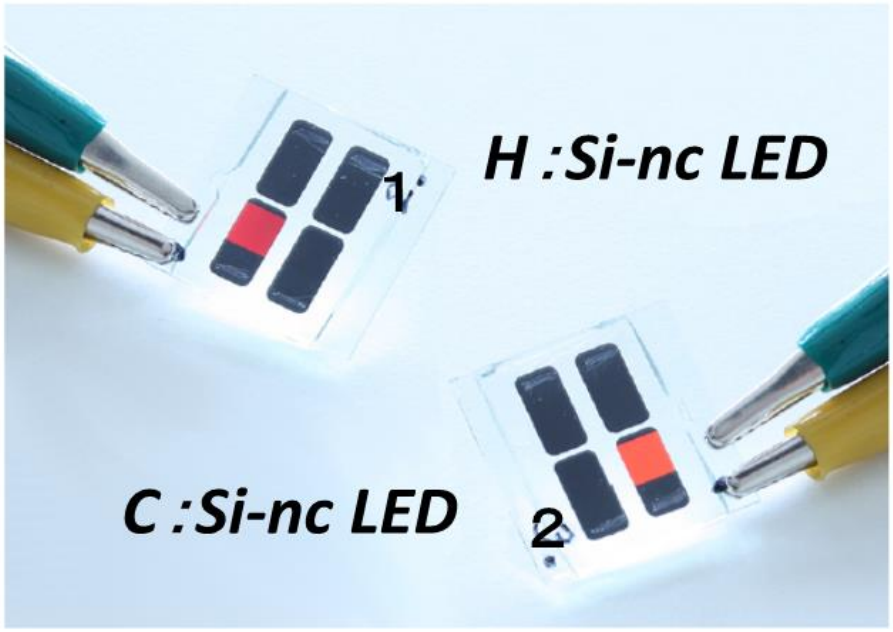

Figure 1.5. H and C: Si-ncs for LEDs application.[37]

1.5 Fabrication approach of Si-ncs.

Top-down and bottom-up approaches are used for the formation of Si-nc materials. The

bottom-up approach is more advantageous than the top-down approach because the former has a better chance of producing nanostructures with less defects, more homogenous chemical composition, and better short- and long-range ordering. In a bottom up synthesis method, the nanostructures are synthesized onto the substrate by stacking atoms onto each other, which gives rise to crystal planes and further crystal planes stacking, resulting in the synthesis of the nanostructures. Bottom-up approach can thus be considered as a synthesis approach where the building blocks are added onto the substrate to form the nanostructures. In a top down synthesis method, the nanostructures are synthesized by etching out crystals planes (removing crystal planes) which are already present on the substrate. A top-down approach can thus be considered as an approach where the building blocks are removed from the substrate to form the nanostructure.

1.5.1 Bottom up synthesis method (Solution-phase synthesis)

Since in 1992, Heath *et al* reported a kind of bottom-up approaches using reducing agents in the presence of silane targets in solvent, and also for first time to preparing a silicon single crystals by liquid-solution-phase technique.[38] This technique showed that mixing $SiCl_4$ and octyltrichlorosilane under high temperature and pressure fabricated Si-ncs.[38] Examples in the previous routes, Baldwin *et al* reported the use of sodium naphthalenide ($NaC_{10}H_8$) as the reducing agent and $SiCl_4$ in solvent,[39] or sodium as the reducing agent and tetraethyl orthosilicate. Li *et al* reported that very high QE Si-ncs can be obtained by using this technique.[40]

1.5.2 Top down synthesis method (Chemical etching)

Technology of Si-nc prepared by electrochemical etching of silicon wafer has been become one of the most popular technology. Herein, Canham *et al* first demonstrated the visible luminescent silicon nanostructures by using electrochemical etching in 1991.[6] The approach for producing colloidal of silicon was reported in 1992 by Heinrich *et al*.[41] Samples of n-type Si have been electrochemically etched to synthesis porous silicon and then dispersed into organic or water solvents, producing a good luminescent Si particles.

However, bottom-up or top-down synthesis method to prepare the Si-nc also need two

steps, e.g., the formation of nanoparticle and then surface modification (as shown in figure 1.6.). Thus, the complicated preparation processing is hard to satisfy a future mass production of Si-nc.

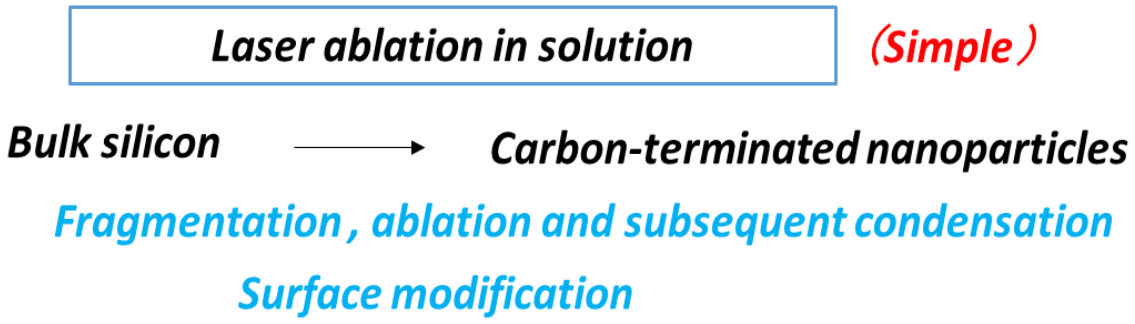

Figure 1.6. Laser ablation processing for prepared Si-ncs

1.5.3 Laser ablation in solution

Laser ablation is conducted in vacuum, gas, or liquids and has been used for the preparation of nanoparticle materials. In particular, the use of laser ablation in liquid is considered an easy way to produce a colloidal nanoparticle solution without any unnecessary reagent[41-44]. In this technique, pulsed laser irradiation causes the vaporization of the material to be ablated subsequently, nanoparticles are grown. The growth of the nanoparticles is complete when the surfactant molecules cover the nanoparticle surface via chemical reactions between the ablated material and liquid, thereby resulting in the formation of a well-passivated nanoparticle surface. Then, formation of nanoparticle and surface passivation can be produced by one step. Thus, as shown in Figure 1.7, the present laser ablation in solution can be for simple production process in silicon research compared with solution-phase synthesis or chemical etching.

Since in 2008, Švrček *et al* reported that blue-luminescent Si-ncs (see Figure 1.7 (a)) can be fabricated by using pulsed laser ablation of bulk Si in water. The prepared Si-ncs showed the quantum confinement effect due to their size and are prepared with an environmentally compatible process. Moreover, oxide termination around the particle core formed during laser processing in water offers the conditions for the confinement of excitons that allows for stable blue photoluminescence in water.[45]

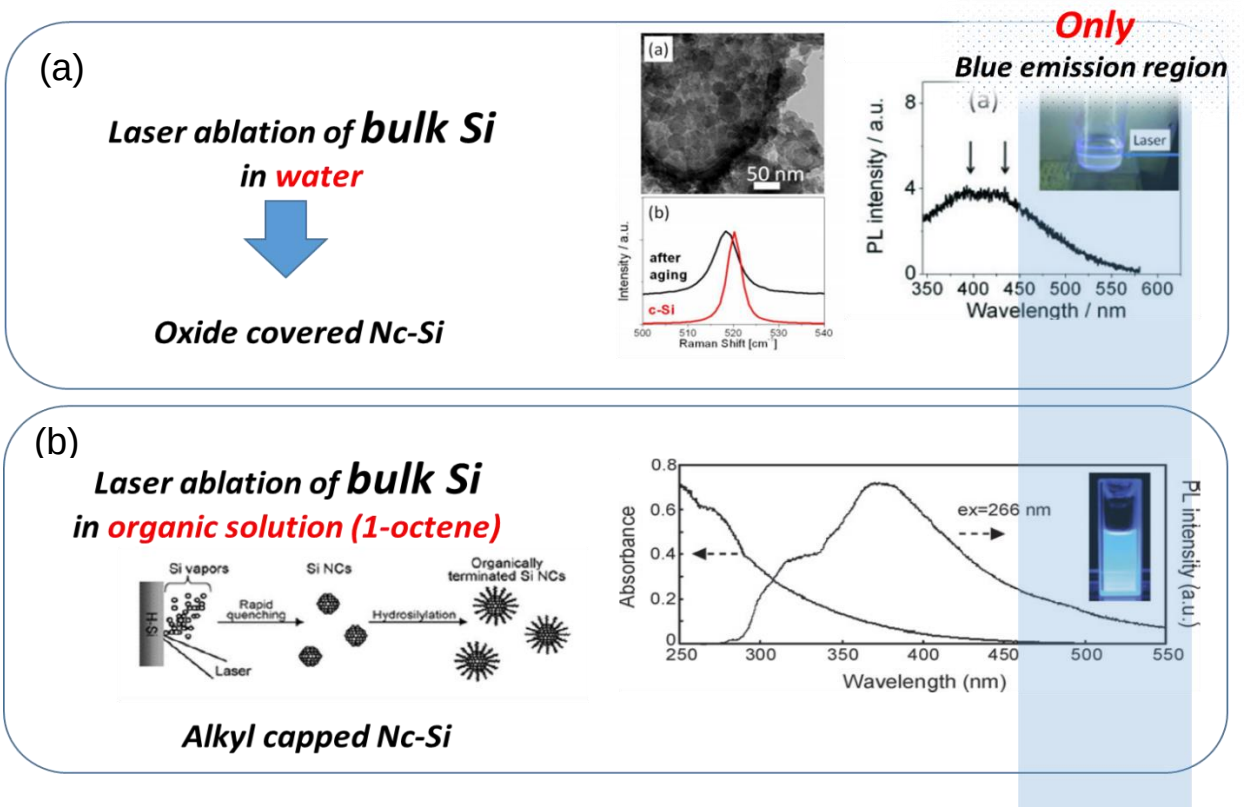

Figure 1.7. Research for luminescent Si-nc prepared by laser ablation in (a) water [45] and (b) 1-octene, [46] respectively.

Shirahata *et al* reported a quick and simply technology for preparing luminescent colloidal Si-ncs with organic monolayers. This technology allows the simultaneous achievement of nanocrystal fabrication and subsequent organic surface modification in a single step by performing laser ablation of bulk silicon target in an organic solution. Moreover, the prepared samples are greatly improved in quantum efficiency compared with the sample in water. But unfortunately, as shown in Figure 1.7 (b), the emission color still is blue.[46]

Actually, in almost all researches on colloidal Si-nc prepared by laser ablation, however, the visible luminescence was only blue in color, because the prepared particle sizes were always limited to less than 2 nm. Some works reported possible mechanism for the blue emission of Si-nc, as shown in Figure 1.8. One is due to direct recombination at the Γ point direct-transition-like, recombination of quantum confined electron–hole pairs [46, 47] or direct-transition-like recombination via the Si–Si self-trap states. Another one is due to recombination via oxygen-related defect states. Furthermore, with conventional laser-

ablation technologies, it is difficult to control the size distribution of synthesized Si-ncs and obtain samples with a high QE and large-scale mass-production. Therefore, further exploration of new fabrication routes is still a challenging issue toward versatile control of visible luminescent Si-nc.

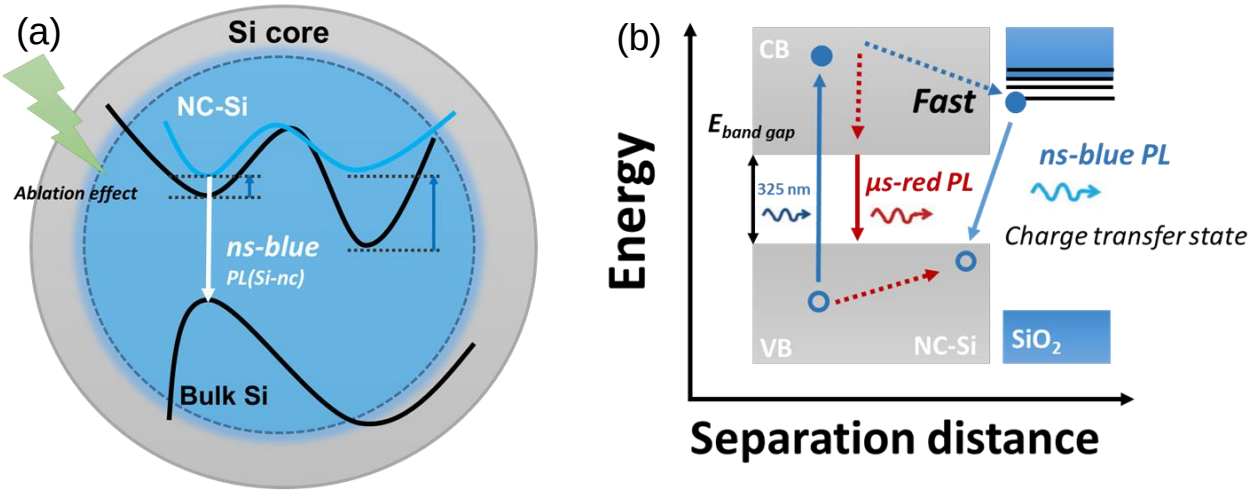

Figure 1.8. Schematic illustration of colloidal Si-nc blue emission mechanism. (a) Quantum confinement effect and (b) surface defect states effect.

1.5.4 Starting material for improving laser ablation

Some years ago, we reported a new method for preparing blue emitting colloidal Si-nc by the laser ablation of a nanostructured Si assembly (PSi) in liquid (1-octene).[51] PSi has a large surface area and high chemical and physical reactivities.[52,53] Thus, we can achieve efficient production of colloidal Si-nc by the highly selective laser ablation of PSi instead of bulk Si.

Figure 1.9 shows the plot of the integrated PL intensity I_{PL} of colloidal Si-nc versus the I_{PL} of PSi synthesized at various stain etching times, t_e = 0–40 min. The inset of Figure 1.9 shows the PL spectra of colloidal Si-nc and PSi powder for t_e =0, 12, 30, and 40 min. The PL intensity of the PSi powder increases with increasing t_e, as shown in the inset of Figure 1.9. This is because the surface porous layer volume increases with increasing t_e. The PL intensity in the colloidal Si-nc sample also increases with increasing t_e. As shown in Figure 3, the I_{PL} values of the colloidal Si-nc linearly increase with the increase in PSi

powder. This proportionality relationship indicates that the number of colloidal Si-ncs is limited by the starting PSi layer volume itself. Of course, almost no colloidal Si-nc can be formed by the laser ablation of Si powder without stain-etching (bulk Si powder) under the present ablation condition, i.e., the I_{PL} for the sample at t_e = 40 min is ~30 times larger than that for t_e = 0 min (bulk Si powder). This indicates that the yield of the colloidal Si-nc obtained by using the laser ablation of PSi is one order of magnitude higher than the ablation of bulk Si. We note that the irradiation needs to generally possess a considerably large high power density to result in the formation of colloidal Si-nc from bulk Si, as noted in the literature.[44] The PL intensity of colloidal Si-nc samples will decrease with decreasing irradiation laser power density, and no colloidal Si can be produced below the plasma ablation threshold.

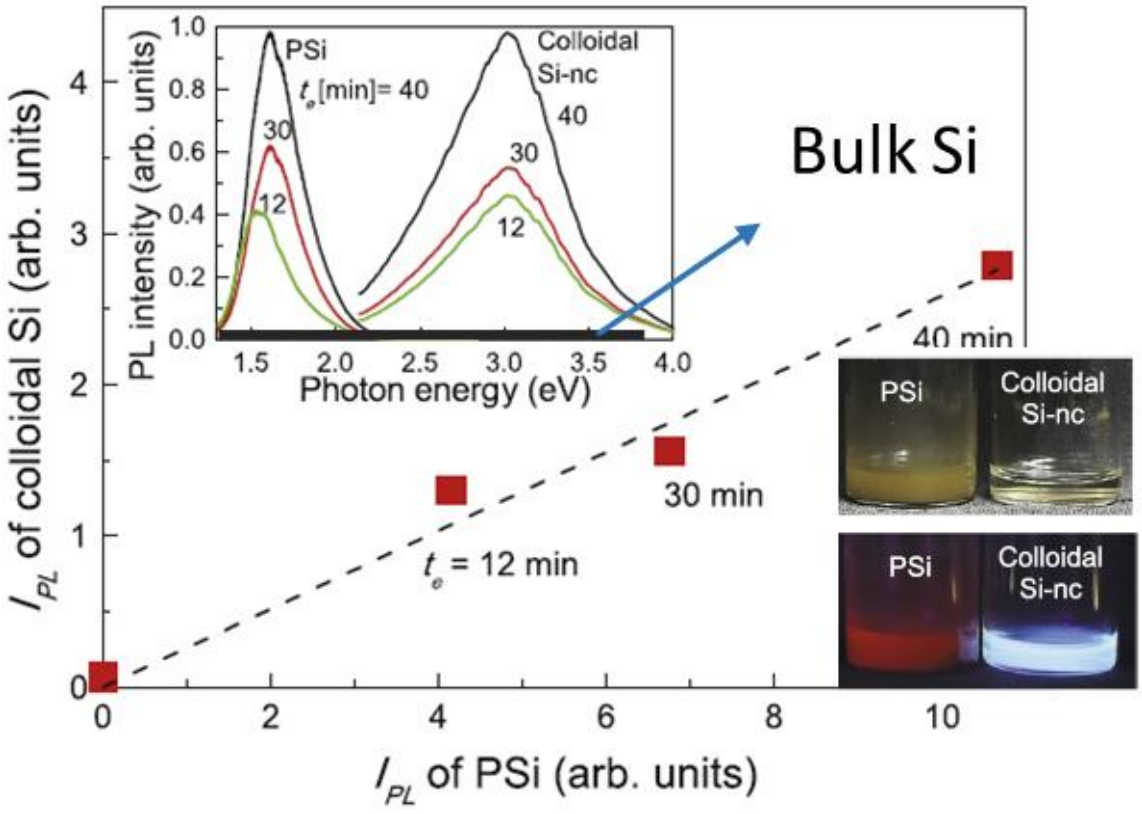

Figure 1.9. Integrated PL intensity I_{PL} of colloidal Si-nc versus I_{PL} of PSi powder for various etching times t_e. The dashed curve represents the result of linear fitting. Inset shows the PL spectra of the colloidal Si-nc and PSi powder prepared for t_e = 0 (Bulk Si), 12, 30, and 40 min.

One possible reason for the high yield of colloidal Si-nc from PSi as observed above is the considerably lower thermal conductivity of PSi. The irradiated light is absorbed by Si, and

subsequently, Si vaporization occurs as a result of rapid heating by light absorption. Subsequently, the Si atoms and/or Si clusters are rapidly cooled at the liquid (1-octene) interface, and condensation results in the colloidal Si-nc formation. Because porous materials have a lower thermal conductivity as a result of nanostructured geometrical effects,[54] local heating at the porous layer easily occurs in response to laser irradiation when compared with the case of bulk Si, and porous layer is selectively ablated. This may possibly enable easier formation of the colloidal Si-nc from PSi than from Si powder without a porous structure at a fixed laser power density. The high yield of colloidal Si-nc from PSi may also result form its large surface area. Thus, highly porosity of PSi as starting material of laser ablation approach is greatly to solve the low preparation of colloidal Si-nc.

1.6 Motivation, objectives and outline

Comparing with the conventional laser ablation methods fby using bulk Si as a starting material, the PSi is a new approach strategy for the fabrication of luminescent colloidal Si-nc with high production efficiency. However, in almost all researches of colloidal Si-nc prepared by laser ablation methods, however, the visible luminescence was only blue in color, very difficult efficient to control the emission color and particle size. Moreover, the lower quantum efficiency (~6-20%) of prepared colloidal Si-ncs is insufficient for light emitting device application.

In this thesis, we developed a series of improved fabrication techniques for luminescent colloidal Si-nc by pulsed laser irradiation of porous silicon (PSi). We realized high yield fabrication of luminescent colloidal Si-nc and its luminescence color control via nanoparticle size control from orange to red regions. These color changes are attributed to the different formation mechanisms of nanoparticles from the porous nanostructures. We also succeeded in obtaining more homogeneous size distribution Si-nc samples with higher QE up to ~70% by using highly reactive solvent, i.e., HF-contained organic solvent than conventional pulsed laser irradiation technique in organic solvent.

In chapter 2, the preparation of multicolor luminescent colloidal Si-nc's by chemical etching combined with pulsed UV laser irradiation. The target of the UV laser irradiation was PSi, which is an assembly of wire-like Si nanostructures with low-efficiency luminescence prepared by stain-etching of bulk Si. We found the multicolor luminescent colloidal Si-nc is produced by the fragmentation of different-sized Si nanostructures in PSi.

In chapter 3, the preparation of chlorine-terminated colloidal Si-ncs (Cl:Si-nc) via the laser ablation of porous silicon (PSi) in an organochloride solution. We demonstrated a reversible transformation from Cl:Si-nc to carbon-terminated Si-ncs (C:Si-nc) having a higher PL quantum efficiency and different size distribution (changing the emission color) by using irradiation and lower thermal conductive solvent the colloidal Si-ncs solution with a laser.

In chapter 4, further improvement of fabrication technique for the orange emittting colloidal Si-nc by pulsed UV laser irradaition of PSi in liquid. The pulsed laser irradiation in a HF-contained organic solution generates bright luminescent colloidal Si-nc (QE = ~50−70%) with a homogeneous size distribution. Furthermore, the preparation yield of the present samples is found to be larger than that of the previous orange-emitting ones. We found that these improvements are attributed to the promotion of the laser induced fragmentation process due to the removal of the oxide layer on PSi surface.

Chapter 5 gives the general conclusions and future perspective of this thesis.

1.7 Reference

(1) Takeoka, S. Size-dependent photoluminescence from surface-oxidized Si nanocrystals in a weak confinement regime. *Phys. Rev. B.* **2000**, 62, 16, 820.

(2) Kang, Z.; Liu, Y.; Tsang, CHA; Ma, DDD; Fan, X.; Wong, N-B; Lee, S-T. Water-soluble silicon quantum dots with wavelength-tunable photoluminescence. *Adv. Mater.* **2009,** 21, 661–4.

(3) Dohnalova, K.; Ondič, L.; Kůsova, K.; Pelant, I.; Rehspringer, J. L.; Mafouana, R-R. White-emitting oxidized silicon nanocrystals: Discontinuity in spectral development with reducing size. *J. Appl. Phys.* **2010**, 107 053102.

(4) Tan, D.; Xu, B.; Chen, P.; Dai, Y.; Zhou, S.; Ma, G.; Qiu, J. One-pot synthesis of luminescent hydrophilic silicon nanocrystals. *R. Soc. Chem. Adv.* **2012**, 2 8254-7.

(5) Dohnalova, K.; Poddubny, A. N.; Prokofiev, A. A.; de Boer, W. DAM; Umesh, C. P.; Paulusse, J. MJ; Zuilhof, H.; Gregorkiewicz, T. Surface brightens up Si quantum dots: direct bandgap-like size-tunable emission. *Light: Sci. Appl.* **2013,** 2 e47.

(6) Canham, L. T. Silicon quantum wire array fabrication by electrochemical and chemical dissolution of wafers. *Appl. Phys. Lett.* **1990**, 57, 1046.

(7) Colvin, V. L.; Schlamp, M. C.; Alivisatos, A. P. Light-emitting diodes made from cadmium selenide nanocrystals and a semiconducting polymer. *Nature.* **1994**, 370,354–357.

(8) Tessler, N.; Medvedev, V.; Kazes, M.; Kan, S.; Banin, U. Efficient near-infrared polymer nanocrystal light-emitting diodes. *Science* **2002**, 295, 1506–1508.

(9) Sun, Q.; Wang, Y. A.; Li, L. S.; Wang, D.; Zhu, T.; Xu, J.; Yang, C.; Li, Y. Bright, Multicoloured Light-emitting Diodes Based on Quantum Dots. *Nat. Photonics* **2007**, 1, 717–722.

(10) Caruge, J. M.; Halpert, J. E.; Wood, V.; Bulovic, V.; Bawendi, M.G. Colloidal quantum-dot light-emitting diodes with metal-oxide charge transport layers. *Nat. Photonics* **2008**, 2, 247–250.

(11) Cho, K.-S.; Lee, E. K.; Joo, W.-J.; Jang, E.; Kim, T.-H.; Lee, S. J.;Kwon, S.-J.; Han, J. Y.; Kim, B.-K.; Choi, B. L.; Kim, J. M. High-performance crosslinked colloidal quantum-dot light-emitting diodes. *Nat. Photonics* **2009**, 3, 341–345.

(12) Cheng, K.-Y.; Anthony, R.; Kortshagen, U. R.; Holmes, R. J. Hybrid Silicon Nanocrystal–Organic Light-Emitting Devices for Infrared Electroluminescence. *Nano Lett.* **2010**, 10, 1154–1157.

(13) Puzzo, D. P.; Henderson, E. J.; Helander, M. G.; Wang, Z.; Ozin, G. A.; Lu, Z. Visible Colloidal Nanocrystal Silicon Light-Emitting Diode. *Nano Lett.* **2011**, 11, 1585−1590.

(14) Cheng, K.-Y.; Anthony, R.; Kortshagen, U. R.; Holmes, R. J. High-Efficiency Silicon Nanocrystal Light-Emitting Devices. *Nano Lett.* **2011**, 11, 1952−1956.

(15) Anthony, R.; Cheng, K.-Y.; Holman, Z. C.; Holmes, R. J.;Kortshagen, U. R. An All-Gas-Phase Approach for the Fabrication of Silicon Nanocrystal Light-Emitting Devices. *Nano Lett.* **2012**, 12, 2822−2825.

(16) Kwak, J.; Bae, W. K.; Lee, D.; Park, I.; Lim, J.; Park, M.; Cho, H.;Woo, H.; Yoon, D. Y.; Char, K.; Lee, S.; Lee, C. Bright and Efficient Full-Color Colloidal Quantum Dot Light-Emitting Diodes Using an Inverted Device Structure. *Nano Lett.* **2012**, 12, 2362−2366.

(17) Bourvon, H.; Le Calvez, S.; Kanaan, H.; Meunier-Della-Gatta, S.; Philippot, C.; Reiss, P. Langmuir–Schaeffer Monolayers of Colloidal Nanocrystals for Cost-Efficient Quantum Dot Light-Emitting Diodes. *Adv. Mater.* **2012**, 24, 4414−4418.

(18) Sun, L.; Choi, J. J.; Stachnik, D.; Bartnik, A. C.; Hyun, B.-R.;Malliaras, G. G.; Hanrath, T.; Wise, F. W. Bright Infrared Quantum-Dot Light-Emitting Diodes through Inter-Dot Spacing Control. *Nat. Nanotechnol.* **2012**, 7,369−373.

(19) Barillaro, G.; Strambini, L. M. Color tuning of light-emitting-diodes by modulating the concentration of red-emitting silicon nanocrystal phosphors. *Appl. Phys. Lett.* **2014**, 104, 091102.

(20) Draeger, E. W.; Grossman, J. C.; Williamson, A. J.; Galli, G. Optical properties of passivated silicon nanoclusters: the role of synthesis. *J. Chem. Phys.* **2004**, 120 10807–14.

(21) Eyre, R. J.; Goss, J. P.; Briddon, P. R. Density functional study of oxygen migration processes for silicon quantum dots. *Phys. Rev. B.* **2007**, 76 245325.

(22) Kudo, T.; Nagase, S. Theoretical study of silanone. Thermodynamic and kinetic stability. *J. Phys. Chem.* **1984**, 88 2833–40.

(23) Djurabekova, F.; Nordlund, K. Atomistic simulation of the interface structure of Si nanocrystals embedded in amorphous silica. *Phys. Rev. B.* **2008**, 77 115325.

(24) Prendergast, D.; Grossman, J. C.; Williamson, A. J.; Fattebert, J-L.; Galli, G. Optical properties of silicon clusters in the presence of water: a first principles theoretical analysis. *J. Am. Chem. Soc.* **2004**, 126 13827–37.

(25) Dohnalová, K.; Kůsová, K.; Pelant, I. Time-resolved photoluminescence spectroscopy of the initial oxidation stage of small silicon nanocrystals. *Appl. Phys. Lett.* **2009**, 94 211903.

(26) Mariotti, D.; Mitra, S.; Švrček, V. Surface-engineered silicon nanocrystals. *Nanoscale* **2013**, 5 1385–98.

(27) Švrček, V.; Dohnalová, K.; Mariotti, D.; Trinh, M. T.; Limpens, R.; Mitra. S.; Gregorkiewicz, T.; Matsubara, K.; Kondo, M. Dramatic Enhancement of Photoluminescence Quantum Yields for Surface-Engineered Si Nanocrystals within the Solar Spectrum. *Adv. Funct. Mater.* **2013**, 23 6051–8.

(28) Dohnalová, K.; Poddubny, A. N.; Prokofiev, A. A.; de Boer, W. DAM; Umesh, C. P; Paulusse, J. MJ.; Zuilhof, H.; Gregorkiewicz, T. Surface brightens up Si quantum dots: direct bandgap-like size-tunable emission. *Light: Sci. Appl.* **2013**, 2 e47.

(29) Stewart, M. P.; Buriak, J. M. New Approaches Toward the Formation of Silicon-Carbon Bonds on Porous Silicon. *Commun. Inorg. Chem.* **2002**, 23 179–203.

(30) Walsh, R. Bond dissociation energy values in silicon-containing compounds and some of their implications. *Acc. Chem. Res.* **1981**, 14 246–52.

(31) Wolkin, M. V.; Jorne, J.; Fauchet, P. M.; Allan, G.; Delerue, C. Electronic states and luminescence in porous silicon quantum dots: The role of oxygen. *Phys. Rev. Lett.* **1999**, 82 197–200.

(32) Gupta, A.; Swihart, M. T.; Wiggers, H. Luminescent Colloidal Dispersion of Silicon Quantum Dots from Microwave Plasma Synthesis: Exploring the Photoluminescence Behavior Across the Visible Spectrum. *Adv. Funct. Mater.* **2009**, 19 696–703.

(33) Zou, J.; Baldwin, R. K.; Pettigrew, K. A.; Kauzlarich, S. M. Solution Synthesis of Ultrastable Luminescent Siloxane-Coated Silicon Nanoparticles. *Nano Lett.* **2004**, 4 1181–6.

(34) Sato, S.; Swihart, M. T. Propionic-Acid-Terminated Silicon Nanoparticles: Synthesis and Optical Characterization. *Chem. Mater.* **2006**, 18 4083–8.

(35) Li, X.; He, Y.; Swihart, M. T. Surface Functionalization of Silicon Nanoparticles Produced by Laser-Driven Pyrolysis of Silane followed by $HF-HNO_3$ Etching. *Langmuir* **2004**, 20 4720–7.

(36) Hua, F.; Swihart, M. T.; Ruckenstein, E. Efficient Surface Grafting of Luminescent Silicon Quantum Dots by Photoinitiated Hydrosilylation. *Langmuir* **2005**, 21 6054–62.

(37) Maier-Flaig, F.; Rinck, J.; Stephan, M.; Bocksrocker, T.; Bruns, M.; Kbel, C.; Powell, A. K.; Ozin, G. A.; Lemmer, U. Multicolor Silicon Light-Emitting Diodes (SiLEDs). *Nano Lett.* **2013**, 13 475–80.

(38) Heath, J. R. A liquid-solution-phase synthesis of crystalline silicon. *Science* **1992**, 258, 1131–1133.

(39) Baldwin, R. K.; Pettigrew, K. A.; Ratai, E.; Augustine, M. P.; Kauzlarich, S. M. Solution reduction synthesis of surface stabilized silicon nanoparticles. *Chem. Commun.* **2002**, 1822–1823.

(40) Li, Q.; He, Y.; Chang, J.; Wang, L.; Chen, H.; Tan, Y.-W.; Wang, H.; Shao, Z. Surface-Modified Silicon Nanoparticles with Ultrabright Photoluminescence and Single-Exponential Decay for Nanoscale Fluorescence Lifetime Imaging of Temperature. *J. Am. Chem. Soc.* **2013,** 135,14924–14927.

(41) Mafuné, F.; Kohno, J.; Takeda, Y.; Kondow, T.; Sawabe, H. Formation and size control of silver nanoparticles by laser ablation in aqueous solution Formation and Size Control of Silver Nanoparticles by Laser Ablation in Aqueous Solution. *J. Phys. Chem. B.* **2000**, 104 9111–7.

(42) Tsuji, T.; Nakanishi, M.; Mizuki, T.; Ozono, S.; Tsuji, M.; Tsuboi, Y. Preparation and shape-modification of silver colloids by laser ablation in liquids: a brief review. *Sci. Adv. Mater.* **2012**, 4 391–400.

(43) Anikin, K.; Melnik, N.; Simakin, A.; Shafeev, G.; Voronov, V.; Vitukhnovsky, A. Formation of ZnSe and CdS quantum dots via laser ablation in liquids. *Chem. Phys. Lett.* **2002**, 366 357–60.

(44) Shirahata, N.; Hirakawa, D.; Masuda, Y.; Sakka, Y. Size-dependent color tuning of efficiently luminescent germanium nanoparticles. Langmuir **2013**, 29 7401–10.

(45) Švrček, V.; Mariotti, D.; Kondo, M. Ambient-stable blue luminescent silicon nanocrystals prepared by nanosecond-pulsed laser ablation in water. *OPTICS EXPRESS* **2009**, 17, 520-7.

(46) Holmes, J. D.; Ziegler, K. J.; Doty, R. C.; Pell, L. E.; Johnston, K. P.; Korgel, B. A. Highly luminescent silicon nanocrystals with discrete optical transitions. *J. Am. Chem. Soc.* **2001**, 123 3743–48.

(47) Wilcoxon, J. P.; Samara, G. A.; Provencio, P. N. Optical and electronic properties of Si nanoclusters synthesized in inverse micelles *Phys. Rev. B.* **1999**, 60 2704–14.

(48) Dasog, M.; Yang, Z.; Regli, S.; Atkins, T. M.; Faramus, A.; Singh, M. P.; Muthuswamy, E.; Kauzlarich, S. M.; Tilley, L. D.; Veinot, J. G. C. Chemical insight into the origin of red and blue photoluminescence arising from freestanding silicon nanocrystals. *ACS Nano.* **2013**, 72676–85.

(49) Hua, F.; Erogbogbo, F.; Swihart, M. T.; Ruckenstein, E. Organically capped silicon nanoparticles with blue photoluminescence prepared by hydrosilylation followed by oxidation. *Langmuir* **2006**, 22 4363–70.

(50) Portolés, M. J. L.; Diez, R. P.; Dell'Arciprete, M. L.; Caregnato, P.; Romero, J. J.; Mártire, D. O.; Azzaroni, O.; Ceolín, M.; Gonzalez, M. C. Understanding the parameters affecting the photoluminescence of silicon nanoparticles. *J. Phys. Chem. C.* **2012**, 116 11315–25.

(51) Nakamura, T.; Yuan, Z.; Adachi, S. High-yield preparation of blue-emitting colloidal Si nanocrystals by selective laser ablation of porous silicon in liquid. *Nanotechnology* **2014**, 25, 275602.

(52) Sailor, M. J.; Lee, E. J. Surface chemistry of luminescent silicon nanocrystallites. *Adv. Mater.* **1997**, 9 783–93.

(53) Kovalev, D.; Timoshenko, V. Y.; Künzner, N.; Gross, E.; Koch, F. Strong explosive interaction of hydrogenated porous silicon with oxygen at cryogenic temperatures. *Phys. Rev. Lett.* **2001**, 87 68301.

(54) Ben-Chorin, M.; Möiler, F.; Koch, F.; Schirmacher, W.; Eberhard, M. Hopping transport on a fractal: ac conductivity of porous silicon. *Phys. Rev. B.* **1995**, 51 2199–213.

Chapter 2

Bright and multicolor luminescent colloidal Si nanocrystals prepared by pulsed laser irradiation in liquid

2.1 Introduction

Colloidal Si nanocrystal (Si-nc), which is nanometer sized (~1–10 nm) crystalline Si particle, is known to exhibit a size tunable and efficient visible luminescence at room temperature due to the quantum confinement effect.[1] Because of its environmental friendliness and low cost, colloidal Si-nc is a promising material for future light-emitting devices and biomedical applications.[2] Various preparation techniques for colloidal Si-nc, such as wet-chemical synthesis[3] and high-temperature thermal processing,[4] have been developed. These techniques consist of at least two processes: the formation of nanoparticles and passivation of their surfaces. The latter process is necessary because various surface states strongly affect luminescence properties such as the luminescence efficiency and color.[5]

Pulsed laser irradiation in liquid is a simple top-down method for preparing colloidal Si-nc.[6–8] By irradiating bulk Si crystal with a high power-density pulsed laser light, nanoparticles can be generated from the ablation and/or fragmentation of Si crystal. Their surfaces are simultaneously passivated by chemical reactions at the liquid/nanoparticle interface.[8] Because of the method's simplicity, however it is difficult to control the size of the Si nanoparticles. Furthermore, the size distribution is usually very wide.[6] Thus, the nanoparticles need to be separated into various sizes after their preparation to obtain the required emission color.[9]

In this work, we report on the preparation of bright and multicolor luminescent colloidal Si-nc's by chemical etching combined with pulsed UV laser irradiation. The target of the UV laser irradiation was porous Si (PSi), which is an assembly of wire-like Si

nanostructures with low-efficiency luminescence prepared by stain-etching of bulk Si. By changing the stain-etchant composition and, as a result, the size of nanostructures in PSi, the emission color of colloidal Si-nc can be varied and its luminescence efficiency is strongly enhanced compared to virgin PSi samples. Multicolor luminescent colloidal Si-nc is thought to be produced by the fragmentation of different-sized Si nanostructures in PSi. The bright luminescence can be attributed to the enhanced radiative decay rate and suppressed surface defects due to organic passivation.

2.2 Experimental section

2.2.1 Preparation of PSi powder

PSi was prepared by stain-etching of metallurgical grade polycrystalline Si powder.[10] The etching was performed in an aqueous HF/HNO_3 solution. To obtain PSi samples with different porosities, the HNO_3 concentration was changed from 3 to 5 vol. %, while the HF concentration was fixed to 20 vol. %. The etching time was 40 min. After etching, the PSi powders were collected by filtering of the etching solution and dried under ambient conditions for 24 h. Figure 2.1(a) shows the two different PSi powders prepared by etching in low (3 vol. %) and high HNO_3 (5 vol. %) concentration solutions. Both the PSi powders exhibited red luminescence upon UV-light excitation. The emission color of the powder prepared at the low HNO_3 concentration was darker than that at the high concentration, which indicates that these two PSi samples had different porosities.[10]

2.2.2 Preparation of colloidal Si-nc

For the preparing of the colloidal Si-nc samples, 100 mg of PSi powder was first dispersed in an organic solvent (1-octene) with a quartz cuvette. Second, pulsed UV laser light was irradiated at 266 nm from a Q-switched Nd:YAG laser (Continuum) with a pulse duration of 5 ns and repetition of 15 Hz for 3 h. During laser irradiation, the PSi/1-octene solution was constantly stirred by a magnetic stirrer. The laser light was irradiated into the PSi dispersed solution through the lens at a focal length of 120 mm. The distance between the lens and the front of the cuvette was set to 180 mm. The laser fluence was ~0.5 J/cm^2. After laser irradiation, the supernatant part of liquid was filtered by centrifugation at 13 000 rpm for 20 min with a membrane filter having a pore size of ~200

nm. By using the two different PSi samples prepared at different HNO_3 concentrations, we obtained two colloidal dispersion samples. Under UV illumination, each solution exhibited bright photoluminescence (PL) with different colors: orange and red for the colloidal

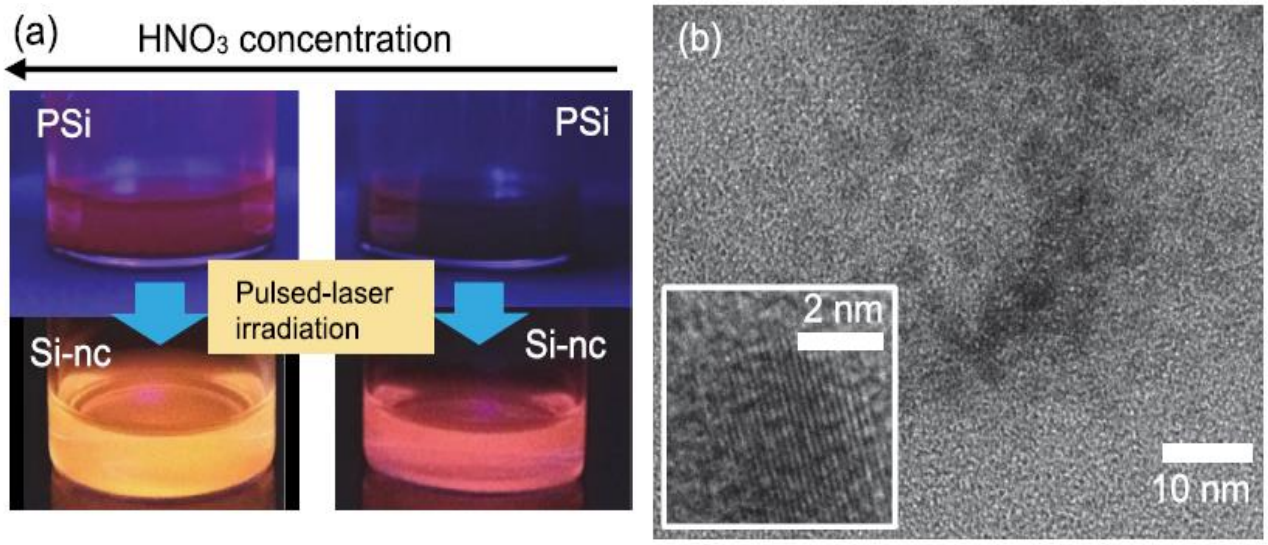

Figure 2.1. (a) Photographs of PSi (upper panels) and colloidal Si-nc (lower panels) dispersed in trichloroethylene (PSi) and 1-octene (colloidal Si-nc) under UV light illumination. The left and right panels show the samples prepared at high (5 vol. %) and low HNO_3 (3 vol. %) concentrations. (b) TEM image of colloidal Si-nc. The inset shows the high-resolution TEM image of a Si-nc.

dispersion samples obtained from the PSi etched at the low and high HNO_3 concentrations, respectively [lower part of Fig. 2.1(a)]. We also confirmed that colloidal solution can be obtained with laser irradiation even for 1 h and its density gradually increases with increasing irradiation time.

2.2.3 Analytical technique

The prepared colloids were characterized by using transmission electron microscope (TEM) (JEOL, TEM-2010). The surface chemistry of the colloids was monitored by using a Fourier-transform infrared (FTIR) spectrometer (Thermo Scientific, Nicolet iS50). The PL was measured by using a single monochromator equipped with a chargecoupled device (Princeton Instruments, PIXIS 100B). A He–Cd laser (Kimmon, IK3302R-E) was used as the excitation light source. The PL excitation (PLE) was measured by using a fluorescence

spectrometer (Hitachi, F-4500). PL decay curves were measured by using a frequency-tripled 355-nm light pulse from a Nd:YAG laser (Teemphotonics, STV-01E). The decay data at the microsecond scale were recorded by using a Peltier-device-cooled photomultiplier tube (Hamamatsu, R375) and multichannel scaler (Stanford Research, SR430). At the nanosecond scale, the data were detected by using a time-correlated single-photon counting module (Becker & Hickl, SPC-130EM) and single-photon avalanche photodiode (Micro Photon Device, SPD-050). Optical measurements were performed on samples in a quartz cuvette at room temperature.

2.3 Results and discussion

Figure 2.1(b) shows the TEM image of a colloidal sample deposited on a copper grid mesh. Spherical nanoparticles with a diameter of 2–5nm were observed. The high resolution TEM image in the inset of Fig. 2.1(b) reveals that the nanoparticle had lattice spacings of ~0.19 and 0.16 nm [Si (220) and (311) planes]. Thus, the synthesized colloidal particles are understood to be nanocrystalline Si.

FTIR measurements of the colloidal samples showed absorption peaks characterized by the bonding between silicon atoms and hydrocarbon chains such as Si–CH_3 at 1270 cm^{-1} and 850 cm^{-1} and Si–C at 677 cm^{-1}. This indicates that colloidal Si-nc is passivated by

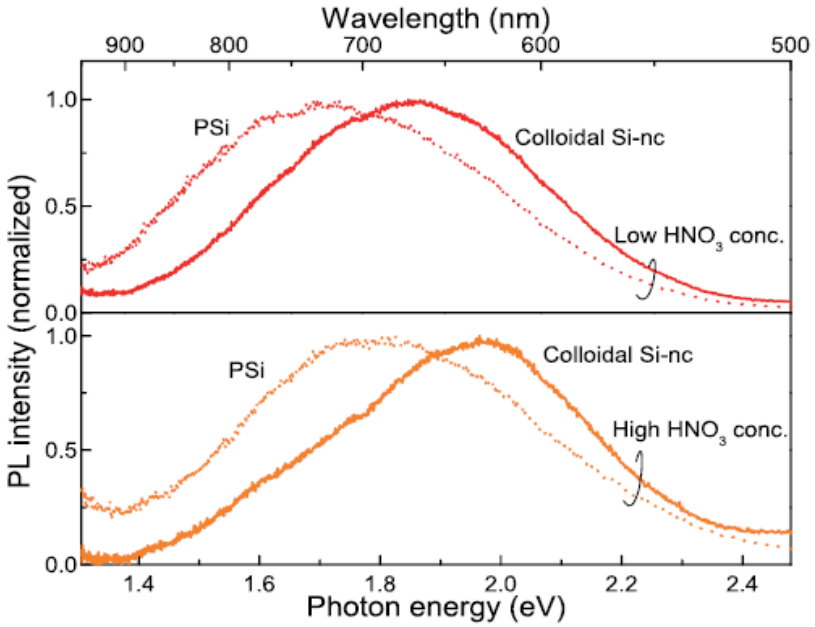

Figure 2.2. PL spectra of PSi (dashed curves) and colloidal Si-nc (solid curves) prepared at different HNO_3 concentrations.

alkyl groups. An absorption peak related to the Si–O–Si bridge bond at 1000–1200 $cm^{-1}$was also observed. This suggests that part of the surface area should be oxidized. However, because the solubility of our colloidal particles in polar solvents such as ethanol and water was very poor, the colloidal Si-nc surface is thought to be considerably covered with Si–C bonds.[11]

Figure 2.2 shows the PL spectra of PSi and colloidal Si-nc samples at low (3 vol.%) and high (5 vol.%) HNO_3 concentrations. The peak energy of PSi was clearly higher at 5 vol.% (~1.8 eV) than at 3 vol.% (~1.7 eV). Furthermore, as shown in Table I, the PSi sample at 5 vol. % had a higher PL efficiency. These features were due to the higher porosity of the PSi sample stain-etched at 5 vol.%. Because the porous layer in the PSi samples consists of the interconnected wire-like crystalline nanostructure network,[12] the higher porosity/ larger pore size indicates the presence of smaller sized/narrower wire dimensions. As a result, the bandgap energy and radiative recombination rate are higher because of the strong

	PSi		Colloidal Si-nc	
Sample HNO_3 conc. (vol. %)	3	5	3	5
Peak energy (eV)	1.70	1.78	1.93	1.97
Spectral width (meV)	570	590	510	550
Quantum efficiency (%)	1	3	23	20
Diameter (nm)	2.71	2.52	2.74	2.65

Table I. Properties of PSi and colloidal Si-nc.

quantum confinement effects,[13] in the 5 vol.% stain-etched PSi sample. Delerue *et al.*[14] calculated the bandgap energy for PSi as a function of the width (diameter) of cylindrical Si wire. From these calculated results and our measured PL peak energies, the diameters of the wire nanostructures for the PSi samples stain-etched at 3 and 5 vol.% are estimated to be 2.71 and 2.52 nm, respectively (Table I).

As similar to PSi samples, the PL peak energy was higher for the colloidal Si-nc generated from the PSi stain etched at 5 vol.% than at 3 vol. %. This indicates that the diameter of spherical nanocrystalline particles decreases as the HNO_3 concentration

increases. In the literature,[14] the bandgap energy versus diameter has also been calculated for spherical nanocrystalline Si. By comparing these calculated results with our observed PL peak energies, we can estimate the diameter of colloidal Si-nc to be 2.74 and 2.65 nm for samples with stain-etching at 3 and 5 vol. %, respectively. These diameter values agree quite well with those of the PSi samples, which suggest that laser irradiation of PSi with a particular size distribution causes the formation of colloidal Si-nc with an analogous size distribution. In fact, the PL spectral width of each colloidal Si-nc sample, which reflects the homogeneity of nanocrystalline size, was similar to that of the relevant PSi sample (Table I).

A possible mechanism for the formation of the present colloidal Si-nc is the ablation of the porous layer by laser irradiation, similar to that for blue-emitting colloidal Si-nc:[15] The irradiated light is efficiently absorbed by the PSi layer. Due to the local heating effects, the Si is then ejected in atomic and/or cluster form. The ejected Si species condense at the interface with the liquid to form nanoparticles. For this laser ablation mechanism, the nanoparticle size distribution is expected to be broad and can be determined as a kind of ablated material and liquid.[16] In other words, the size and shape of the ablated material do not affect the nanoparticle size distribution. In the present case, the size distribution of colloidal Si-nc surely reflects the size of the starting PSi material. Because of this, such a laser ablation mechanism should be excluded here. Another possible mechanism for the formation of the colloidal Si-nc is the pulsed laser-induced fragmentation of porous layer. The pulsed laser-induced shock waves can cause the fragmentation of interconnected wire nanostructures of PSi.[17] This can produce nanoparticles having nearly the same diameter as the nanowire width. With this mechanism, the nearly identical size distributions/PL peak energy and spectral width of the PSi and colloidal Si-nc can beexplained without a problem.

Another possible mechanism for the formation of the colloidal Si-nc is the pulsed laser-induced fragmentation of porous layer. The pulsed laser-induced shock waves can cause the fragmentation of interconnected wire nanostructures of PSi.[17] This can produce nanoparticles having nearly the same diameter as the nanowire width. With this mechanism, the nearly identical size distributions/PL peak energy and spectral width of the PSi and colloidal Si-nc can be explained without a problem.

A surface passivation process is necessary to obtain efficient luminous materials including Si-nc.[5] In the laser ablation process used to synthesize blue-emitting Si-nc in an organic solvent (1-octene),[9] the dangling bonds on the Si-nc surface are passivated with

organic species via a chemical reaction with unsaturated hydrocarbon chains in the solvent. On the other hand, the possible surface passivation considered here is photochemical hydrosilylation assisted by UV light. The surface of hydrogen-terminated Si is known to react with unsaturated organic compounds such as 1-octene under UV (<350 nm) light illumination at room temperature.[18] As a result of this reaction, a homolytic cleavage of Si–H bonds occurs. Subsequently, a hydrocarbon monolayer is formed and bonds to the Si surface (hydrosilylation). In the present case, only the UV laser irradiation at 266 nm generated luminescent nanoparticles. Thus, photochemical hydrosilylation occurred simultaneous to the fragmentation of PSi. This type of hybrid effect has never been reported.

In Table I, the PL quantum efficiencies of colloidal Si-nc (20%–23%) were much higher than those of PSi (1%–3%). A possible reason for this is the enhancement of the radiative recombination rate due to the change in the surface bonding species from hydrogen to carbon, as reported in the literature.[11,19,20] Another reason may be the suppression of nonradiative recombination channels caused by the decreased surface defects and dangling bonds. This is supported by the fact that the dissociation energy of Si–C bond (3.83 eV) is higher than that of Si–H bond (3.32 eV); thus, the former case promises a highly stable surface.5 In fact, the present colloidal Si-nc sample exhibits relatively high durability, confirmed by no large change in the PL quantum efficiency (~23%) measured before and after aging several months.

Figure 2.3(a) shows the PL decay curves of PSi and colloidal Si-nc samples (5 vol%) measured at the microsecond scale. Because the colloidal Si-nc sample has a nanosecond decay component, we also measured the decay curve of this sample at the nanosecond scale and plotted these data. The inset of Fig. 2.3(a) shows the PL decay curves of the colloidal Si-nc on a log –log scale. Integrating the decay curve data in Fig. 2.3(a), we obtained the PL intensities for the slow (I_{slow}) and fast (I_{fast}) decay components of the colloidal Si-nc sample. The intensity ratio between the fast and slow decay components (I_{slow} / I_{fast}) was ~16. Thus, the PL intensity of the colloidal Si-nc was mainly due to the slow decay component. It should be noted that the organically capped Si-nc samples usually exhibit PL decay time at the "nanosecond" scale.[11] The reason for our slower decay component at the microsecond scale may come from shorter organic passivation time (~3 h) compared with about 3 months.[11]Mastronardi *et al.*[21] also observed PL decay times in the microsecond scale for samples organic-passivated for 14 h.

Figure 2.3(b) shows the recombination rates estimated from the fitting of the PL decay

curves in Fig. 2.3(a). The recombination rate of the fast decay component for the colloidal Si-nc was almost independent of the emission energy, while the rate of the slow component increased with the emission energy. The recombination rate of the PSi decreased with the emission energy, similar to the colloidal Si-nc, but over a limited energy range (>1.8 eV). At the lower energy side (<1.8 eV), an increase in the decay rate was observed. This was probably due to the increased non-radiative recombination rates.[22] The recombination rate of PSi was also high compared with that of the slow-component colloidal Si value.

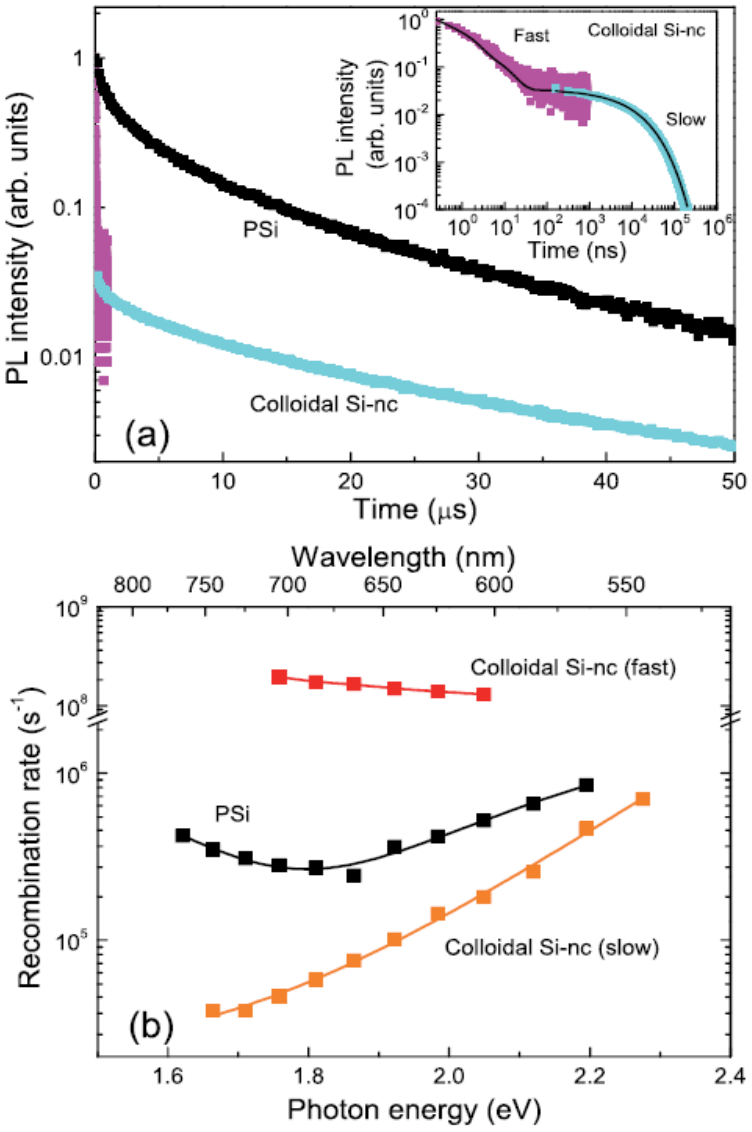

Figure 2.3. (a) PL decay curve of PSi measured in the microsecond region and those of colloidal Si-nc in the nanosecond and microsecond regions at 1.9 eV. The inset shows the decay curves of colloidal Si-nc up to millisecond range. (b) Recombination rates as a function of the emission energy for PSi and colloidal Si-nc.

The recombination rate of band-to-band transitions in quantum confined Si-nc is on the order of 104–106 s^{-1}, but in a particular case of organic passivated Si-nc, much larger values of up to ~109 s^{-1} were reported.[20] Note that the rate increases with decreasing nanocrystalline size due to the quantum confinement effect. On the other hand, the radiative recombination rate at defect and/or surface states is larger (~109 s^{-1}) than that of the band-to-band transition and is independent of the emission energy.[23] Thus, the fast decay component in the colloidal Si-nc is connected with such defect and/or surface states, while the slow decay component is considered to originate from the band-to-band transition.

The radiative w_r and non-radiative recombination rates (w_{nr}) can be estimated from the measured decay rate w by using the relations $\eta = w_r/(w_r + w_{nr})$ and $w = w_r + w_{nr}$, where η is the PL quantum efficiency. The estimated recombination radiative rates w_r at 1.92 eV were 2 x 10^5 and 3 x 10^4 s^{-1} for colloidal Si-nc and PSi, respectively, which indicates that its value was enhanced when the surface termination chemical species was changed from hydrogen (PSi) to carbon (colloidal Si-nc). In fact, the theoretical calculation by Poddubny and Dohnalov`a[24] showed an increase in the radiative rate from ~10^4 s^{-1} to ~10^5 s^{-1} when the chemical species was changed from atomic hydrogen to carbon on the Si-nc surface. Note that the estimated non-radiative recombination rate w_{nr} of colloidal Si-nc (8 x 10^5 s^{-1}) was smaller than that of PSi (3 x 10^6 s^{-1}). This supports our conjecture that the non-radiative recombination center is passivated by the strongly bonded organic species with Si atoms (Si–CH_n).

Figure2.4 shows the PL and PLE spectra of PSi and colloidal Si-nc at 5 vol.%. The PLE intensity of the PSi sample continuously increased with the photon energy and showed no clear peak. This PLE spectral feature indicates that the hydrogen-terminated PSi has a bulk-like indirect bandgap electronic structure.[25] However, interestingly, the PLE spectrum of colloidal Si exhibited a clear peak at ~4.4 eV. Furthermore, the PLE intensity of the colloidal Si-nc at the absorption edge (~3 eV) is higher than that of PSi. These differences suggest that the electronic band structure in the latter sample is modified by the organic passivation of Si–CH_n. In fact, Poddubny and Dohnalov`a's calculation[24] showed that the electron density of states of the conduction band at the Γ point strongly increases due to the carbon termination of Si-nc. As a result, the direct optical transition rates at the higher lying bandgap states (3.5–4.5 eV) are strongly enhanced. The PLE peak energy observed in this study (~4.4 eV) is in reasonably agreement with their calculation results. Thus, the absorption peak at ~4.4 eV is considered to be due to such an enhanced electronic density of state at the Γ point by the organic Si–CH_n formation.

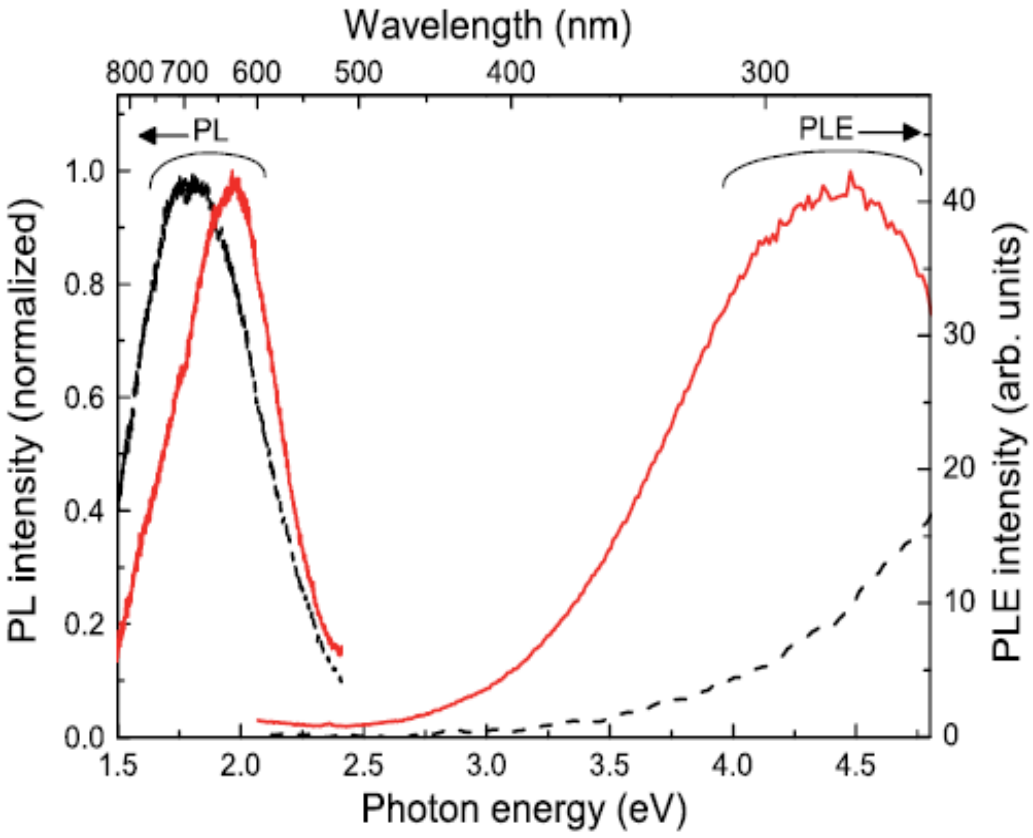

Figure 2.4. PL and PLE spectra of PSi (dashed curves) and colloidal Si-nc (solid curves). The detection energies of the PLE spectra were 1.8 eV (PSi) and 2.0 eV (colloidal Si-nc).

2.4 Conclusion

In conclusion, we reported a simple route to produce bright and multicolor luminescent colloidal Si-nc. The colloidal Si-nc was produced by pulsed UV laser irradiation of PSi in an organic solvent (1-octene). The emission color of the colloidal Si-nc's reflected that of PSi, which indicates that colloidal Si-nc has a size distribution analogous to that of the starting PSi. Furthermore, the PL quantum efficiencies of the colloidal Si-nc were much larger than those of Psi samples. This enhancement in the PL quantum efficiencies was attributed to an organic passivation. The formation of the colloidal Si-nc was caused by the fragmentation of the PSi nanostructures. The organic passivation simultaneously occurred via UV light-induced hydrosilylation. The present simple preparation method and

emission-color tenability will allow us to develop a top-down and low-cost mass production process for luminescent colloidal Si-nc's over a wide spectral range in the future.

2.5 Reference

(1) Hybertsen, M, S.; Absorption and emission of light in nanoscale silicon structures. *Phys. Rev. Lett.* **1994**, 72, 1514.

(2) Cheng, X.; Lowe, S. B.; Reecec, P. J.; Gooding, J. J. Colloidal silicon quantum dots: from preparation to the modification of self-assembled monolayers (SAMs) for bio-applications. *Chem. Soc. Rev.* **2014**, 43, 2680.

(3) Heath, J. R. A liquid-solution-phase synthesis of crystalline silicon. *Science.* **1992**, 258, 1131.

(4) Henderson, E. J.; Kelly, J. A.; Veinot, J. G. C. Influence of $HSiO_{1.5}$ Sol−Gel Polymer Structure and Composition on the Size and Luminescent Properties of Silicon Nanocrystals. *Chem. Matter.* **2009**, 21, 5426.

(5) Dohnalova´, K.; Gregorkiewicz, T.; K°usova´, K. Silicon quantum dots: surface matters. *J. Phys.: Condens. Matter* **2014**, 26, 173201.

(6) ˇSvrcˇek, V.; Sasaki, T.; Shimizu, Y.; Koshizaki, N. Blue luminescent silicon nanocrystals prepared by ns pulsed laser ablation in water. *Appl. Phys. Lett.* **2006**, 89, 213113.

(7) Umezu, I.; Senoo, H. Synthesis of photoluminescent colloidal silicon nanoparticles by pulsed laser ablation in liquids. *J. Phys.: Conf. Ser.* **2007**, 59, 392.

(8) Shirahata, N.; Hirakawa, D.; Sakka, Y. Interfacial-related color tuning of colloidal Si nanocrystals. *Green Chem.* **2010**, 12, 2139.

(9) Shirahata, N.; Hirakawa, D.; Masuda, Y.; Sakka, Y. Size-dependent color tuning of efficiently luminescent germanium nanoparticles. *Langmuir* **2013**, 29, 7401.

(10) Limaye, S.; Subramanian, S.; Goller, B.; Diener, J.; Kovalev, D. Scaleable synthesis route for silicon nanocrystal assemblies. *Phys. Status Solidi A.* **2007**, 204, 1297.

(11) K°usova´, K.; Cibulka, O.; Dohnalova´, K.; Pelant, I.; Valenta, J.; Fucˇkova´, A.; ˇZidek, K.; Lang, J.; Englich, J.; Matˇejka, P.; ˇStˇepa´nek, P.; Bakardjieva, S. Brightly Luminescent Organically Capped Silicon Nanocrystals Fabricated at Room Temperature and Atmospheric Pressure. *ACS Nano.* **2010**, 4, 4495.

(12) Cullis, A. G.; Canham, L. T.; Calcott, D. J. The structural and luminescence properties of porous silicon. *J. Appl. Phys.* **1997**, 82, 909.

(13) Kovalev, D.; Heckler, H.; Polisski, G.; Koch, F. Optical Properties of Si Nanocrystals. *Phys. Status Solidi B.* **1999**, 215, 871.

(14) Delerue, C.; Allan, G.; Lannoo, M. Theoretical aspects of the luminescence of porous silicon. *Phys. Rev. B.* **1993**, 48, 11024.

(15) Nakamura, T.; Yuan, Z.; Adachi, S. High-yield preparation of blue-emitting colloidal Si nanocrystals by selective laser ablation of porous silicon in liquid. *Nanotechnology.* **2014**, 25, 275602.

(16) Werner, D.; Hashimoto, S. Controlling the Pulsed-Laser-Induced Size Reduction of Au and Ag Nanoparticles via Changes in the External Pressure, Laser Intensity, and Excitation Wavelength. *Langmuir.* **2013**, 29, 1295.

(17) Lau, M.; Barcikowski, S. Quantification of mass-specific laser energy input converted into particle properties during picosecond pulsed laser fragmentation of zinc oxide and boron carbide in liquids. *Appl. Surf. Sci.* **2015,** 348, 22.

(18) Buriak, J. M. Organometallic Chemistry on Silicon and Germanium Surfaces. *Chem. Rev.* **2002**, 102, 1271.

(19) K°usova´, K.; Hapala, P.; Valenta, J.; Jelı´nek, P.; Cibulka, O.; Ondicˇ, L.; Pelant, I. Silicon Nanocrystals: Direct Bandgap Silicon: Tensile-Strained Silicon Nanocrystals. *Adv. Mater. Interfaces* **2014**, 1, 1300042.

(20) Dohnalova´, K.; Poddubny, A. N.; Prokofiev, A. A.; Boer, W. D. de; Umesh, C. P.; Paulusse, J. M.; Zuilhof, H.; Gregorkiewicz, T. Surface brightens up Si quantum dots: direct bandgap-like size-tunable emission. *Light: Sci. Appl.* **2013**, 2, e47.

(21) Mastronardi, M. L.; Maier, F. F.; Faulkner, D.; Henderson, E. J.; K¨ubel, C.; Lemmer, U.; Ozin, G. A. Size-Dependent Absolute Quantum Yields for Size-Separated Colloidally-Stable Silicon Nanocrystals. *Nano Lett.* **2012**, 12, 337.

(22) Nakamura, T.; Ogawa, T.; Hosoya, N.; Adachi, S. Effects of thermal oxidation on the photoluminescence properties of porous silicon. *J. Lumin.* **2010**, 130, 682.

(23) Wen, X.; Zhang, P.; Smith, T. A.; Anthony, R. J.; Kortshagen, U. R.; Yu, P.; Feng, Y.; Shrestha, S.; Coniber, G.; Huang, S. Tunability Limit of Photoluminescence in Colloidal Silicon Nanocrystals. *Sci. Rep.* **2015**, 5, 12469.

(24) Poddubny, A. N.; Dohnalova´, K. Direct band gap silicon quantum dots achieved via electronegative capping. *Phys. Rev. B.* **2014**, 90, 245439.

(25) Matsui, Y.; Adachi, S. Optical Properties of Porous Silicon Layers Formed by Electroless Photovoltaic Etching. *ECS J. Solid State Sci. Technol.* **2012**, 1, R80.

2.6 Supporting Information

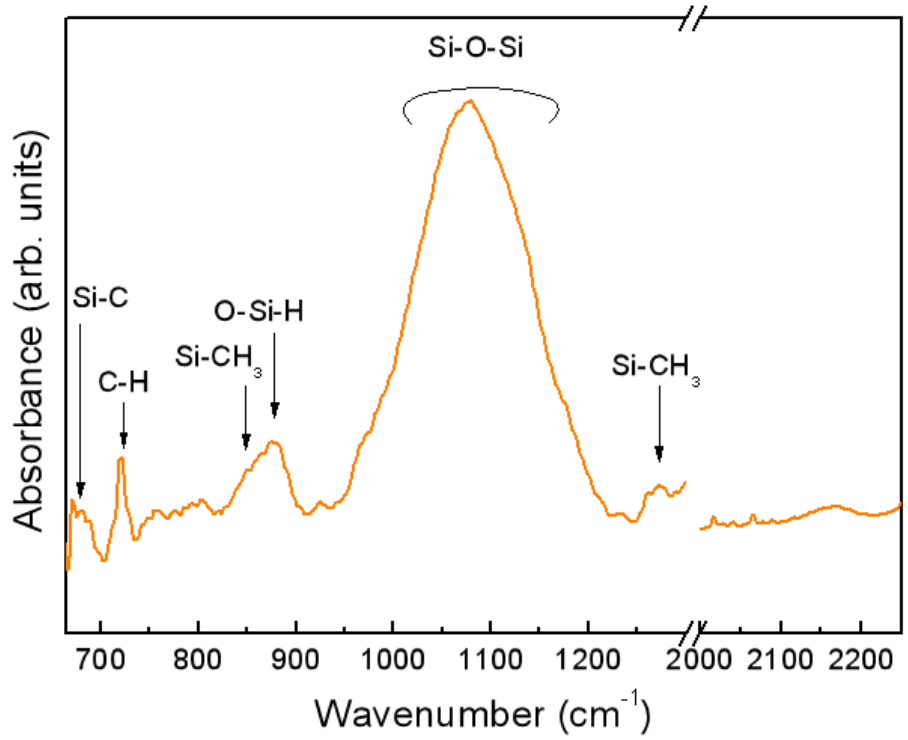

Figure S1 FTIR spectra of the colloidal Si-nc samples prepared in the 1-decene solution.

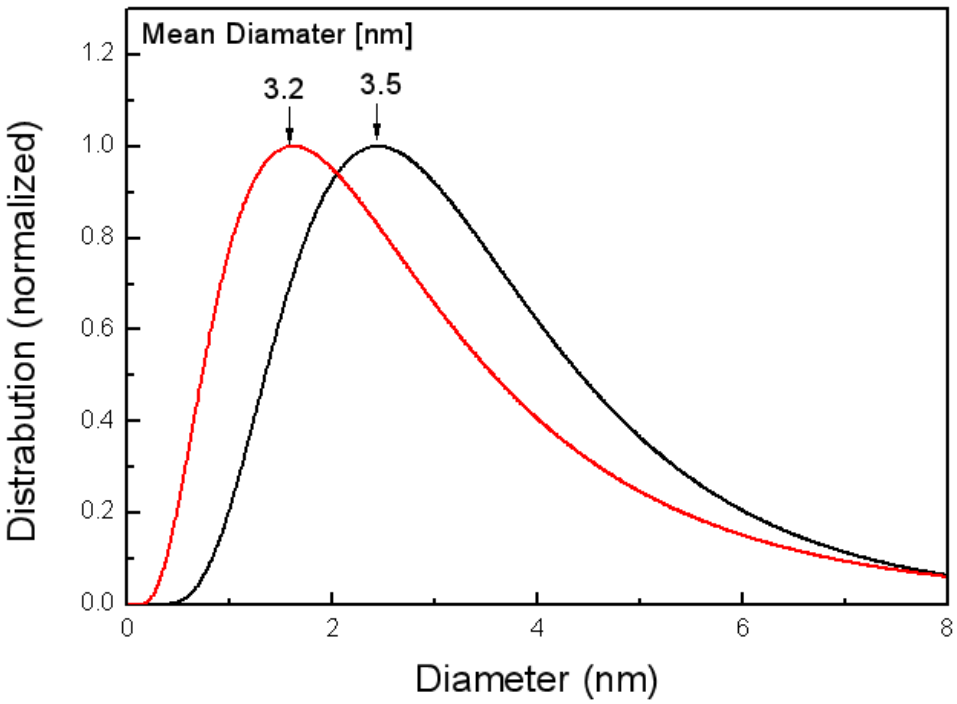

Figure S2 Small Angle X-ray Scattering (SAXS) spectra of the colloidal Si-nc samples prepared at high (5 vol.%) (Red curves) and low HNO_3 (3 vol.%) (Black curves) concentrations, respectively.

Chapter 3

Luminescence color control and quantum-efficiency enhancement of colloidal Si nanocrystals by pulsed laser irradiation in liquid

3.1 Introduction

Si nanocrystals (Si-ncs) are ~1–10 nm in size and exhibit size-tunable luminescence at room temperature owing to quantum-confinement effects.[1] The luminescence properties of Si-ncs are sensitive to the surface termination.[2–4] This is because of the substantially increased surface-to-volume ratio in a decreased crystallite-size sample, which strongly influences the degree of interaction between the photo excited carries and surface states. Moreover, in the case of colloidal Si-ncs, dispersibility in a solvent is usually determined by the terminated chemical species.

Various kinds of surface termination, such as hydrogen[5] and carbon (organic molecule) termination,[6–10] have been performed on colloidal Si-nc surfaces. In principle, various organic molecules (mainly the derivatives of alkenes chains) can be grafted to the surface of Si-ncs. The carbon termination was reported to be less reactive than the termination of other chemical species (e.g., hydrogen, oxygen, and fluorine[11]). The organic-capped Si-ncs also showed good resistance to surface oxidation[5]. Moreover, the surface capping with longer organic ligands prevented the aggregation of nanocrystals and improved their long-term stability.[12, 13] The carbon termination also changed the material properties of the Si-ncs (e.g., direct-bandgap transitions were observed because of the enhanced photoluminescence (PL) efficiency[13–15]).

Halogen termination can be used for the improvement of the luminescence properties of compound semiconductors (e.g., CdS) nanocrystals by passivating undesirable surface states.16 Moreover, halogen termination provides several benefits. For example, different halogen (Cl) termination allows the Si nanocrystal shapes to be changed, and the higher

reactivity of the halogen-terminated surface facilitates the subsequent functionalization of these nanocrystals with other organic groups.[5] However, there have been few reports on halogen-terminated colloidal Si-ncs.

Plasma[17–19] and chemical solution-based syntheses19–20 are popular bottom-up preparation methods for colloidal Si-ncs. These techniques provide better control of the size and shape,[5, 16] high-yields[5], and easy surface modification.[11, 12] On the other hand, chemical etching is a typical top-down preparation method for colloidal Si-ncs.[21] With this technique, subsequent surface-modification treatment is needed to remove the terminated hydrogen atoms. This is because the surface of Si-ncs prepared by this method is usually terminated by hydrogen atoms. Pulsed laser irradiation of the sample surfaces under liquid is a simple top-down preparation method for colloidal Si-ncs.[22–24] Here, the surface termination of Si-nc can be changed by using various kinds of liquids (solvents). Blue-emitting colloidal Si-ncs were synthesized via the laser ablation of bulk Si in water.[22] Additionally, alkyl-passivated colloidal Si-ncs were prepared using an organic solution and shown to emit blue light with a relatively high PL quantum efficiency (~10%).[24] Furthermore, it has been demonstrated that the femtosecond laser ablation method in solution can efficiently produce colloidal Si-ncs.[25, 26] However, with conventional laser-irradiation methods, it is difficult to control the size distribution of synthesized Si-ncs and obtain samples with a high quantum efficiency.

In this study, we prepare chlorine-passivated colloidal Si-ncs (Cl:Si-ncs) via the laser ablation of porous silicon (PSi) in an organochloride solution. A reversible transformation from Cl:Si-ncs to carbon-terminated Si-ncs (C:Si-ncs) having a higher PL quantum efficiency and different size distribution (changing the emission color) is achieved by irradiating the colloidal Si-nc solution with a laser. The optical properties of the prepared Cl:Si-nc and C:Si-nc samples are investigated in detail by absorption, PL, PL excitation (PLE), and time-resolved PL measurements.

3.2 Experimental section

3.2.1 Preparation of PSi powder

The colloidal Si-nc samples were prepared by pulsed laser ablation in liquid. The PSi samples were used as a target for the laser ablation because they had a large surface area

and high chemical and physical reactivities.[27, 28] Thus, a high preparation yield of colloids was expected[21]. The PSi samples were prepared via the stain-etching of Si powder:[29] First, commercially available metallurgical-grade polycrystalline Si powder (Vesta Ceramics) was immersed in an etching mixture containing HNO_3 (60 wt%) and HF (46 wt%) solutions. Its composition was HF:H_2O:HNO_3 = 4:1:20 by volume. Etching was performed for 30 min. Then, the synthesized PSi powder was collected by filtering the etching solution and dried in ambient conditions for 24 h.

3.2.2 Preparation of colloidal Si-nc

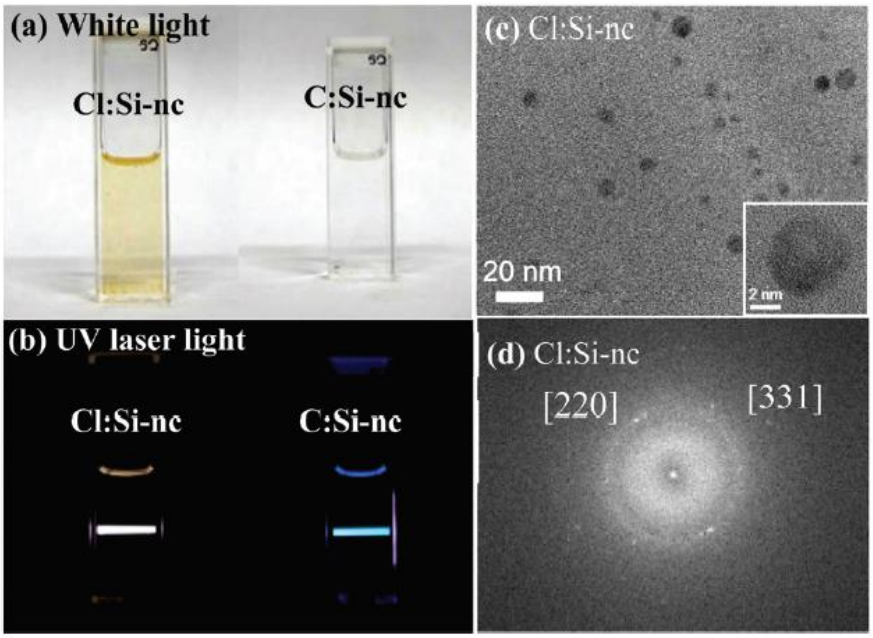

Figure 3.1. Photographs of colloidal Cl:Si-ncs prepared from PSi in trichloroethylene and C:Si-ncs prepared from Cl:Si-ncs in 1-octene. The samples were dispersed in trichloroethylene (Cl:Si-ncs) and 1-octene (C:Si-ncs) and observed under (a) white- and (b) UV-light illuminations. (c) TEM image of Cl:Si-ncs. The inset shows a high-resolution TEM image of a Cl:Si-nc. (d) FFT pattern of the TEM image for the Cl:Si-nc shown in the inset

To prepare colloidal samples, 100 mg of PSi powder was dispersed in 3 mL of an organic solvent. We used trichloroethylene as the solvent to obtain Cl:Si-ncs. Then, the sample was irradiated by pulsed laser light (wavelength of 532 nm, pulse duration of 5 ns, and repetition rate of 15 Hz) from the second harmonic of a Q-switched Nd:YAG laser

(Continuum) for 6 h. During the laser irradiation, the PSi-contained trichloroethylene solution was constantly stirred by a magnetic stirrer. The laser pulse fluence was ~0.4 J/cm^2. After the laser irradiation, the liquid supernatant was separated by centrifugation at 13,000 rpm for 20 min using a membrane filter having a pore size of ~200 nm. This process yielded a yellowish colloidal (Cl:Si-nc) solution, as shown in the left part of figure 3.1(a). Under ultraviolet (UV) laser light (325 nm) illumination, the solution exhibited white emission (the left part of figure 3.1(b))

Pulsed laser irradiation was also performed on an obtained colloidal sample dispersed in a different organic solution. Initially, the colloidal solution (trichloroethylene) with a volume of 5 mL was completely dried in air for a week at room temperature, and then 5 mL of 1-octene of was added to replace the solvent. Next, the colloidal sample solution (1-octene) was irradiated by a 266-nm pulsed laser light from a Q-switched Nd: YAG laser (pulse duration of 5 ns, repetition rate of 15 Hz, fourth harmonic) at ~0.2 J/cm^2 for 6 h. After the UV irradiation, the emission color of the colloidal solution had changed from white to blue, as shown in figure 3.1(b). We also determined whether undesirable byproducts such as carbon nanoparticles were generated by the pulsed laser irradiation at 532 or 266 nm in the solvent (trichloroethylene or 1-octene) without target material(s). Carbon-related byproducts can exhibit PL emission in a blue region. However, we observed no PL emission from the irradiated solvent alone, indicating that carbon-related byproducts were not the origin of the blue emission.

3.2.3 Analytical technique

The structural properties of the prepared colloidal samples were analyzed using a transmission electron microscope (TEM-300F, JEOL). The surface chemistry of the samples was investigated using a Fourier-transform infrared (FTIR) spectrometer (iS50, Nicolet). PL measurements were performed using a single monochromator equipped with a charge-coupled device (Princeton Instruments, PIXIS 100). The fourth harmonic (266 nm) of a Nd:YAG laser (Continuum) with a pulse duration of 5 ns at a repetition rate of 15 Hz was used as an excitation light source. PLE measurements were performed using a fluorescence spectrometer (Hitachi, F-4500). Time-resolved PL measurements were performed using a frequency-tripled 355-nm light pulse (pulse width of 300 ps) from a Nd:YAG laser (third harmonic, STV-01E, TEEM Photonics) as an excitation source. The PL data were recorded using a time-correlated single-photon counting module (SPC-130EM,

Becker & Hickl) and a single-photon avalanche photodiode (SPD-050, Micro Photon Devices). The PL relative quantum efficiency was measured using a He-Cd laser (325 nm, Kinmon) or a diode laser (405 nm, Toptica Photonics) as an excitation source, a single monochromator equipped with a charge-coupled device (Princeton Instruments) as a detector, and $K_2SiF_6:Mn^{4+}$ or courmarin 314 excited at 325 and 405 nm, respectively, as standards for the PL quantum efficiency.[30,31] Optical measurements were performed on the samples in a quartz cuvette at room temperature.

3.3 Results and discussion

Figure 3.1(c) shows an transmission electron microscopy (TEM) image of the as-prepared sample, which exhibits white-light emission (left part of figure 1(b)). Well-monodispersed particles several nanometers in size are clearly observed. The inset shows a high-resolution TEM (HRTEM) image of a spherical nanoparticle with a diameter of ~7 nm. The corresponding fast Fourier transform (FFT) diffraction pattern of the HRTEM image is shown in figure 1(d) and indicates lattice spacings of 1.9 and 1.2 Å for the Si (220) and (311) planes, respectively. Thus, the colloidal particles prepared by the pulsed laser irradiation of PSi had a nanocrystalline morphology. We also confirmed that the colloidal particles prepared by the post-laser irradiation emitted blue light (right side of figure 1(b)) and were single-crystalline, with a size distribution clearly different from that of particles prepared without post-laser irradiation (see figure 3(c) below).

Figure 3.2 shows the FTIR spectra of (a) an as-prepared white-emitting colloidal sample and (b) a post-laser irradiated blue-emitting colloidal sample. The absorption peaks at 527 and 586 cm^{-1} for the as-prepared sample correspond to the vibration modes of the Si–Cl bond.[32] The present observations suggest that the as-prepared sample was comprised of Cl:Si-ncs. However, other absorption peaks arising from the carbon-related modes, such as the Si–C and Si-CH3 modes, are also observed. On the other hand, the C:Si-nc sample prepared with post-laser irradiation (figure 3.2(b)) exhibited FTIR peaks originating from the bonds between Si and carbon-related species at 1,470 cm^{-1} ($Si–CH_3$) and 795 cm^{-1} (Si–C).[15] This indicates that the post-laser-irradiated colloidal sample (C:Si-nc) was passivated by alkyl groups. In addition, the (Si–O–Si)-related absorption peaks observed at 1,000–1,200 cm^{-1} (Ref. 15) in both samples suggest that the surfaces of the samples were partly oxidized by the laser-irradiation processes in the organic solvents. The Cl:Si-nc sample had

an inhomogeneous surface-passivation layer because of the numerous surface defects and different termination species, such as chlorine, carbon, and oxygen.

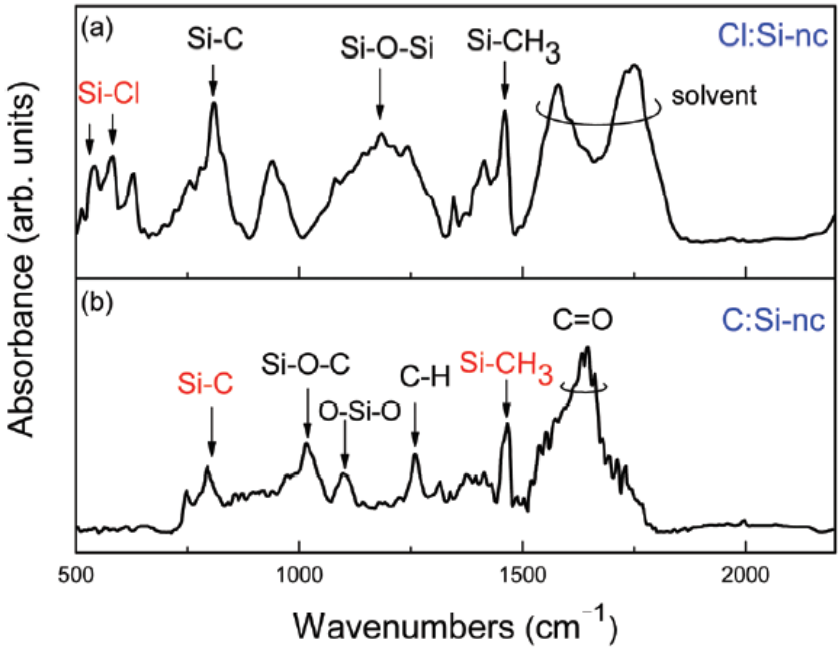

Figure 3.2. FTIR spectra of the colloidal (a) Cl:Si-ncs prepared from PSi in trichloroethylene and (b) C:Si-ncs prepared from Cl:Si-ncs in 1-octene. The FTIR frequencies are obtained from the literature.[15,28]

Figure 3.3(a) shows the PL spectra of the as-prepared (Cl:Si-nc) and post-laser-irradiated (C:Si-nc) samples. The PL peak energies of the C:Si-nc and Cl:Si-nc samples are ~3.3 and ~2.5 eV, respectively. Furthermore, the PL emission for the Cl:Si-nc sample covers the entire visible region (350-700 nm), while the PL spectrum for C:Si-nc is limited to the blue-UV region (300-500 nm). These differences in the PL spectral features correspond to the different emission colors, i.e., white and blue, as shown in figure 3.1(b). The emission intensity for the Cl:Si-nc sample is weaker than that for the C:Si-nc sample. The C:Si-nc sample was irradiated again by intense pulsed UV laser light of ~0.2 J/cm^2 at 266 nm in trichloroethylene for 6 h. Interestingly, its PL spectrum almost returned from blue to white (red dashed curve in figure 3(a). The PL quantum efficiencies of the Cl:Si-nc and C:Si-nc samples were~7% and~13% excited at 405 and 355 nm, respectively. The PL quantum efficiency of the twice post-laser-irradiated sample (red dashed curve in figure 3(a)) was almost the same (~6%) as that of the as-prepared (Cl:Si-nc) sample. FTIR measurements confirm that the sample that was post-laser irradiated twice had a chlorine-passivated surface, matching the original colloidal sample surface (i.e., Cl:Si-nc).

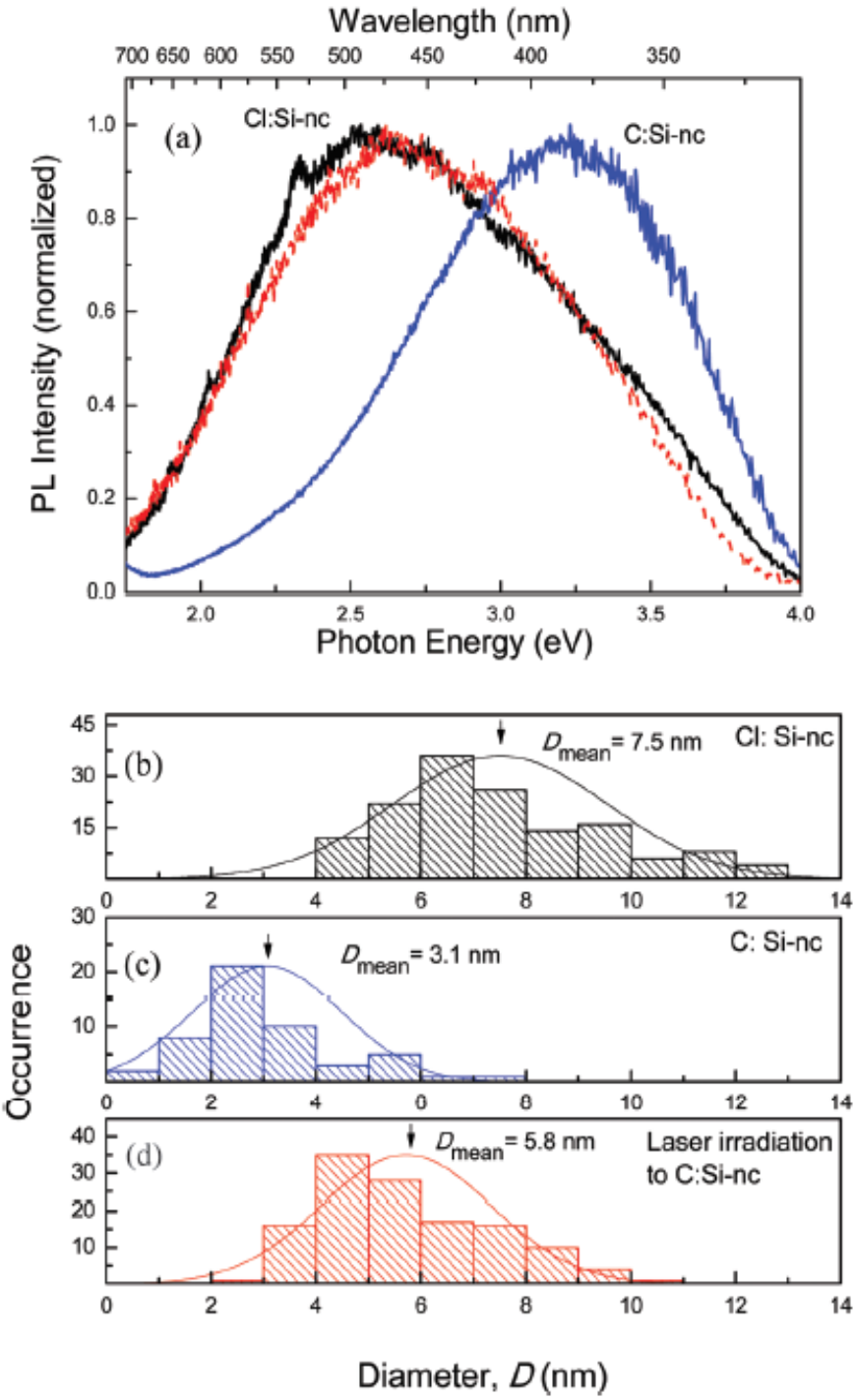

Figure 3.3. PL spectra of colloidal Cl:Si-nc and C:Si-nc solutions (see figure 1(a)). Size-distribution histograms of the colloidal (b) Cl:Si-ncs, (c) C:Si-ncs, and (d) Cl:Si-ncs formed by laser-ablating C:Si-nc samples in trichloroethylene. The red dashed curve in (a) represents the PL spectrum of the Cl:Si-nc sample of (d).

One possible reason for the change in the PL peak energy from 2.5 to 3.3 eV and vice versa observed after the second laser irradiation is the decrease or increase of the colloidal Si-nc sizes due to the first or second post-processing, respectively. This is because the PL peak energy of Si-nc depends on its diameter owing to the quantum-confinement effect.[22, 33] To confirm this, we examined the size distribution of the different colloidal Si-nc samples according to the TEM images. The results are shown in figures 3.3(b)–3.3(d). Here, we observe that the size distribution clearly changed before and after the first or second post-laser irradiation. These statistical data provide the results of $D_{mean} \approx 7.5$ nm (Cl:Si-ncs; figure 3.3(b)), 3.1 nm (C:Si-ncs; figure 3.3(c)), and 5.8 nm (second post-laser-irradiated Cl:Si-ncs; figure 3.3(d)). Surprisingly, the second post-laser-irradiated Cl:Si-nc sample had a D_{mean} of 5.8 nm, which is clearly larger than that of the first post-laser-irradiated C:Si-nc sample (3.1 nm). Thus, there is a clear correlation between the experimental PL peak energies and the colloidal Si-nc sizes observed in figure 3.3: lager colloidal Si-ncs yield a lower PL peak energy, which agrees with the quantum-confinement theory.

An interesting feature in figure 3.3 is that the size distribution strongly depends on the post-laser irradiation processing in different solvents—1-octene (figure 3.3(c)) and trichloroethylene (figure 3.3(d))—despite the same irradiation laser wavelength and power of 266 nm and ~0.2 J/cm^2, respectively. The present result indicates that the Si-nc size distribution is mainly determined by the organic solvent used (1-octene or trichloroethylene). In the literature,[34] the size of Ge nanoparticles prepared by laser ablation in n-octane was larger than that for 1-octene. This result was explained by the fact that n-octane has a lower reactivity with the Ge nanoparticle surface than 1-octene. Our observed laser-ablated Si-nc size difference between in trichloroethylene and 1-octene can also be explained by the different reactivity of these solvents with Si nanoparticle surfaces. The details are as follows. First, Si particles dispersed in an organic solvent are ablated by the pulsed laser irradiation, and then each ablated Si atom re-condenses to form Si nanoparticles. Simultaneously, the surface should be terminated by a chemical species in the solvent. The resultant encapsulation tends to the inhibit further condensation of Si nanoparticles. In the case of trichloroethylene, which has a lower reactivity than 1-octene, Si surface passivation occurs more slowly (or in the later stage of ablation), resulting in larger nanoparticles, regardless of whether the starting material is PSi (figure 3.3(b) or C:Si-nc (figure 3.3(d)). Thus, the present results indicate that the ablated nanoparticle size can be determined only by the kind of the solvent, i.e., the reactivity of the solvent in the ablation process, as confirmed by the Ge nanoparticle size difference between in 1-octene

and n-octane.34 The average size of the twice post-laser-irradiated sample (~5.8 nm) is smaller than that of the original Cl:Si-ncs (~7.5 nm), as indicated by figures 3.3(b) and 3.3(d). This is probably due to the lower concentration of available Si in trichloroethylene, which suppressed the nanoparticle growth.

The PL quantum efficiency of ~7% excited at 405 nm for the colloidal Cl:Si-nc samples prepared in trichloroethylene (figures 3.3(b) and 3.3(d)) is considerably lower than that for the sample prepared in 1-octene (~13% excited at 325 nm; figure 3.3(c)). Therefore, we expect insufficient (or incomplete) surface passivation by the chlorine termination formed in the trichloroethylene solvent due to its lower reactivity with the Si-nc surface. Many surface defects and, consequently, many surface states should be produced on the chlorine-terminated Si-nc surfaces. As discussed later (figure 3.7), this results in increased non-radiative recombination rates and thus decreased PL quantum efficiencies.

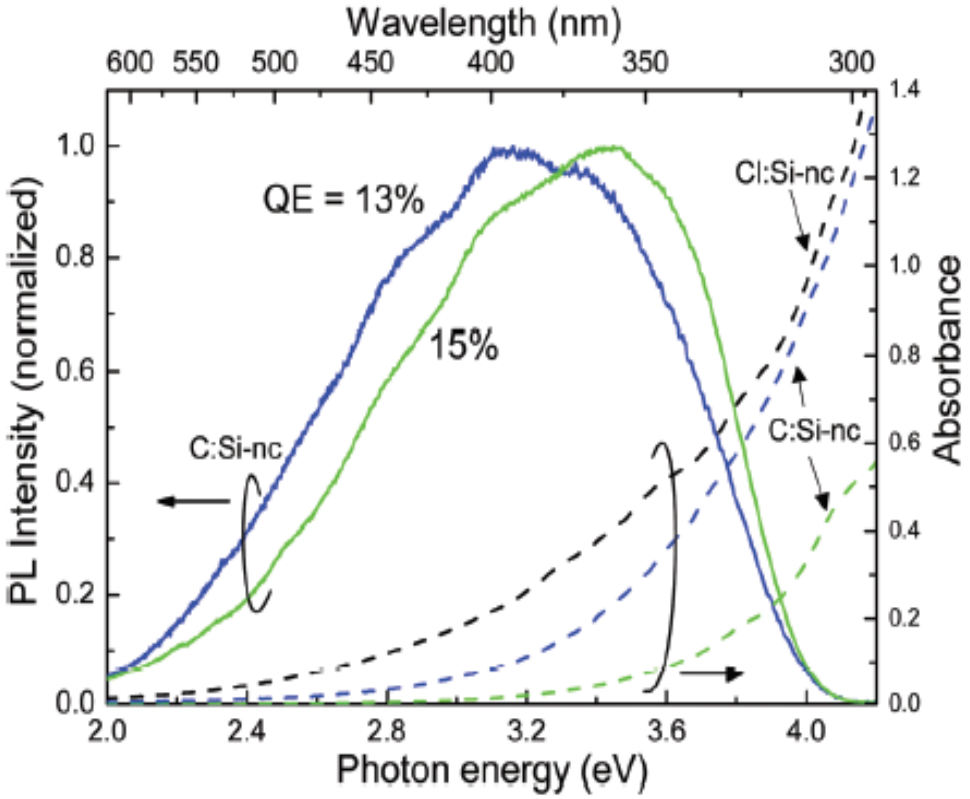

Figure 3.4. PL and absorbance spectra of the post-laser irradiation-prepared C:Si-nc sample in 1-octene (blue curves) and C:Si-ncs directly prepared by the laser ablation of PSi in 1-octene (green curves). The absorbance spectrum of Cl:Si-ncs prepared from PSi in trichloroethylene is also plotted (black dashed curve).

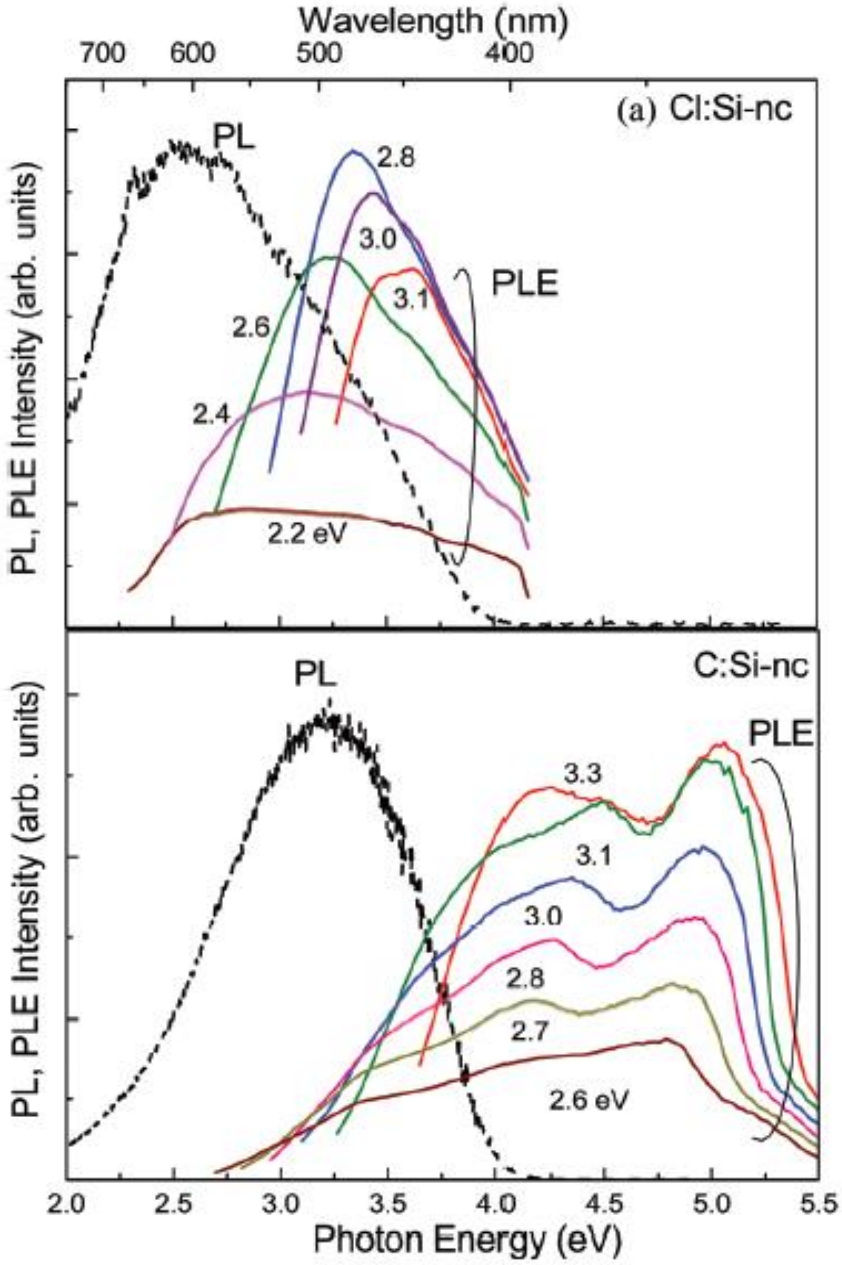

Figure 3.5. PLE spectra of (a) the Cl:Si-nc sample prepared from PSi in trichloroethylene and (b) the C:Si-nc sample prepared from Cl:Si-nc in 1-octene, measured at various emission energies (E_{em}), together with their PL spectra measured by excitation at 266 nm (~4.7 eV).

Figure 3.4 shows the PL and absorbance spectra of the C:Si-nc sample. For comparison, those of the colloidal carbon-passivated Si-nc sample, which was directly prepared by laser ablating PSi in 1-octene (directly-prepared C:Si-ncs),[33] are also shown. The directly

prepared C:Si-ncs and Cl:Si-ncs samples were both prepared with the same amount of starting material (100 mg of PSi). These carbon-terminated samples exhibit the essentially same PL spectra and PL quantum efficiencies (13–15%). However, the absorbance of ~0.6 for the C:Si-ncs at 325 nm is larger than the value of ~0.2 for the directly-prepared C:Si-ncs. The results indicate that the preparation yield of the C:Si-ncs was higher than that of the directly-prepared C:Si-ncs. (The absorbance is proportional to the colloidal nanoparticle light-absorber density.) Furthermore, as shown in the figure, the absorbance of the Cl:Si-ncs is higher than that of the directly-prepared C:Si-ncs, indicating that the preparation

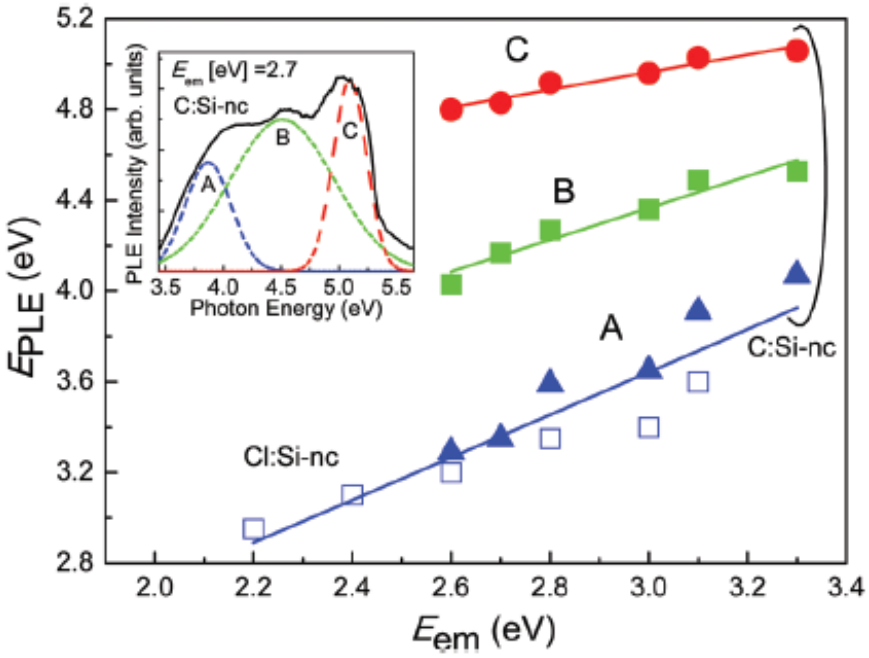

Figure 3.6. PLE peak energies (E_{PLE}) for the Cl:Si-nc sample prepared from PSi in trichloroethylene (open symbols) and the C:Si-nc sample prepared from Cl:Si-nc in 1-octene (solid symbols) with respect to E_{em}. The inset shows the Gaussian-decomposition results for the PLE spectrum at E_{em} = 2.7 eV.

yield of C l:Si-ncs was also higher.

The difference in the preparation yields between the Cl:Si-nc and directly-prepared C:Si-nc samples may reflect the different ablation efficiencies between trichloroethylene and 1-octene. The laser-ablation efficiency is mainly determined by the heat generated by laser irradiation. The degree of heat generation depends not only on the laser fluence but also on the laser wavelength and the target material properties (absorption coefficient,

geometrical shape, etc.).[35] Because the laser-induced heat is dissipated in the surrounding liquid (in this case, resulting in boiling), its thermal conductivity is one of the most important factors determining the target heat dissipation.[35] Trichloroethylene (Cl:Si-ncs) has a lower thermal conductivity (0.090 W/mK at 100°C) than 1-octene (0.1107 W/mK at 100 °C). Thus, the heat-dissipation rate in trichloroethylene should be lower than that in 1-octene, promising a higher laser-ablation efficiency and thus a higher preparation yield (Cl:Si-ncs).

The PLE spectra of the Cl:Si-nc and C:Si-nc samples measured at various emission energies (E_{em}) are shown in figures 3.5(a) and (b), respectively. The PL spectra measured by excitation at 266 nm (4.7 eV) are also shown. The PLE spectra for the Cl:Si-nc shown in figure 3.5(a) clearly depend on E_{em} and shift towards the high-energy side with increasing E_{em} and spectral narrowing. For the C:Si-nc sample of figure 3.5(b), the PLE spectra consist of several excitation bands, and each of their peak positions shifts towards the high-energy side with increasing E_{em}. The PLE peak energies (E_{PLE}) for the Cl:Si-nc and C:Si-nc samples in figure 3.5 are plotted as a function of E_{em} in figure 3.6. Each E_{PLE} value for the C:Si-nc sample was determined via fitting with the three Gaussian components A, B, and C. The inset of figure 3.6 shows an example of the decomposition results for the PLE spectrum measured at E_{em} = 2.7 eV.

As shown in figure 3.6, the A, B, and C peak values for the C:Si-nc sample gradually increase with increasing E_{em}. This result is very similar to that observed in our previous study (directly-prepared C:Si-nc in 1-octene from PSi).[33] Thus, the three PLE bands A, B, and C are attributed to the direct interband transitions at the □□and X points. The increased E_{PLE} with increasing E_{em} can be explained by the increased dipole-transition energies at the higher bandgap energies (i.e., the no direct transitions caused by the effect of the size reduction in Si-ncs).[33] The dependence of E_{PLE} on E_{em} for the Cl:Si-nc sample is very similar to that of the A band in the C:Si-nc sample. Thus, these PLE bands have the same origin. Furthermore, no separated higher excitation bands such as B and C are observed for Cl:Si-nc. The reason for the absence of these bands in the Cl:Si-nc sample is unclear. However, the different passivation states on the sample surfaces between Cl:Si-nc and C:Si-nc may cause the modification of the electron density of states at the higher energy levels, as theoretically predicted.[36] Furthermore, it was recently demonstrated that different surface-termination species on Si-nc, such as chlorine and amine ligands, yield different surface states with various excited energy levels, resulting in the different tunability of PL emission wavelength.[37] Thus, the difference in the PL emission peaks

between the Cl:Si-nc and C:Si-nc samples may be partly caused by the different surface species.

Figure 3.7 shows the PL decay rate of the colloidal Si-nc samples obtained from the PL decay curves measured at E_{em} = 2.0–3.1 (Cl:Si-nc) and 2.2–3.1 eV (C:Si-nc). The inset shows the PL decay curves for the Cl:Si-nc and C:Si-nc samples measured at E_{em} = 3.0 eV. As shown in the inset, the samples exhibit decay characteristics on the nanosecond scale. Furthermore, the decay curves are observed to deviate from the single-exponential shape, implying the existence of various recombination pathways. The decay rate was obtained by fitting the PL decay curve with a convoluted curve of the measured instrument response function (IRF) and the three-exponential model function [$F(t) = a_1\exp(t/\tau_1) + a_2\exp(t/\tau_2) + a_3\exp(t/\tau_3)$] to extract the averaged time constant of the decay curve using a data-analysis software (SPC image, Becker & Hickel GmbH). The solid curves in the inset of figure 3.7 show these fitting results. The decay rate (w) was calculated according to the fit-obtained parameters using the equation $w = 1/\tau_m = (a_1 + a_2 + a_3) / (a_1\tau_1 + a_2\tau_2 + a_3\tau_3)$.

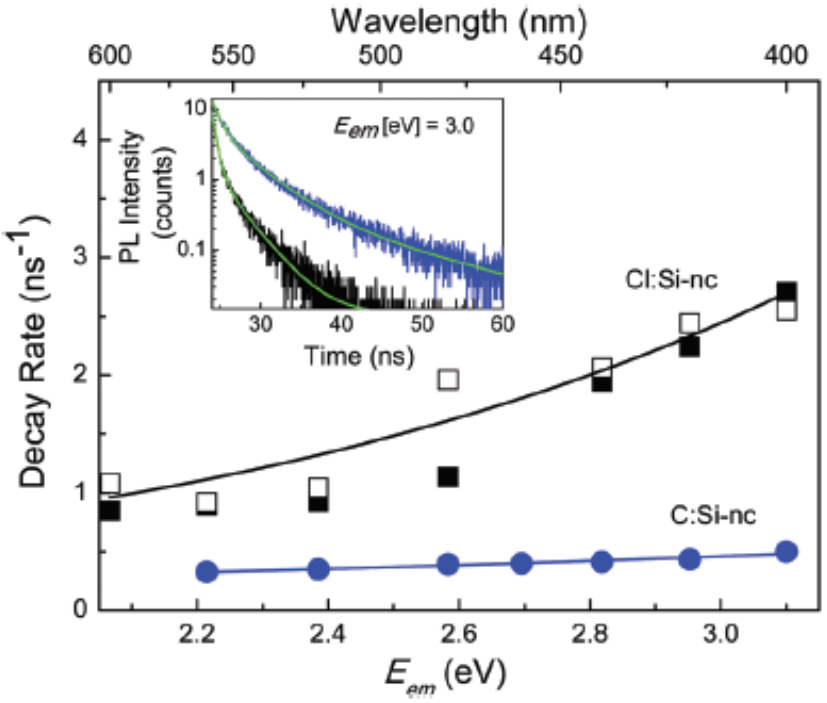

Figure 3.7. PL decay rate with respect to the emission energy E_{em} for the Cl:Si-nc sample prepared from PSi in trichloroethylene (solid squares) and the C:Si-nc sample prepared from Cl:Si-nc in 1-octene (solid circles). The decay rate for the Cl:Si-nc sample with the second laser irradiation is also plotted (open squares). The solid curves are for visual guidance. The inset shows the PL decay curves of the Cl:Si-ncs (black curve) and C:Si-ncs (blue curve) measured at E_{em} = 3.0 eV.

Hydrogen- and oxygen-passivated Si-nc samples usually exhibit microsecond decays owing to their inherent indirect bandgap nature.[38-40] On the other hand, carbon-passivated Si-ncs can exhibit nanosecond decays.[14, 15] The fast decays are attributed to the enhanced radiative-decay rates in C:Si-nc samples. Several mechanisms for the radiative decay-rate enhancement have been suggested (e.g., resonantly enhanced mixing between the electron states in the X valley and the hole states in the Γ valley[36]). For the present Cl:Si-nc and C:Si-nc samples, we expect such an enhancement of the radiative decay rates caused by the different surface modifications.

The PL decay rates (figure 3.7) clearly increase with increasing E_{em} for both the C:Si-nc (solid squares) and Cl:Si-nc (solid circles) samples. This tendency may indicate the size (emission energy) dependence of the radiative-decay rate of the Si-ncs.[41.] However, the measured decay rate can be determined by the sum of the radiative and non-radiative decay rates, which depend on the emission energy.[42] Thus, to further discuss the origin of the emission-energy dependence of the decay rate, the estimation of the radiative and non-radiative decay rates of Si-ncs at different emission energies is necessary.[41-43]

The decay rates for the Cl:Si-ncs were larger than those for the C:Si-ncs, regardless of E_{em}. Because the PL quantum efficiency (~7%) for the Cl:Si-ncs was smaller than that for the C:Si-ncs (~13%), the non-radiative decay rate for the former sample was larger than that for the latter sample (C:Si-nc). The reason for this is as follows. The measured decay rates w and the internal quantum efficiency Φ can be defined as $w = w_r + w_{nr}$ and $\Phi = w_r/w = w_r/(w_r + w_{nr})$, respectively, where the w_r and w_{nr} are the intrinsic radiative and non-radiative decay rates, respectively. Assuming that the radiative-decay rate for the C:Si-ncs is similar to that for the Cl:Si-ncs, the larger w_{nr} value for the Cl:Si-ncs promises larger w and smaller Φ values owing to the aforementioned relationship. This is because of the formation of numerous surface defect states due to the insufficient surface-passivation quality of the Cl:Si-nc sample. This result supports the conjecture that the solvent trichloroethylene has a lower reactivity, producing a considerable amount of surface defect states on Si-ncs, compared with 1-octene. The decay rates for the Cl:Si-nc sample subjected twice-post-laser irradiation (open squares in Figure 3.7) are similar to those of the original Cl:Si-nc sample.

3.4 Conclusions

We prepared Cl:Si-ncs by the laser ablation of PSi in trichloroethylene. We achieved a change in the emission color from white to blue, as well as an PL quantum efficiency increase from 7% (Cl:Si-nc) to 13% (C:Si-nc), by performing a post-laser ablation treatment on the Cl:Si-nc samples in 1-octene to form a stable carbon-passivated Si-nc surface. Such improved PL properties of the post-laser ablation-prepared C:Si-nc sample arose from its nanoparticle-size reduction and improved surface passivation due to the higher reactivity of 1-octene compared with trichloroethylene. Moreover, the preparation yield of the Cl:Si-nc sample prepared in trichloroethylene and that of the C:Si-nc sample prepared by the post-laser ablation of Cl:Si-nc in 1-octene were substantially larger than that of a directly laser ablation-prepared C:Si-nc sample synthesized from PSi powder in 1-octene. The higher preparation yield of the Cl:Si-nc sample in trichloroethylene is ascribed to its low heat-dissipation rate of the solvent (i.e., its low thermal conductivity). We also investigated the PL properties of similar colloidal Si-nc samples. A Cl:Si-nc sample exhibited an excitation band in the 3.0–4.0 eV spectral region, which is similar to that of the C:Si-nc sample prepared in 1-octene; However, the Cl:Si-nc sample did not exhibit an excitation band above ~4 eV, in direct contrast to the latter sample (C:Si-nc). These Cl:Si-nc and C:Si-nc samples exhibited faster decay —on the nanosecond scale—than that usually observed (on the millisecond scale), probably because of the electronic energy-band structure modification of the present samples via surface passivation effect(s), as previously reported. The controllability of the PL properties by changing the organic solvents used in the laser-ablation process may help us to understand the complicated physical processes of nanoparticle formation by laser ablation in liquid.

3.5 References

(1) Hybertsen, M. S. Absorption and emission of light in nanoscale silicon structures. *Phys. Rev. Lett.* **1994**, 72, 1514–7.

(2) Kang, Z.; Liu, Y.; Tsang, C H A.; Ma, D, D, D.; Fan, X.; Wong, N.B.; Lee, S.T. Water-soluble silicon quantum dots with wavelength-tunable photoluminescence. *Adv. Mater.* **2009**, 21 661–4

(3) Dohnalova, K.; Ondič, L.; Kůsova, K.; Pelant, I.; Rehspringer, J.; Mafouana, R,R. White-emitting oxidized silicon nanocrystals: Discontinuity in spectral development with reducing size. *J. Appl. Phys.* **2010**, 107, 053102.

(4) Tan, D.; Xu, B.; Chen, P.; Dai, Y.; Zhou, S.; Ma, G.; Qiu, J. One-pot synthesis of luminescent hydrophilic silicon nanocrystals. *R. Soc. Chem.* Adv. **2012**, 2, 8254–7.

(5) Shirahata, N.; Hozumi, A.; Yonezawa, T. Monolayer-derivative functionalization of non-oxidized silicon surfaces. *Chem. Rec.* **2005**, 5, 145–9.

(6) Hua, F, J.; Erogbogbo, F.; Swihart, M.; Swihart, M, T.; Ruckenstein , E. Capped silicon nanoparticles with blue photoluminescence prepared by hydrosilylation followed by oxidation. *Langmuir*. **2006**, 22, 4363–70.

(7) Warner, J, H.; Rubinsztein, D, H.; Tilley, R, D. Surface morphology dependent photoluminescence from colloidal silicon nanocrystals. *J. Phys. Chem. B* **2005**, 109, 19064–7.

(8) Heintz, A, S.; Fink, M, J.; Mitchell, B, S. Mechano chemical synthesis of blue luminescent alkyl/alkenyl-passivated silicon nanoparticles. *Adv. Mater.* **2007**, 19, 3984–8.

(9) Chao,Y.; Sˇiller, L.; Krishnamurthy, S.; Coxon, P.; Bangert, U.; Gass, M.; Kjeldgaard, L.; Patol, S.; Lie, L.; O'Farrell, N.; Alsop, T.; Houlton, A.; Horrocks, B. Evaporation and deposition of alkyl-capped silicon nanocrystals in ultrahigh vacuum. *Nat. Nanotechnol.* **2007**, 2, 486–9.

(10) Rogozhina, E.; Eckhoff, D.; Gratton, E.; Braun, P. Carboxyl functionalization of ultrasmall luminescent silicon nanoparticles through thermal hydrosilylation. *J. Mater.Chem.* **2006**, 16, 1421–30.

(11) Stewart, M, P.; Buriak, J, M. New approaches towards the formation of silicon-carbon bonds on porous silicon. *Commun. Inorg. Chem.* **2002**, 23, 179–203.

(12) Li, X.; He, Y.; Swihart, M, T. Surface functionalization of silicon nanoparticles produced by laser-driven pyrolysis of silane followed by HF-HNO_3 etching. *Langmuir*. **2004**, 20, 4720–7.

(13) Warner, J, H.; Hoshino, A.; Yamamoto, K.; Tilley, R, D. Water-soluble photoluminescent silicon quantum dots. Angew. *Chem. Int. Ed*. **2005**, 44, 4550–4.

(14) Dohnalova, K.; Poddubny, A, N.; Prokofiev, A, A.; Boer, W, D, A, M.; Umesh, C, P.; Paulusse, J, M, J.; Zuilhof, H.; Gregorkiewicz, T. Surface brightens-up Si quantum dots: Direct bandgap-like size-tunable emission Light. *Sci. Appl.* **2013**, 2 e47.

(15) Kůsová, K.; Cibulka, O.; Dohnalová, K.; Pelant, I.;Valenta, J.; Fucíková, A.; Zídek, K.; Lang, J.; Englich, J.; Matejka, P.; Stepánek, P.; Bakardjieva, S.; Brightly luminescent organically capped silicon nanocrystals fabricated at room temperature and atmospheric pressure. *ACS Nano.* **2010**, 4 4495–504.

(16) Alexander, H, I.; Susanna, M, T.; Sjoerd, H.; Oleksandr, V.; David, Z.; Ratan, D.; Larissa, L.; Lisa, R, JK.; Zhijun, N.; André, J, L.; Kang, W, C.; Aram, A.; Edward, H, S. Hybrid passivated colloidal quantum dot solids. *Nat. Nanotechnol.* **2012**, 7, 577−82.

(17) Mangolini, L.; Thimsen, E.; Kortshagen, U. High-yield plasma synthesis of luminescent silicon nanocrystals. *Nano Lett.* **2005**, 5, 655–9.

(18) Kanemitsu, Y.; Ogawa, T.; Shiraishi, K.; Takeda, K. Visible photoluminescence from oxidized Si nanometer-sized spheres: Exciton confinement on a spherical shell. *Phys. Rev. B.* **1993**, 48, 4883–6.

(19) Bhavin, N, J.; Nicolaas, J, K.; Cristina P, M.; David, C, B.; M. C. M. van de Sanden.; Paul, S.; Cristian, V, C.; Sumit, A. Surface hydride composition of plasma-synthesized Si nanoparticles. *J. Phys. Chem. C.* **2011**, 115, 20375–9.

(20) Shirahata, N. Colloidal Si nanocrystals: A controlled organic–inorganic interface and its implications of color-tuning and chemical design toward sophisticated architectures. *Phys. Chem. Chem. Phys.* **2011**, 13, 7284–94.

(21) Ghosh, B.; Shirahata, N. Colloidal silicon quantum dots: Synthesis and luminescence tuning from the near-UV to the near-IR range. Sci. *Tech. Adv. Mat.* **2014**, 15, 014207.

(22) Švrček, V.; Sasaki, T.; Shimizu, Y.; Koshizaki, N.; Blue luminescent silicon nanocrystals prepared by ns pulsed laser ablation in water. *Appl. Phys. Lett.* **2006**, 89, 213113.

(23) Umezu, I.; Senoo, H. Synthesis of photoluminescent colloidal silicon nanoparticles by pulsed laser ablation in liquids. *J. Phys.: Conf. Ser.* **2007**, 59, 392–5.

(24) Shirahata, N.; Hirakawa, D.; Sakka, Y. Interfacial-related color tuning of colloidal Si nanocrystals. *Green Chem.* **2010**, 12, 2139–41.

(25) Tan, D.; Z. Ma, B. Xu, M. B.; Dai, Y. ; Ma, G.; He, M.; Jin, Z. ; Qiu, J. Surface passivated silicon nanocrystals with stable luminescence synthesized by femtosecond laser ablation in solution. *Phys. Chem. Chem. Phys.* **2011**, 13, 20255-61.

(26) Tan, D.; Zhoua, S.; Qiu, J.; Khusroa, N. *J.* Preparation of functional nanomaterials with femtosecond laser ablation in solution. *Photochem. Photobio. C,* **2013**, 17, 50-68.

(27) Sailor, M, J.; Lee,E, J. Surface chemistry of Luminescent Silicon Nanocrystallites. *Adv. Mater.*, **1997**, 9, 783–93.

(28) Kovalev, D.; Timoshenko, V, Y.; Künzner, N. ; F. Gross,; Koch, E. Rectification Properties of Carbon Nanotube "Y-Junctions". *Phys. Rev. Lett.*, **2001**, 87, 068301.

(29) Limaye,S.; Subramanian,S.; Goller,B.; Diener,J.; Kovalev,D. Scaleable synthesis route for silicon nanocrystal assemblies. *Phys. Status Solidi A.*, **2007**, 204, 1297–301.

(30) Fletcher, A. N.; Bliss,D. E. Effect of Chemical Substituents of Bicyclic Dyes Upon Photodegradation Parameters. *Appl. Phys.* **1978**, 16, 289-95.

(31) Nakamura,T.; Yuan,Z.; Adachi,S. Micronization of red-emitting K2SiF6:Mn4+phosphor by pulsed laserirradiation in liquid. *Appl. Phys. Sci.* **2014**, 320, 514-18

(32) Sandrine, R.; Yves, J, C. Chlorination of hydrogen-terminated silicon (111) surfaces. *J. Vac. Sci. Technol. A* **2005**, 23, 1100-6.

(33) Nakamura, T.; Yuan, Z.; Adachi, S.; High-yield preparation of blue-emitting colloidal Si nanocrystals by selective laser ablation of porous silicon in liquid. *Nanotechnology.* **2014**, 25, 275602.

(34) Shirahata, N.; Hirakawa, D.; Masuda, Y.; Sakka, Y. Size-dependent color tuning of efficiently luminescent germanium nanoparticles, *Langmuir*, **2013**, 29 7401−10.

(35) Pyatenko, A.; Wang, H.; Koshizaki, N.; Tsuji, T. Mechanism of pulse laser interaction with colloidal nanoparticles, *Laser Phys. Rev.* **2013**, 7, 596−04.

(36) Poddubny, A, N.; Dohnalová, K. Direct band gap silicon quantum dots achieved via electronegative capping. *Phys. Rev. B.* **2014**, 90, 245439.

(37) Li,Q.; Luo,T.-Y.; Zhou,M.; Abroshan, H.; Huang, J.;Kim, H.J.; Rosi, N.L.; Shao, Z.; Jin,R. Silicon Nanoparticles with Surface Nitrogen: 90% Quantum Yield with Narrow Luminescence Bandwidth and the Ligand Structure Based Energy Law. *ACS Nano*, **2016**, 10, 8385−93.

(38) Delerue, C.; Allan,G.; Lannoo, M. Theoretical aspects of the luminescence of porous silicon. *Phys. Rev. B.*, **1993**, 48, 11024−36.

(39) Kovalev, D.; Heckler, H.; Polisski, G.; Koch, F. Optical properties of Si nanocrystals. *Phys. Status Solidi B*, **1999**, 215, 871−32.

(40) Takeoka, S.; Fujii, M.; Hayashi, S. Size-dependent photoluminescence from surface-oxidized Si nanocrystals in a weak confinement regime. *Phys. Rev.* **2000**, 62, 16820−5.

(41) Stobbe, S.; Johansen, J.; Kristensen, P, T.; Hvam, J, M.; Lodahl, P. Frequency dependence of the radiative decay rate of excitons in self-assembled quantum dots: Experiment and theory. *Phy. Rev. B.* **2009**, 80, 155307

(42) Miura,S.; Nakamura,T.; Fujii, M. Hayashi, S. Size dependence of photoluminescence quantum efficiency of Si nanocrystals. *Phys. Rev., B.* **2006**, 73, 245333

(43) Leistikow, M, D.;Johansen, J.; Kettelarij, A, J.; Lodahl, P.; Vos, W, L.; Size-dependent oscillator strength and quantum efficiency of CdSe quantum dots controlled via the local density of states. *Phys. Rev B.* **2009**, 79, 045301.

3.6 Supporting Information

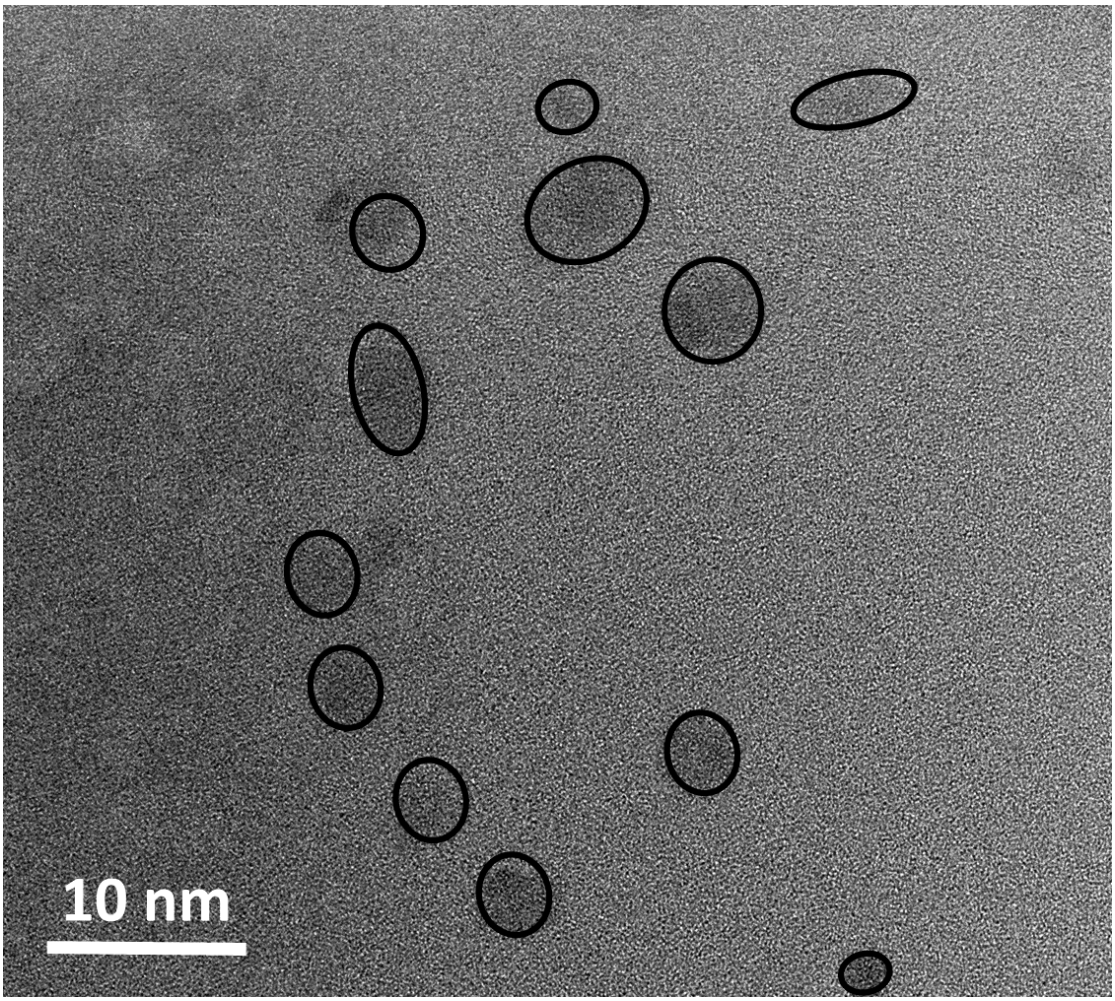

Figure S1 Transmission electron microscope image of the colloidal Cl: Si-ncs.

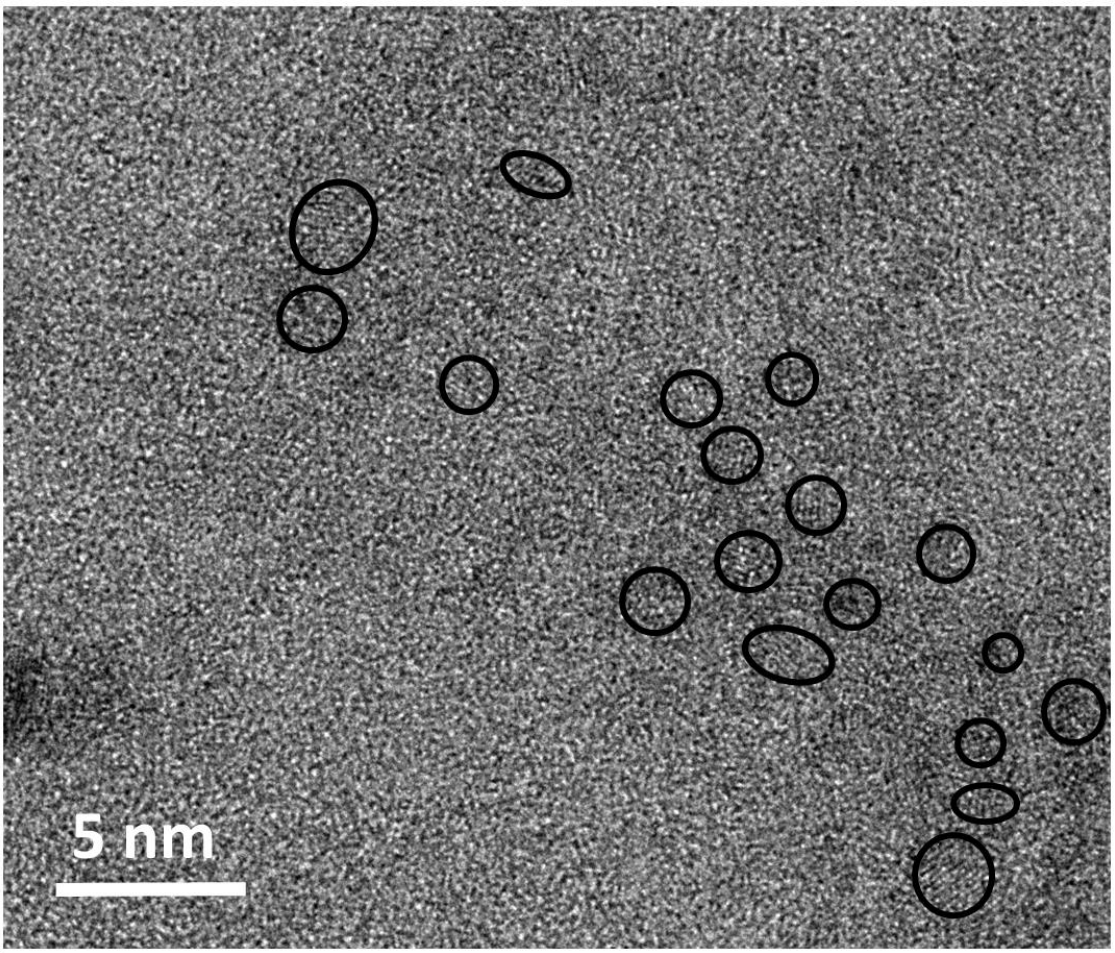

Figure S2 Transmission electron microscope image of the colloidal C: Si-ncs.

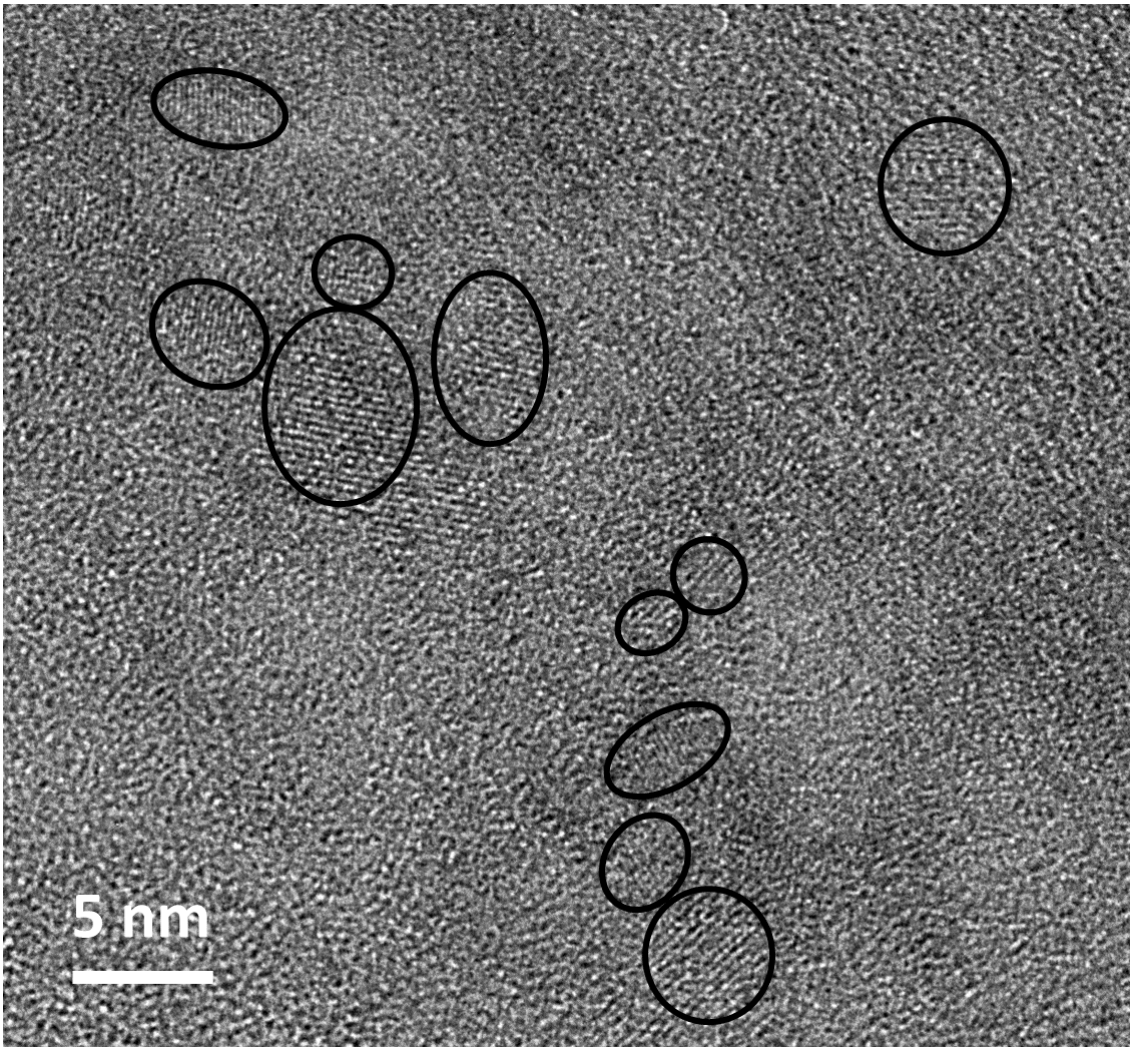

Figure S3 Transmission electron microscope image of the colloidal Cl: Si-ncs formed by laser-ablating C:Si-nc samples in trichloroethylene..

Chapter 4

Improvement of laser processing for colloidal silicon nanocrystal formation in a reactive solvent

4.1 Introduction

Silicon nanocrystal (Si-nc) is a promising material for use in various applications in light emitting devices,[1,2] photovoltaics, biological labeling,[3] etc. This is owing to its unique properties such as the quantum confinement-induced intense luminescence, emission color tunability, and environmentally friendliness. There are various forms of Si-nc, e.g., porous silicon (PSi) which is an assembly of wire-like Si-nc,[4] the nanoparticles embedded in a glass matrix,[5] and free-standing "colloidal" nanoparticles.[6-8] In particular, the "colloidal Si-nc" dispersed in solutions has attracted attention for low-cost, easiness of the handling in solution-based technology.[2] Surface functionalization of the colloidal Si-nc also allows us to control its optical properties6 and chemical reactivity.[7,8]

Freestanding colloidal Si-nc with hydrogen termination is reported to exhibit tunable PL in the entire visible region.[9-11] However, such surface can be easily oxidized in ambient air, resulting in the degradation of PL from Si-nc. This effect is problematic for light-emitting device applications and, therefore, further efficient surface protection technique is required. The effective approach for a stable functionalization of Si surface is termination by some alkyl groups.[12-14] Such alkyl terminated Si-nc is reported to have relatively high PL efficiency without showing degradation in ambient air.

Various techniques, such as electrochemical reduction,[15] plasma deposition of silane,[16] wet-chemical synthesis,[17] have been proposed for preparing colloidal Si-nc with alkyl termination. It should be noted that laser irradiation method in an organic solvent has some advantages (i.e., one-pot production and a concise preparation setup[18-20]) in preparing alkyl-terminated colloidal Si-nc. However, this synthesis process makes difficult to control the sizes of the colloidal nanoparticles and its size distribution is known to be wider.18 Furthermore, the productivity or preparation yield of this process is relatively low due to

its necessity of using high power pulsed lasers. The PL quantum efficiency (QE) of colloidal Si-nc prepared by laser irradiation process (~10-20%)[18,21] is also usually lower than those prepared by other methods (~50-90%).[22,23] Thus, it is important to improve the QE of alkyl-terminated Si-nc prepared by laser irradiation method.

In this work, we demonstrate that the pulsed-UV-laser irradiation of PSi in a HF-contained organic solution generates bright luminescent colloidal Si-nc (QE = ~50-70%) with a homogeneous size distribution. In previous works,[21,24] we reported the preparation of blue- and orange-emitting colloidal Si-nc by pulsed-laser irradiation of PSi in ordinary organic solution (i.e., without HF). These prepared samples exhibit the lower QE values (15~20%) than the present samples, and its detailed size distribution through a microscopic technique such as transmission electron microscope is unclear. Furthermore, the preparation yield of the present samples is found to be larger than that of the previous orange-emitting ones. By systematically changing HF concentration, we investigate in detail the effects of HF addition in the organic solvent on the PL properties, size distribution, and preparation yield. We also discuss underlying mechanisms for the production of Si-nc with the highly improved laser processing in the reactive solvent proposed in the present study.

4.2 Experimental section

4.2.1 Preparation of PSi powder

The colloidal Si-nc samples were prepared by pulsed-UV-laser irradiation onto PSi in liquid. The reason for the use of PSi as a target in this laser processing is its large surface area[25] and lower thermal conductivity nature,[26] which allow us to realize high productivity of the colloidal Si-nc.[24] The PSi powder used was prepared by stain-etching of metallurgical-grade polycrystalline Si powder, which has a diameter range in the range of 3–11 μm (Vesta Ceramics). Etching was performed in a mixture of aqueous HF and HNO_3 solutions. Its composition was HF (50%) : H_2O: HNO_3 (14.5N) = 4:1:20 in volume ratio. Etching time was 30 min. After etching, the PSi powder was collected by filtering the etchant solution and then dried under ambient conditions.

4.2.2 Preparation of colloidal Si-nc

For preparing the colloidal Si-nc samples, a 100 mg of PSi powder was firstly dispersed in an organic solvent (1-decene) with a quartz cuvette. Then, a small amount of aqueous HF solution was added in the organic solution. The concentration of aqueous HF solution was varied from 0 to 3 vol%. Finally, pulsed UV laser at 266 nm from a Q-switched Nd:YAG laser (Continuum) was irradiated with a pulse duration of 5 ns and a repetition rate of 15 Hz for 6 h. The laser fluence was ~0.2 J/cm^2. During laser irradiation, the PSi power dispersed in the HF/1-decene solution was constantly stirred by a magnetic stirrer. The laser light was irradiated into the solution through the lens with a focal length of 120 mm. The distance between the lens and the front of the cuvette was set at 180 mm. After laser irradiation, the supernatant part of liquid was filtered by centrifugation at 13,000 rpm for 20 min with a membrane filter having a pore size of ~200 nm. This process enabled obtaining colloidal solution. As shown in Figure 4.1, the color of the colloidal solution obtained by adding the HF solution at 3 vol% became yellowish in color. The colloidal solution with HF exhibited bright orange emission under UV illumination, as shown in the inset of Figure 4.2(a). Note that the colloidal solution without HF also exhibited an orange emission, but its emission intensity was observed to be lower (see Figure 4.3 below).

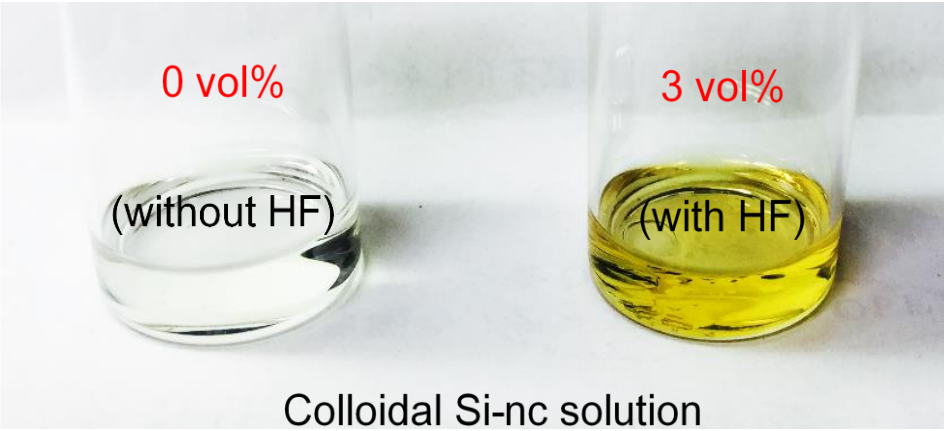

Figure 4.1. Photograph of the colloidal Si-nc samples prepared in the 1-decene solution without (left) and with HF solution (3 vol%, right) taken under room light.

4.2.3 Analytical technique

The structural properties of the prepared Si-nc colloids were analyzed using a transmission electron microscope (TEM) (JEOL, TEM-2100). The surface chemistry of the samples was investigated using a Fourier-transform infrared (FTIR) spectrometer (Nicolet, iS50). The photoluminescence (PL) spectra were measured by using a single monochromator equipped with a charge-coupled device (Princeton Instruments, PIXIS 100B). A He–Cd laser (Kimmon, IK3302R-E) was used as the excitation light source. From the measurements of the emission spectra for pure solution samples, we confirmed that the effects of Rayleigh and Raman scattering on PL spectra of Si-nc contained samples by changing the solution composition (i.e., the addition of HF) are neglected. The optical absorption spectra were measured by using a V-570 (JASCO) spectrometer. Note that we also confirmed that no change in the absorbance spectra due to Rayleigh scattering occurs by the addition of HF. PL decay curves were measured by using a frequency-tripled 355 nm light pulse with a pulse width of 300 ps from a Nd:YAG laser (Teemphotonics, STV-01E). The laser pulse fluence was 21 J/cm^2. Note that we confirmed that this laser power is low enough not to cause any undesired effects such as increase in non-radiative decay rates. The PL decay data were recorded by using a Peltier-device-cooled photomultiplier tube (Hamamatsu, R375) and multichannel scaler (Stanford Research, SR430). The relative QE was measured using He-Cd laser (325 nm, Kimmon) as the excitation source, a single monochromator equipped with a charge-coupled device (Princeton Instruments) as the detector, and Rhodamine 6G (Sigma Aldrich) as the reference sample.[27] Optical measurements for the colloidal solution samples were performed in a quartz cuvette at room temperature.

4.3 Results and discussion

A representative high-resolution TEM (HRTEM) image of the nanoparticle with a diameter of ~3.2 nm is shown in Figure 4.2(a), obtained from the colloidal solution with the HF concentration at 3 vol%. The clear lattice fringe for the nanoparticle can be observed. The corresponding fast Fourier transform (FFT) diffraction pattern of the HRTEM image is shown in Figure S1. The lattice spacing of 3.2 Å is realized, corresponding to the (111) plane of the Si crystal. Thus, the prepared colloidal nanoparticles are concluded to be single-crystalline Si. The colloidal sample prepared in the organic solution without HF (0 vol%) was also confirmed nanoparticles from the TEM measurements to be crystalline Si.

In previous work,[21] we confirmed single crystalline nanoparticles with a several nanometers (3~4 nm) by the UV pulsed laser irradiation of PSi in similar organic solvent (1-octene) without HF. Note that the laser ablation of PSi with a pulsed visible laser light causes the formation of crystalline nanoparticles with relatively small sizes (~2 nm).[24] The size distributions for the present two samples will be discussed later.

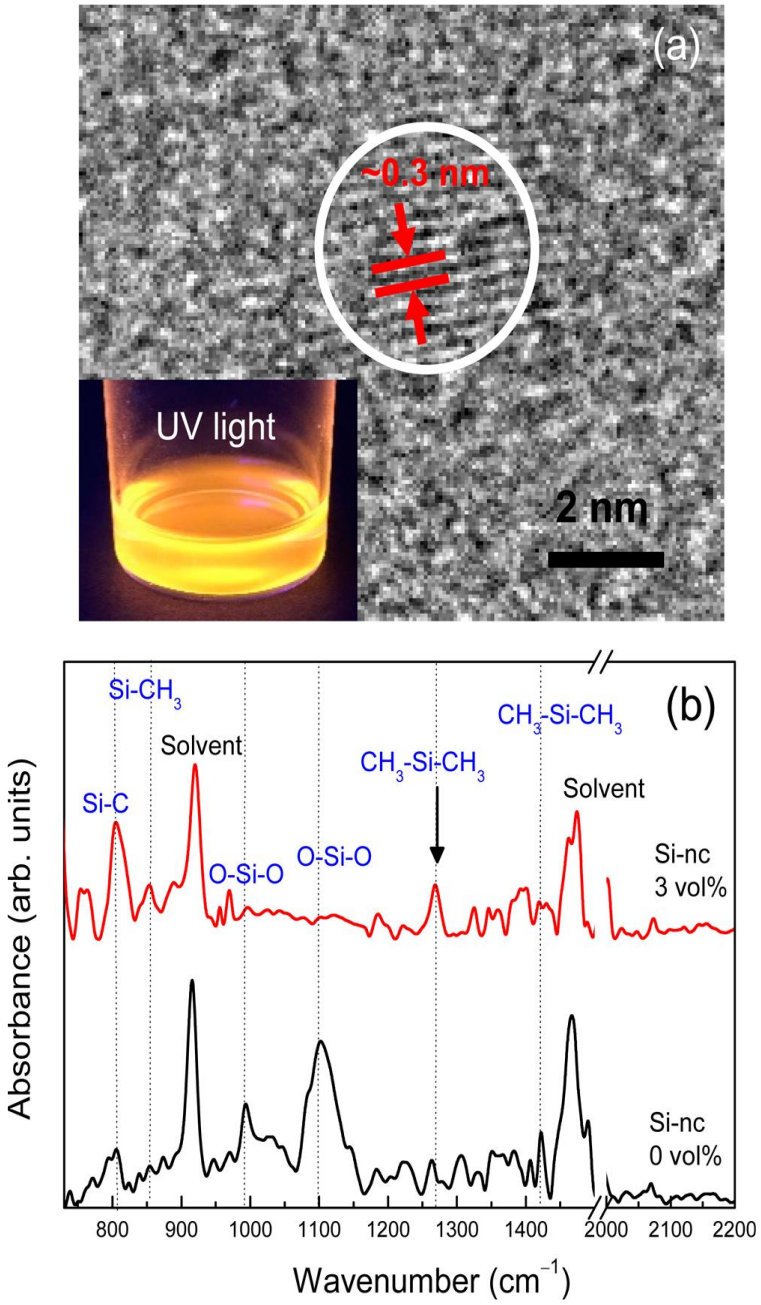

Figure 4.2. (a) High-resolution TEM image of the colloidal Si-nc. Inset shows the photograph of the colloidal Si-nc dispersed in the 1-decene solution taken under UV illumination. (b) FTIR spectra of the colloidal Si-nc samples prepared in the 1-decene solution without (0 vol%, black curve) and with HF solution (3 vol%, red curve).

Figure 4.2(b) shows the FTIR spectra of the colloidal Si-nc samples prepared at the HF concentrations of 0 (black curve) and 3 vol.% (red curve). The clear absorption peak at 760 cm^{-1} (Si-C) and those at 850, 1270, 1470 cm^{-1} (Si-CH_3) (Ref. 28) were observed for the sample prepared at the HF concentration of 3 vol.%. The fact indicates that the colloidal Si-nc sample at 3 vol.% was terminated by some alkyl species. On the other hand, the colloidal Si-nc sample (0 vol.%) exhibited the absorption peaks at 990 and 1100 cm^{-1} due to the O-Si-O vibration modes,[28] together with the alkyl-related peaks. The alkyl-related absorption intensities for the sample with HF are also observed to be larger than those for the sample without HF. These results imply that the oxide-free alkyl-terminated layer was formed on the colloidal Si-nc surface prepared in the HF-contained organic solution with the alkyl termination coverage larger than that for the sample without HF.

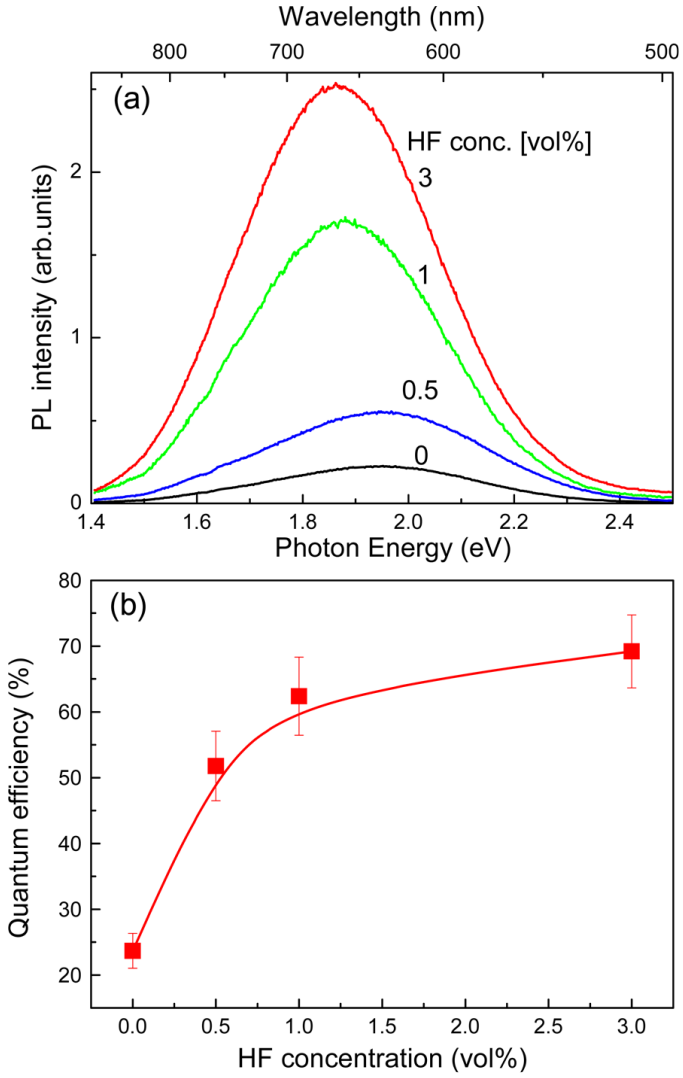

Figure 4.3. (a) PL spectra of the colloidal Si-nc samples for various HF concentrations from 0 to 3 vol% in 1-decene. (b) The PL quantum efficiencies of colloidal Si-nc samples as a function of HF concentration in 1-decene.

Figure 4.3(a) shows the PL spectra of the colloidal Si-nc samples prepared at various HF concentrations, 0-3 vol.%. A broad emission band peaking at ~1.9 eV (~750 nm) is observed for all samples. The PL intensity clearly increases with increasing the HF concentration. Thus, the addition of HF considerably improves QE and/or the preparation yield of Si-nc. On the contrary, the changes in their spectral shapes (i.e., their widths and peak energies) are relatively small. In the previous work,[21] the PL emission of the colloidal Si-nc prepared by the pulsed-UV-laser irradiation of PSi in an organic solution (1-octene) was mainly attributed to the band-to-band transitions of the electron hole pairs in quantum confined Si-nc cores. The present Si-nc sample prepared by the UV laser irradiation in the 1-decene solution has essentially the same properties as the Si-nc sample previously prepared in 1-octene.[21] Thus, no large change in the spectral shape in Figure 4.3(a) suggests that the origin of the PL emission for the colloidal Si-nc prepared in the HF-contained solution should be the band-to-band transition in Si-nc core, the same as that prepared in the solution without HF. The reason for the higher PL peak energy for the sample without HF (~1.94 eV) compared with HF at 3 vol.% (~1.87 eV) may be due to the size reduction of the colloidal Si-nc in the former sample caused by thinner surface oxide growth or deposition after the HF-free synthesis treatment and resultant bandgap widening of the Si-nc particles. Note that the PL emission of Si-nc samples obtained by laser ablation with a visible laser light appears in a different wavelength region (300-500 nm) from the present samples.[24] This is mainly due to a smaller size of the Si-nc (~2-3 nm) compared to that for the present sample (~3-4 nm).

The HF concentration dependence of the relative QE of the colloidal Si-nc is shown in Figure 4.3(b). The QE values of the colloidal Si-nc prepared in the HF-contained solution (QE: ~50%-70%) are higher than that of the Si-nc without HF (QE: ~20%) and show slight increase with increasing HF concentration from 0.5 to 3 vol%. The increase in the QE by the addition of HF is considered to be due to an improvement in the alkyl passivation quality (i.e., a decrease in the surface defect density).[29] In fact, the FTIR spectra in Figure 4.2(b) showed that the Si-nc in the HF-contained sample has an efficiently alkyl-terminated surface that may result in passivation of the surface dangling bonds (i.e., in the low surface defect density).

To investigate the mechanism for the increase in the PL efficiency due the addition of HF, we measured the PL decay curves for the colloidal Si-nc sample prepared in the HF-contained solution (3 vol.%) and that in the solution without HF (0 vol.%). These results are shown in Figure 4.4. The PL decay for the Si-nc at 3 vol.% becomes slower compared to

that for the Si-nc at 0 vol.%. Furthermore, the decay curves for these samples have slow (several tens of microseconds) and fast components (below several microseconds), as also observed in our previous work.[21] The fast and slow components are to be due to the recombination via non-radiative defect centers and band-to-band recombination of the electron-hole pairs in the Si-nc cores, respectively. As seen in Figure 4.4, the slow-decay processes seem to be almost the same between them, while the fast decay component for the sample at 3 vol.% is slower than the 0 vol.% sample. To further qualitatively evaluate such PL decay processes, the measured PL decay curves were fitted with the "bistretched" exponential function, $I(t) = I_s \exp(t/\tau_s)^{\beta_s} + I_f \exp(t/\tau_f)^{\beta_f}$, where Is $I_{s(f)}$, $\tau_{s(f)}$, and $\beta_{s(f)}$ are the intensity, decay time, and β factor for the slow (fast) component, respectively. Note that the "stretched" exponential function has been popularly used for PL decay curve analysis of Si-nc core samples.[30,31] In the present fitting procedure, the common decay time and β factor for the slow decay component (τ_s and β_s) are considered for both samples to reduce freedom of the fitting parameters.

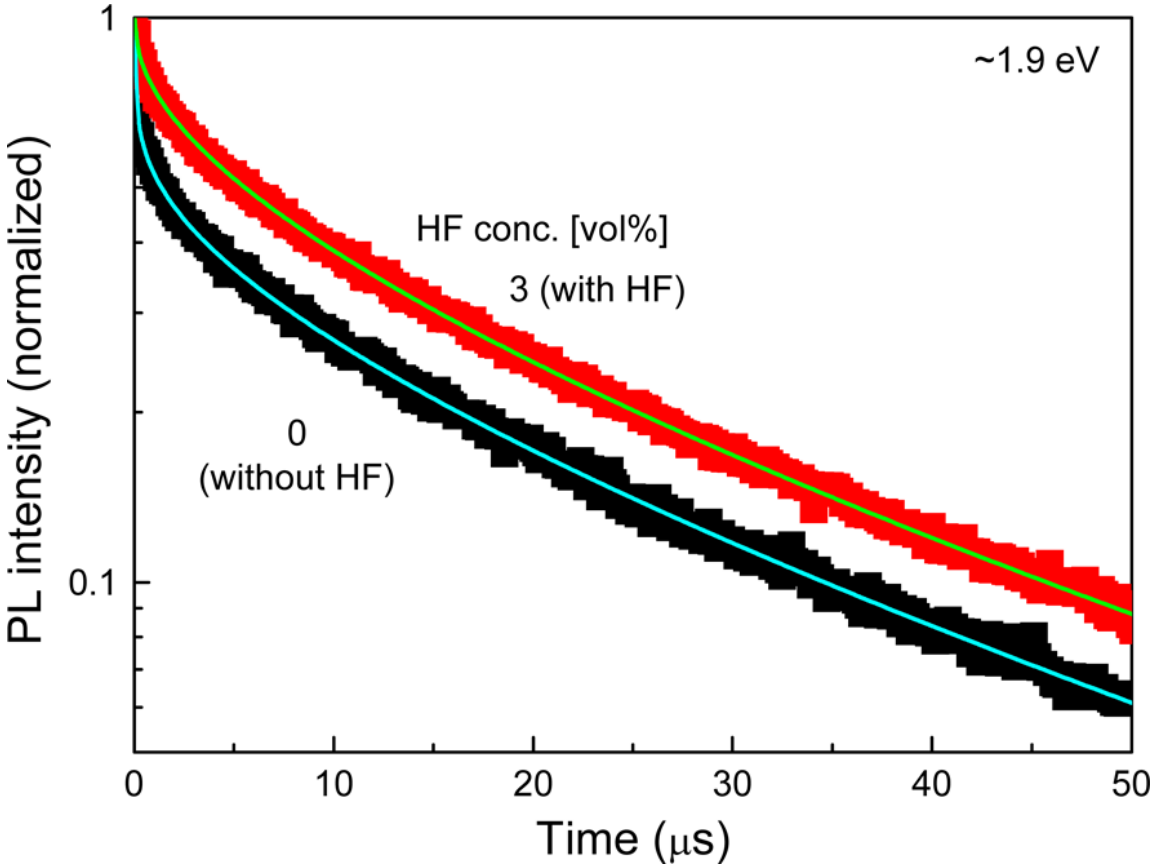

Figure 4.4. PL decay curves of the colloidal Si-nc samples for HF concentrations of 0 and 3 vol.% in 1-decene detected at ~1.9 eV. The solid curves represent the fitting results of the bistretched exponential function.

The fitting results using the bistretched exponential function are shown as solid curves in Figure 4.4. The fitting curves are in reasonable agreement with the experimental data. The fit-obtained parameters for the slow component are τ_s = 18.2±0.2 μs, β_s = 0.74±0.01. Those for the fast component are also determined to be τ_f = 3.37±0.06 s (0.32±0.2 s) and β_f = 0.41±0.01 (0.29±0.02) for the sample with (without) HF, respectively. The intensity ratios of the fast and slow components for the samples with and without HF are I_f/I_s = 0.76±0.01 and 1.19±0.1, respectively. These results indicate that the decay time for the fast component obtained by the addition of the HF in the organic solvent becomes much slower. Because the fast component represents the recombination via non-radiative defect centers, the slower decay time for the fast component observed for the Si-nc prepared in the HF-contained solution implies the decreased surface defect density. This result is evidently responsible for the increase in the QE values in Figure 4.3(b).

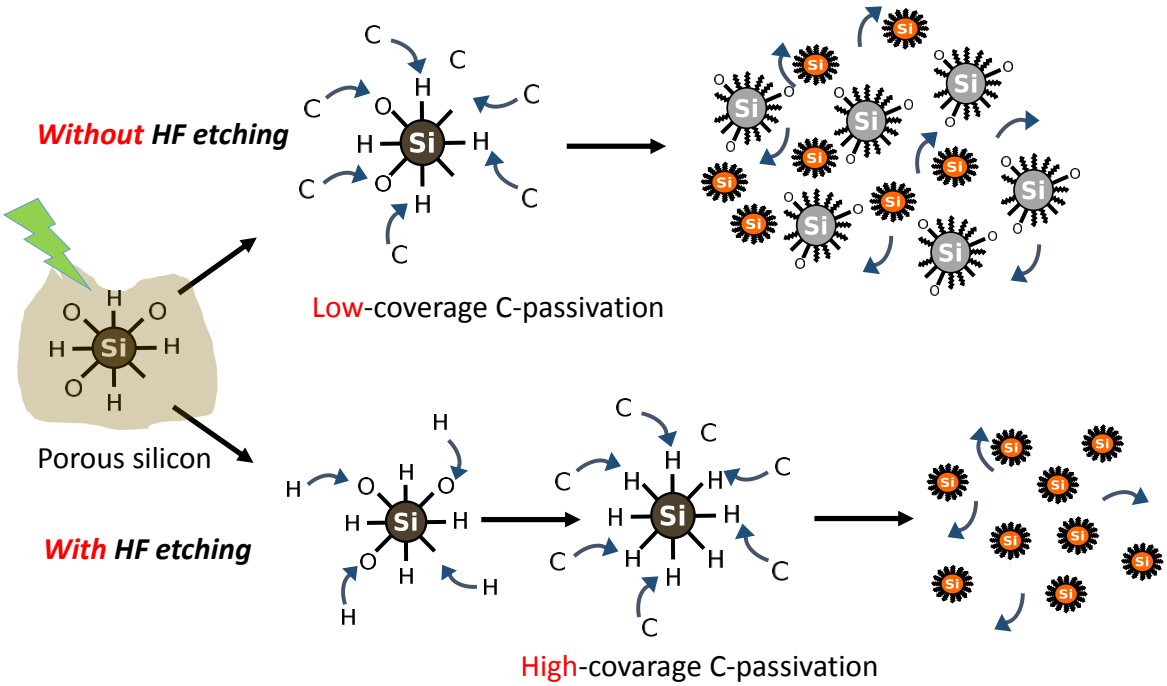

Scheme 1. Schematic representation for the formation processes of alkyl-terminated Si-nc in an organic solvent with and without HF.

The present colloidal Si-nc samples are considered to be formed by the fragmentation of PSi target by the intense pulsed-laser irradiation.[21] The Si surface can be simultaneously terminated by the alkyl groups due to the UV laser-assisted hydrosilation between the Si-H surface and unsaturated bonds of organic solvent. Thus, the addition of HF in the organic

solvent during laser irradiation considerably promotes such hydrosilation reaction process and results in oxygen-free, alkyl-terminated Si-nc surface with relatively high coverage, as observed in Figure 4.2(b). This is because HF can etch-remove undesirable oxide from Si surface and then uniform hydride surface can be formed. Therefore, the laser processing of PSi in HF-contained organic solution produces highly efficient colloidal Si-nc with considerably low defect density, as shown in Figure 4.3(b) (see also Figure 4.4). The similar increase in the QE of Si-nc via an enhancement in the hydrosilation reaction due to HF addition has also been reported in the literature.[22,32] The above-mentioned alkyl termination mechanism for the increased QE by the HF addition is schematically shown in Scheme 1.

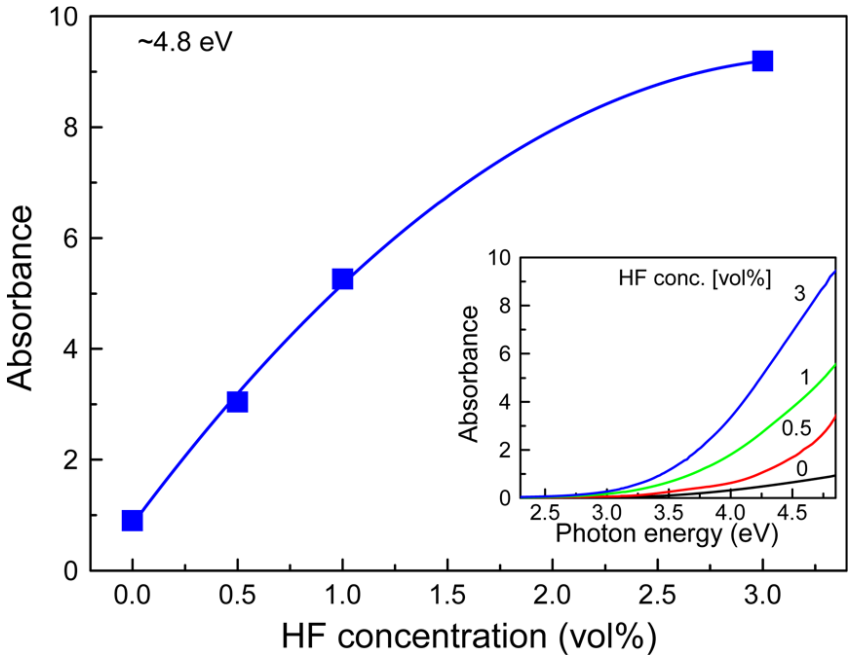

Figure 4.5. Absorbance of the colloidal Si-nc samples at 4.8 eV as a function of HF concentration in 1-decene. Inset shows the absorbance spectra of the colloidal Si-nc samples for HF concentrations from 0 to 3 vol.% in 1-decene. The solid curve represents guide to the eye.

To investigate the effects of the HF addition on the preparation yield of colloidal Si-nc, the absorbance spectra of the samples prepared in the different HF concentrations were measured. In Figure 4.5, we plotted absorbance value at 4.8 eV as a representative for the absorption of Si-nc in a UV region. Inset shows the corresponding spectra. The absorption

in the UV region (< ~3 eV) increases with increasing HF concentration. Because the Si-nc size of several nanometers is much smaller than the investigated absorption light wavelengths, light scattering can be safely neglected. Thus, the absorbance is assumed to be proportional to the preparation yield. As shown in Figure 5, the absorbance at 4.8 eV increases with increasing HF concentration, implying the preparation yield to be increased with increasing HF concentration. Note that the similar gradual increase in the absorbance is also observed for the absorbance values above ~3 eV. One possible reason for the increase in the preparation yield by the addition of HF is the removal of native oxide overlayer on the PSi target surface. Because hydrogen-terminated Si surface will have lower mechanical strength than that covered with native oxide, the UV-laser-induced fragmentation occurs more efficiently in samples of native oxide-free PSi surfaces. The removal of oxide overlayer may also generate a mechanical stress in the porous Si network that will further affect the laser-induced fragmentation process to occur more effectively.

Let us now discuss the size difference of the colloidal Si-nc samples prepared without and with HF addition. Figures 4.6(a) and 4.6(b) show a wide-view TEM images of the Si-nc samples prepared without and with HF addition (3 vol.%), respectively. The relatively smaller particles are observed for the sample with HF than without HF. The magnified TEM images are also shown in Figure 6(c) and 6(d) to more clearly observe their lattice fringes. The single-crystalline Si particles with a diameter of ~2-3 nm are observed for both samples (see white circles in Figures 4.6(a) and 4.6(b). However, the larger nanoparticles are observed only in the Si-nc sample without HF (Figure 4.6(c) and Figure S2 in the Supporting Information). Note that some larger nanoparticles exhibit the polycrystalline nature (black circles in Figure 4.6(c)). From these TEM images, we obtained histograms of the Si-nc size distribution. These results are shown in Figures 4.6(e) and 4.6(f). In the construction of the histograms, we counted the nanoparticles with clear lattice fringes.

The size distribution for the sample without HF in Figure 4.6(e) exhibits the bimodal distribution behavior, while the distribution for the sample with HF is monomodal (Figure 4.6(f). The average diameters estimated from the bimodal distribution are ~3.1 and ~5.5 nm. The average diameter of Si-nc for the sample with HF (~2.9 nm) is also observed to be nearly the same as the smaller diameter (~3.1 nm) obtained for the sample without HF. This result is in agreement with the fact that the two samples exhibit similar PL peak energies at ~1.9 eV, which strongly reflect the sizes of Si nanocrystallite. In other word, larger nanoparticles with larger size distribution (average diameters of ~5.5 nm) are considered not to contribute to the PL emission. This may be due to the insufficient surface

terminations for the larger nanoparticles particle because of difficulties in the uniform surface passivation in the larger nanoparticles. Another possible reason is the polycrystalline nature of the larger nanoparticles shown in Figure 4.6(c). The emission efficiency of these nanoparticles may be lower due to the migration of the excited carriers than single crystalline particles. However, the clear underlying mechanism is not clear in present.

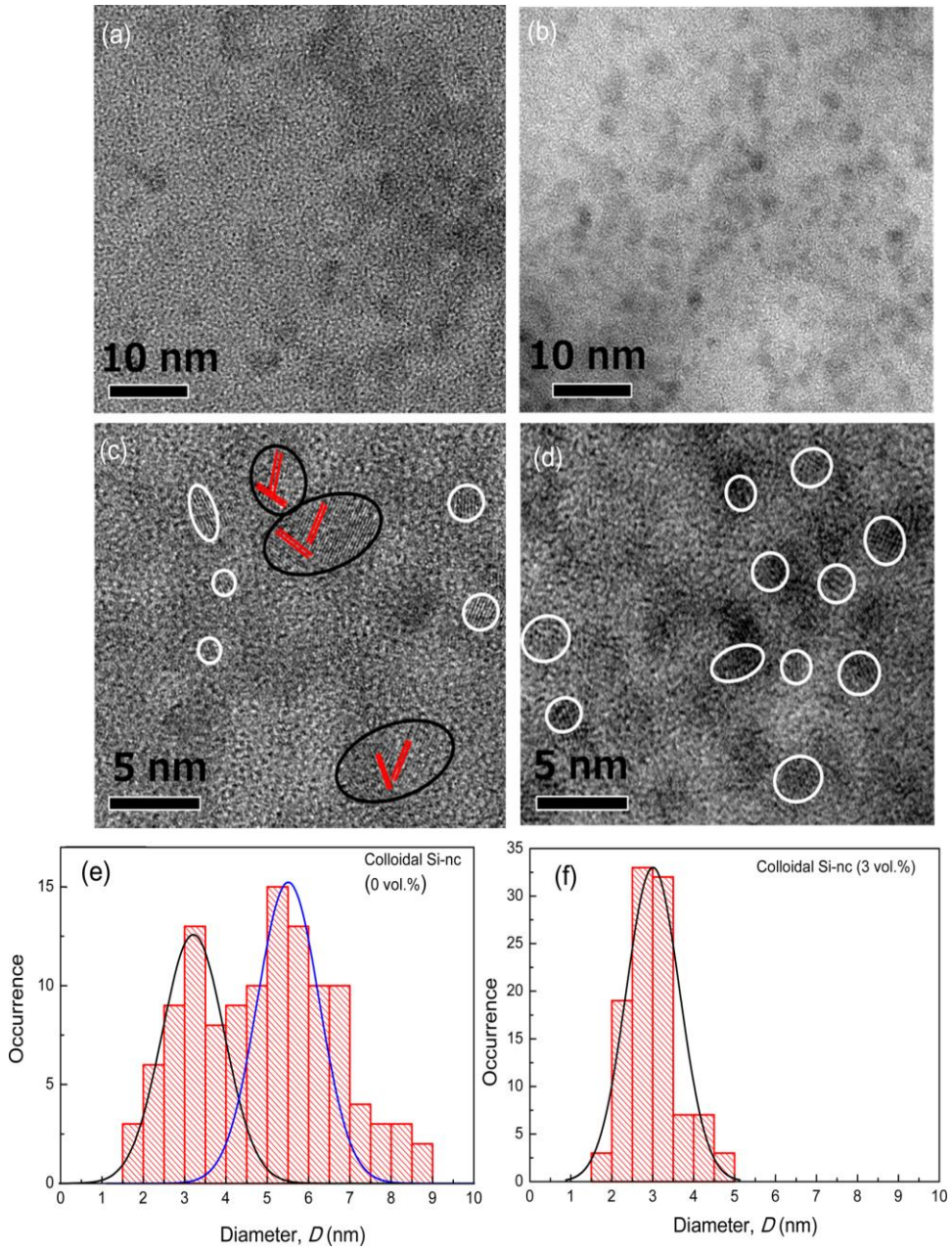

Figure 4.6. TEM images of the colloidal Si-nc samples prepared in the 1-decene solution without HF [(a), (c)] and HF (3 vol.%) [(b), (d)]. The histograms of the colloidal Si-nc sizes prepared in the 1-decene solution (e) without and (f) with HF solution (3 vol.%) derived from the TEM images in (c) and (d), respectively.

Possible reason for the distinguishable difference in the size distribution observed in this study may be the different degree of the UV-laser-induced fragmentation of the PSi target in the solvent with or without HF. As mentioned before, the addition of HF etch-removes the oxide overlayer on the PSi surface and makes the mechanical strength weaker. Thus, the irradiated laser power thoroughly fragments the porous network until the small nanoparticles generate, as illustrated in Scheme 1. This conjecture is consistent with higher preparation yield in the HF-contained solution via an efficient UV-laser-induced fragmentation process. On the contrary, the laser-induced fragmentation in the solvent without HF occurs insufficiently that produces the particles in still large size. The bimodal distribution coming from the thoroughly fragmented nanoparticles and remained larger particles justifies the above-mentioned speculation. The bimodal distribution has been occasionally observed in laser-induced size reduction process of metal nanoparticles.[33]

4.4 Conclusions

In conclusion, we demonstrated the highly improvement of formation processes for colloidal Si-nc by pulsed-UV-laser irradiation on porous silicon in a reactive HF-contained organic solution. The Si-nc samples exhibit a higher PL quantum yield (~50-70%) than that in an ordinary organic solvent without HF (~20%). This enhancement of the quantum yield is caused by the HF-induced removal of the surface oxide overlayer on Si-nc and subsequent hydrogen termination. These reactions promote the efficient hydrosilylation between the hydrogen surface and organic solvent, resulting in the lower defect density of the Si-nc surface. The preparation yield also increases by an order of the magnitude compared to that without HF and the size distribution of Si-nc becomes homogeneous, in direct contrast to the bimodal size distribution obtained in the ordinary solvent without HF. These results are owing to effective pulsed-laser-induced fragmentation by the removal of oxide overlayer and the resultant weakening of mechanical strength of the PSi target layer. The present novel improvement approach of laser processing using a reactive solvent containing HF for the preparation of colloidal Si-nc is expected to utilize as the future formation technology of novel nanomaterials, including semiconductor nanocrystals and other materials.

4.5 References

(1) Walters, R.; Atwater, H.; Bourianoff, G. Field-effect Electroluminescence in Silicon Nanocrystals. *Nat. Mater.* **2005,** 4, 143–146.

(2) Maier-Flaig, F.; Rinck, J.; Stephan, M.; Bocksrocker, T.; Bruns, M.; Kübel, C.; Powell, A. K.; Ozin, G. A.; Lemmer, U. Silicon Light-Emitting Diodes (SiLEDs). *Nano Lett.* **2013**, 13, 475–480.

(3) Cheng, X.; Lowe, S. B.; Reece, P. J.; Gooding, J. J. Colloidal Silicon Quantum Dots: from Preparation to the Modification of Self-assembled Monolayers (SAMs) for Bio-applications. *Chem. Soc. Rev.* **2014**, 43, 2680–2700.

(4) Cullis, A. G.; Canham, L. T.; Calcott, P. D. J. The Structural and Luminescence Properties of Porous Silicon. *J. Appl. Phys.* **1997**, 82, 909–965.

(5) Takeoka, S.; Fujii, M.; Hayashi, S. Size-dependent Photoluminescence from Surface-Oxidized Si Nanocrystals in a Weak Confinement Regime. *Phys. Rev. B* **2000**, 62, 16820–16825.

(6) Yixuan, Y.; Clare, E. R.; Richard D. S.; Brian A. K. Synthesis and Ligand Exchange of Thiol-capped Silicon Nanocrystals. *Langmuir* **2015,** 31, 6886–6893.

(7) Shirahata, N.; Hozumi, A.; Yonezawa, T. Monolayer-derivative Functionalization of Non-Oxidized Silicon Surfaces. *Chem. Rec.* **2005**, 5, 145–149.

(8) Ghosh, B.; Shirahata, N. Colloidal Silicon Quantum Dots: Synthesis and Luminescence Tuning from the Near-UV to the Near-IR range. *Sci. Technol. Adv. Mater.* **2014**, 15, 014207.

(9) Li, X.; He, Y.; Talukdar, S. S.; Swihart, M. T. Photoluminescent Silicon Nanoparticles with Emission Spanning the Visible Spectrum. *Langmuir* **2003**, 19, 8490–8496.

(10) Pi, X. D.; Liptak, R. W.; Nowak, J. D.; Wells, N.; Blank, D. A.; Carter, C. B.; Campbell, S. A.; Kortshagen, U. Air-Stable Full-Visible-Spectrum Emission from Silicon Nanocrystal Ensembles Synthesized by an All-Gas-Phase Plasma Approach. *Nanotechnology* **2008**, 19, 123102.

(11) Hessel, C. M.; Henderson, E. J.; Veinot, J. G. C. Hydrogen Silsesquioxane: A Molecular Precursor for Nanocrystalline Si-SiO_2 Composites and Freestanding Hydride Surface Terminated Silicon Nanoparticles. *Chem. Mater.* **2006**, 18, 6139–6146.

(12) Hessel, C. M.; Reid, D.; Panthani, M. G.; Rasch, M. R.; Goodfellow, B. W.; Wei, J.; Fujii, H.; Akhavan, V.; Korgel, B. A. Synthesis of Ligand-stabilized Silicon Nanocrystals with

Size-dependent Photoluminescence Spanning Visible to Near-infrared Wavelengths. *Chem. Mater.* **2012**, 24, 393−401.

(13) Hessel, C. M.; Rasch, M. R.; Hueso, J. L.; Goodfellow, B. W.; Akhavan, V. A.; Puvanakrishnan, P.; Tunnel, J. W.; Korgel, B. A. Alkyl Passivation and Amphiphilic Polymer Coating of Silicon Nanocrystals for Diagnostic Imaging. *Small* **2010,** 6, 2026−2034.

(14) Yu, Y.; Hessel, C. M.; Bogart, T. D.; Panthani, M. G.; Rasch, M.R.; Korgel, B. Room Temperature Hydrosilylation of Silicon Nanocrystals with Bifunctional Terminal Alkenes. *Langmuir* **2013**, 29, 1533−1540.

(15) Choi, J.; Wang, N. S.; Reipa, V. Electrochemical Reduction Synthesis of Photoluminescent Silicon Nanocrystals. *Langmuir* **2009**, 25, 7097−7102.

(16) Shen, P.; Uesawa, N.; Inasawa, S.; Yamaguchi, Y. Stable and Color Tunable Fluorescence from Silicon Nanoparticles Formed by Single-step Plasma Assisted Decomposition of $SiBr_4$. *J. Mater. Chem.* **2010**, 20, 1669−1675.

(17) Carlisle, J.; Dongol, M.; Germanenko, I.; Pithawalla, Y.; El-Shall, M. Evidence for Changes in the Electronic and Photoluminescence Properties of Surface-oxidized Silicon Nanocrystals Induced by Shrinking the Size of the Silicon Core. *Chem. Phys. Lett.* **2000**, 326, 335−340.

(18) Shirahata, N.; Hirakawa, D.; Sakka, Y. Interfacial-related Color Tuning of Colloidal Si Nanocrystals. *Green Chem.* **2010**, 12, 2139−2141.

(19) Tan, D.; Ma, Z.; Xu, B.; Dai, Y.; Ma, G.; He, M.; Jin, Z.; Qiu, J. Surface Passivated Silicon Nanocrystals with Stable Luminescence Synthesized by Femtosecond Laser Ablation in Solution. *Phys. Chem. Chem. Phys.* **2011**, 13, 20255−20261.

(20) Dewan, S.; Odhner, J. H.; Tibbetts, K. M.; Afsari, S.; Levis, R. J.;Borguet, E. Resolving the Source of Blue Luminescence from Alkyl-capped Silicon Nanoparticles Synthesized by Laser Pulse Ablation. *J. Mater. Chem. C* **2016**, 4, 6894-6899.

(21) Nakamura, T.; Yuan, Z.; Watanabe. K.; and Adachi, S. Bright and Multicolor Luminescent Colloidal Si Nanocrystals Prepared by Pulsed Laser Irradiation in Liquid. *Appl. Phys. Lett.* **2016**, 108, 023105.

(22) Miyano, M.; Endo, S.; Takenouchi, H.; Nakamura, S.; Iwabuti, Y.; Shiino, O.; Nakanishi, T.; Hasegawa, Y. Novel Synthesis and Effective Surface Protection of Air-stable Luminescent Silicon Nanoparticles. *J. Phys. Chem. C* **2014**, 118, 19778−19784.

(23) Li, Q.; Luo, T. Y.; Zhou, M.; Abroshan, H.; Huang, J. C.; Kim, H, J.; Rosi, N. L.; Shao, Z.; Jin, R. Silicon Nanoparticles with Surface Nitrogen: 90% Quantum Yield with

Narrow Luminescence Band Width and the Ligand Structure Based Energy Law. *ACS Nano* **2016**, 10, 8385−8393.

(24) Nakamura, T.; Yuan, Z.; Adachi, S. High-yield Preparation of Blue-emitting Colloidal Si Nanocrystals by Selective Laser Ablation of Porous Silicon in Liquid. *Nanotechnology* **2014**, 25, 275602.

(25) Sailor, M, J.; Lee, E, J. Surface Chemistry of Luminescent Silicon Nanocrystallites. *Adv. Mater.* **1997**, 9, 783–793.

(26) Ben-Chorin, M.; Moller, F.; Koch, F. Hopping Transport on a Fractal: Ac Conductivity of Porous silicon. *Phys. Rev. B* **1995,** 51, 2199-2213.

(27) Fischer, M.; Georges, J. Fluorescence quantum yield of rhodamine 6G in ethanol as a function of concentration using thermal lens spectrometry. Chem. Phys. Lett. **1996**, 260, 115−118.

(28) Kůsová, K.; Cibulka, O.; Dohnalová, K.; Pelant, I.;Valenta, J.; Fucíková, A.; Zídek, K.; Lang, J.; Englich, J.; Matejka, P.; Stepánek, P.; Bakardjieva, S. Brightly Luminescent Organically Capped Silicon Nanocrystals Fabricated at Room Temperature and Atmospheric Pressure. *ACS Nano* **2010**, 4, 4495−4504.

(29) Li, X.; He, Y.; and Swihart, M T. Surface Functionalization of Silicon Nanoparticles Produced by Laser-driven Pyrolysis of Silane Followed by HF-HNO3 Etching. Langmuir 2004, 20, 4720−4727.

(30) Pavesi, L.; Ceschini, M. Stretched-exponential Decay of the Luminescence in Porous Silicon. *Phys. Rev. B* **1993**, 48, 17625−7628.

(31) Kalkman, J.; Gersen, H.; Kuipers, L.; Polman A. Excitation of Surface Plasmons at a SiO_2/Ag Interface by Silicon Quantum Dots: Experiment and Theory. Phys. Rev. B **2006**, 73, 075317.

(32) Oliinyk, B. V.; Lysenko, V.; and Alekseev, S. Determining the Impact of Hydrofluoric Acid on Surface States of As-prepared and Chemically Modified Si Nanocrystals. *RSC Adv.* **2016**, 6, 3723−3728.

(33) Werner, D.; Ueki, T.; Hashimoto, S. Methodological Improvement in Pulsed Laser-Induced Size Reduction of Aqueous Colloidal Gold Nanoparticles by Applying High Pressure. *J. Phys. Chem. C* **2012**, 116, 5482−5491.

4.6 Supporting Information

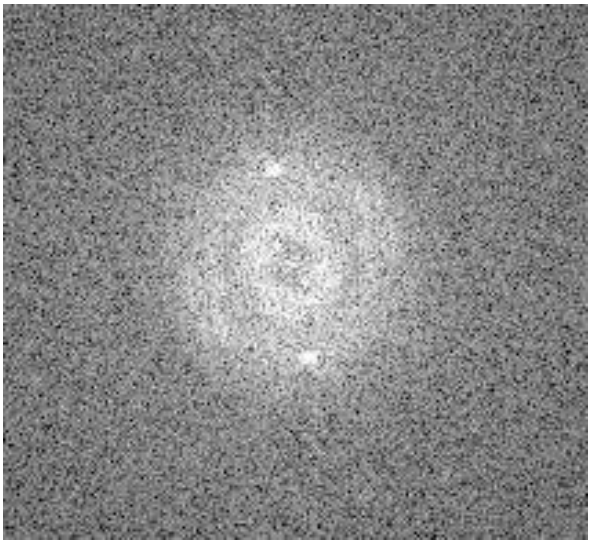

Figure S1 FFT pattern of the transmission electron microscope image in the Figure 4.1a.

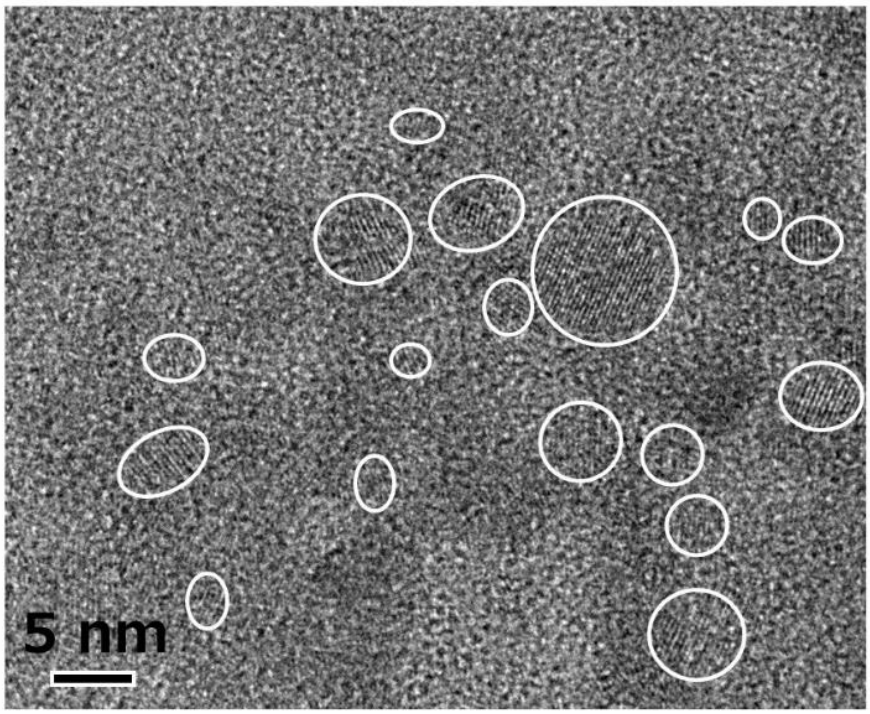

Figure S2 Transmission electron microscope image of the colloidal Si-nc sample prepared in the HF-free solvent (0 vol%).

Chapter 5

Concluding remarks

In Conclusion, we developed improved fabrication techniques for luminescent colloidal Si-nc by pulsed laser irradiation of PSi. We fabricated the different-luminescence-color (blue, white, orange, and red) colloidal Si-nc with different size distributions by changing the different pulsed laser irradiation conditions, such as a kind of the solvent, the wavelength of pulsed laser, properties of PSi target. Such an emission color (size) control is usually difficult in conventional laser irradiation techniques. Furthermore, we succeeded in realizing a high yield preparation of the colloidal Si-nc sample by selecting an appropriate organic solvent and by adding a reactive liquid in the solvent. Our approach to control both PL properties (size) and preparation yields of Si-nc in pulsed laser irradiation techniques will help us to realize a future low-cost mass production of semiconductor nanocrystals.

We reviewed and introduced related research in luminescent colloidal Si-nc for fundamental researches and optical device applications in Chapter 1, and then discussed the correlative problems and difficulty in luminescent colloidal Si-nc research field. Then how to solve those problems and difficulty details are discussed and presented in Chapter 2-4.

In chapter 2, we developed a simple route to produce bright and multicolor luminescent colloidal Si-nc. The colloidal Si-nc was produced by pulsed UV laser irradiation of PSi in an organic solvent (1-octene). The emission color of the colloidal Si-nc's reflected that of PSi, which indicates that colloidal Si-nc has a size distribution analogous to that of the starting PSi.

In chapter 3, we prepared chlorine-passivated colloidal Si-nc (Cl:Si-nc) by laser ablation of PSi in trichloroethylene and demonstrated a change in the emission color from white to blue and also increased PL quantum efficiency from 2% (Cl:Si-nc) to 13% (C:Si-nc) by performing the post-laser ablation of the Cl:Si-nc sample in 1-octene to form stable carbon-passivated Si-nc surface. Such greatly improved PL properties of the post-laser ablation-prepared C:Si-nc sample come from its size reduction and also better surface

passivation, owing to higher reactive nature of 1-octene than that of trichloroethylene. Moreover, the preparation yield of the Cl:Si-nc sample prepared in trichloroethylene and that of the C:Si-nc sample prepared by the post-laser ablation of Cl:Si-nc in 1-octene were observed to be much larger than that of the directly laser ablation-prepared C:Si-nc sample from PSi powder in 1-octene.

In chapter 4, we demonstrated the highly improvement of formation processes for colloidal Si-nc by pulsed-UV-laser irradiation on porous silicon in a reactive HF-contained organic solution. The Si-nc samples exhibit a higher PL quantum yield (~50–70%) than that in an ordinary organic solvent without HF (~20%). This enhancement of the quantum yield is caused by the HF-induced removal of the surface oxide overlayer on Si-nc and subsequent hydrogen termination. These reactions promote the efficient hydrosilylation between the hydrogen surface and organic solvent, resulting in the lower defect density of the Si-nc surface. The preparation yield also increases by an order of the magnitude compared to that without HF and the size distribution of Si-nc becomes homogeneous, in direct contrast to the bimodal size distribution obtained in the ordinary solvent without HF. These results are owing to effective pulsed-laser-induced fragmentation by the removal of oxide overlayer and the resultant weakening of mechanical strength of the PSi target layer.

Publications and Presentations

Journal articles

1. Z. Yuan, T. Nakamura, S. Adachi, and K. Matsuishi "Improvement of Laser Processing for Colloidal Silicon Nanocrystal Formation in a Reactive Solvent" *J. Phys. Chem. C* **121**, 8623−8629 (2017). [IF:4.5]
2. Z. Yuan, T. Nakamura, S. Adachi, and K. Matsuishi, "Luminescence color control and quantum-efficiency enhancement of colloidal Si nanocrystals by pulsed laser irradiation in liquid" *Nanoscale* **9**, 1193 (2017). [IF:7.76]
3. T. Nakamura, Z. Yuan, K. Watanabe, and S. Adachi "Bright and multicolor luminescent colloidal Si nanocrystals prepared by pulsed laser irradiation in liquid"*Applied Physics Letters* **108**, 023105 (2016). [IF:3.14]
4. T. Nakamura, Z. Yuan, and S. Adachi "High-yield preparation of blue-emitting colloidal Si nanocrystals by selective laser ablation of porous silicon in liquid", *Nanotechnology* **25**, pp 275602-1-7 (2014). [IF:3.57]
5. T. Nakamura, Z. Yuan, and S. Adachi, "Micronization of red-emitting $K_2SiF_6:Mn^{4+}$ phosphor by pulsed laser irradiation in liquid", *Applied Surface Science* **320**, pp 514-518 (2014). [IF:3.15]

Oral presentations

1.○袁 澤、中村 俊博、安達　定雄、橋本　修一、多孔質 Si の液中レーザーアブレーションによる青色発光 Si コロイドの作製、第 74 回 応用物理学会秋季講演会報告集、16p-D6-4、同志社大学、2013/9/16-9/20

2.○袁 澤、中村 俊博、安達　定雄、液中レーザーアブレーションによる赤色発光 $K_2SiF_6:Mn^{4+}$ 蛍光体の微粒子化、第 61 回 応用物理学会春季学術講演会報告集、19p-E11-14、青山学院大学、2014/3/17-3/20

3.○渡邊 幹太、袁 澤、中村 俊博、安達 定雄、ポストレーザー照射によるナノ結晶 Si コロイドの発光波長制御、第 62 回 応用物理学会春季学術講演会報告集、12p-A20-13、東海大学、湘南キャンパス、2015/3/11-3/14

4.○袁 澤、中村 俊博、安達 定雄、多孔質 Si の液中レーザーアブレーションによる白色発光 Si ナノ粒子の作製、平成 27 年 電気学会全国大会報告集、2-099, 東京都市大学　世田谷キャ

ンパス、2015/3/24-3/26

5.○**袁 澤**、渡邊 幹太、中村 俊博、安達 定雄、多孔質 Si の液中パルスレーザー照射による多色発光 Si ナノ粒子の作製、第 74 回 応用物理学会秋季講演会報告集、14a-2Q-7、名古屋国際会場、2015/9/13-9/16

6.○渡邊 幹太、**袁 澤**、中村 俊博、安達 定雄、橙色発光 Si ナノ結晶コロイドに対するポストレーザー照射の効果、第 74 回 応用物理学会秋季講演会報告集、14a-2Q-8、名古屋国際会場、2015/9/13-9/16

7.○中村 俊博、**袁 澤**、安達 定雄、多孔質 Si の液中レーザー照射によるナノ結晶 Si 粒子の高効率生成と発光色制御、第 63 回 応用物理学会春季学術講演会報告集、 20p-W321-7 東京工業大学、2016/3/24-3/26

8.○渡邊 幹太、**袁 澤**、中村 俊博、安達 定雄、多孔質 Si の液中紫外レーザー照射による Si ナノ結晶コロイドの作製条件の最適化第 63 回 応用物理学会春季学術講演会報告集、19a-W834-3、 東京工業大学、2016/3/24-3/26

9.○須田 義規、渡邊 幹太、**袁 澤**、中村 俊博、安達 定雄、多孔質 Si の液中紫外レーザー照射により作製した Si ナノ結晶コロイドの発光特性の評価第 63 回 応用物理学会春季学術講演会報告集、19a-W834-4、東京工業大学、2016/3/24-3/26

10.○**袁 澤**、中村俊博、安達定雄、松石清人、高反応性分散液中レーザー照射プロセスによる Si ナノ結晶コロイド粒子の発光効率の改善とサイズ分布の狭小化、第 64 回応用物理学会学術講演会報告集、14p-512-7、パシフィコ横浜、2017/3/14-3/17

11. ○T. Nakamura, **Z. Yuan,** S. Hashimoto, S. Adachi

"Preparation of blue-emitting colloidal Si nanocrystals by laser ablation of porous silicon in liquid"

Advanced Nanoparticle Generation and Excitation by Laser in Liquids (ANGEL) Matsuyama, Japan (19-21 May, 2014)

12. ○T. Nakamura, **Z. Yuan,** S. Adachi

"Fabrication of colloidal Si nanoparticles by pulsed-laser irradiation of porous Si in liquid: Toward high productivity and size control"

The 18th International Symposium on Laser Precision Microfabrication (LPM2017) Toyama, Japan (05-08 June 2017)

Acknowledgments

I would like to express my deepest gratitude to my adviser Professor Kiyoto Matsuishi in the Development of Materials Science at the faculty of Pure and Applied Sciences, University of Tsukuba for his great help, without whom this thesis would have only been a dream. I am indebted for Professor Matsuishi constant assistance, encouragement, guidance and the tremendous support and opportunities when I during studies at University of Tsukuba. I do not have words to express my real appreciation for Professor Matsuishi. He has always been there and gone beyond what I expected from anyone in navigating me towards my educational goals. He has taught me many important lessons in life which will always guide me throughout my PHD program. The many skills I have learnt from Professor Matsuishi will constantly remind me of how great a teacher he is throughout my life.

I would like to express my thesis co-advisor and longtime teacher during my years, Associate Professor Toshihiro Nakamura. I knew Professor Nakamura long before I started my Master's program (Research student period) in Gunma University. He was a mentor and like a big brother to me. He was the reason for me to join the PhD program, because I want to become a researcher like him much. During the PhD process, he always encouraged me to express my ideas. He showed me how to research a problem and achieve goals. He spent endless time reviewing and proofreading my papers, asking me questions to let me think harder, and supported me during the difficult times in my research. He believed in me when I doubted myself. Without his encouragements, continuous guidance and insight, I could not have finished this dissertation. Our weekly progress emails were our means of communication and way to keep in touch that gave me the motivation to work harder and make the best effort possible. His effort and patience will never be forgotten.

I profusely thank Honorary Professor Sadao Adachi, who is my co-advisor, Graduate School of Science and Technology, Gunma University. He is like a father to care of me. He was always eager to help, be it a research issue or a worldly matter. Without his breadth of knowledge in the area of material science, finishing my thesis would have remained a distant dream.

I would like to thank the Committee, Associate Professor Tetsuya Makimura,

Acknowledgments

Associate Professor Kazuhiro Marumoto, Associate Professor Hisanori Tanimoto, for precious wise advices. They were very kind to me but keen and strict with respect to science.

I would thank many other colleagues and research friends in university and other Institutes for every advice and assistance, namely (in family name order) Prof., N. Shirahata (National Institute for Materials Science (NIMS), Japan), Prof., N. Koshida (Department of Electronic and Information Engineering, Graduate School of Engineering, Tokyo University of Agriculture and Technology, Japan), Dr. X.D. He (Department of Physical and Chemical Inspection School of Public Health, Shandong University, China) Thank you all.

I am grateful to University of Tsukuba, Tsukuba City and Japan, where I lived and studied for more than 3 years.

Last but not least, I would like to thank my family for their deep and endless love. I love you.

Ze Yuan

February, 2018

Tsukuba, Japan